**TRIBHUVAN UNIVERSITY**

**INSTITUTE OF ENGINEERING**

**PULCHOWK CAMPUS**

**THESIS NO: S003/075**

# Seismic Vulnerability Assessment of Unreinforced Masonry Residential Buildings in Urban Settlement

by

Dipesh Tiwari

A THESIS

SUBMITTED TO THE DEPARTMENT OF CIVIL ENGINEERING IN PARTIAL FULFILLMENT OF THE REQUIREMENTS FOR THE

DEGREE OF MASTER OF SCIENCE IN

STRUCTURAL ENGINEERING

DEPARTMENT OF CIVIL ENGINEERING

LALITPUR, NEPAL

SEPTEMBER, 2021

## COPYRIGHT ©

**TRIBHUVAN UNIVERSITY**

**INSTITUTE OF ENGINEERING**

**DEPARTMENT OF CIVIL ENGINEERING**

**PULCHOWK CAMPUS**

The undersigned certify that they have read, and recommended to the Institute of Engineering for acceptance, a thesis entitled, **"Seismic Vulnerability Assessment of Unreinforced Masonry Residential Buildings in Urban Settlement"** submitted by Mr. Dipesh Tiwari (075/MSStE/003) in partial fulfillment of the requirements for the degree of Master of Science in Structural Engineering.

……..

Supervisor, Dr. Gokarna Bahadur Motra

Department of Civil Engineering

Institute of Engineering

Pulchowk Campus

……..

External Examiner, Er. Ganga Bahadur Basnet

……..

Committee Chairperson, Dr. Kamal Bahadur Thapa

M.Sc. in Structural Engineering

Institute of Engineering

Pulchowk Campus

Date: September, 2021

## ABSTRACT

Maximum of masonry buildings in urban areas are with large openings in ground floor level and with different stages of construction adding more non-engineered complexity to the structure. This paper shows the analytical methodology of seismic vulnerability assessment through a case study of five unreinforced masonry residential buildings made of brick masonry bonded with the mud mortar, and with different structural deficiencies. These selected prototype buildings represents the buildings situated in urban areas of Nepal. Stepwise procedures of seismic assessment is analyzed through non-linear pushover analysis and fragility functions are generated to define the vulnerability level of the selected prototypes of building. The area elements at potential yielding sections are replaced with Multi-linear plastic non-linear link elements which are defined in finite element software SAP2000. The proposed study has direct implication towards assessing the vulnerability of similar case study of URM residential buildings which may further assists for the development of proper retrofitting strategies assuring life safety requirements.

## ACKNOWLEDGEMENT

I wish to express my deepest and sincere appreciation to my supervisor Prof. Dr. Gokarna Bahadur Motra for the guidance, encouragement, and critical suggestion throughout this study. I am also indebted to Dr. Kshitij Charana Shrestha, without whom, this research and thesis work couldn't achieve this state.

I am thankful to the Department of Civil Engineering, Pulchowk Campus, and MSc Program Coordinator in Structural Engineering. I would like to thank my professors Dr. Prem Nath Maskey, Dr. Hikmat Raj Joshi, Dr. Kamal Bahadur Thapa, Dr. Rajan Suwal, Dr. Jagat Kumar Shrestha and Dr. Bharat Mandal for providing us with technical insight and valuable suggestions.

I would further like to express my sincere thanks to my external supervisor Er. Ganga Bahadur Basnet for his valuable suggestions and guidelines.

Similarly, I am thankful to CRS Nepal, ASF Nepal, CRAterre, Lumanti Group and CARDS office IOE for providing me the opportunity to work on this research field.

Finally, I would like to express my special dedication to my dear parents, friends and SLG group whose love, support, and motivation have encouraged me.

I would like to extend further thanks to all individuals for their direct and indirect help.

Dipesh Tiwari

075/MSStE/003

September, 2021

## TABLE OF CONTENTS

## LIST OF ACRONYMS AND ABBREVIATIONS

| | |
|---|---|
| URM | Unreinforced Masonry |
| BMM | Brick Masonry with Mud Mortar |
| RCC | Reinforced Cement Concrete |
| UNDP | United Nations Development Programme |
| NRA | National Reconstruction Authority |
| CBS | Central Bureau of Statistics |
| FEMA | Federal Emergency Management Agency |
| NL | Non Linear |
| CSM | Capacity Spectrum Analysis |
| ATC | Applied Technology Council |
| TMS | The Masonry Society |
| IO | Immediate Occupancy Level |
| LS | Life Safety Level |
| CP | Collapse Prevention Level |
| GMI | Ground Motion Intensity |
| $V_{bjs}$ | Lateral strength of wall / pier based on bed joint shear strength |
| $v_{me}$ | Expected bed-joint sliding shear strength |
| $A_n$ | Area of net mortared/grouted section |
| $v_{te}$ | Average test value representing bond strength from in-plane push testing |
| $P_{CE}$ | Expected vertical axial gravity compressive force |
| $V_r$ | Lateral rocking strength of wall or pier component |
| $\alpha$ | Factor equal to 0.5 for fixed-free cantilever wall, or equal to 1.0 for fixed-fixed pier |
| $f_a$ | Upper bound of vertical axial compressive stress |

| | |
|---|---|
| $f'_{dt}$ | Lower bound of masonry diagonal tension strength |
| $f'_{m}$ | Lower bound of masonry compressive strength |
| $P_{CL}$ | Lower bound of vertical compressive force |
| $V_{dt}$ | Lateral strength limited by diagonal tension stress |
| $V_{tc}$ | Lateral strength limited by toe compressive stress |
| $f_y$ | Yield strength of steel reinforcement |
| $E_m$ | Modulus of Elasticity of Masonry Wall |
| $E_s$ | Modulus of Elasticity of Reinforcement Steel |
| $G_m$ | Shear modulus of masonry |
| $A_{trib}$ | Tributary Area |
| $A_{m,trib}$ | Tributary area of masonry to nonlinear link |
| $A_{s,trib}$ | Tributary area of reinforcement to nonlinear link |
| $L_{link}$ | Length of nonlinear link elements |
| $V_n$ | Nominal shear strength |
| b | Width of section |
| $d_v$ | Actual depth of member in direction of shear considered |
| $\bar{S}_{d,ds}$ | Median value of spectral displacement at which the building reaches a certain threshold of the damage state $d_s$ |
| $\beta_{ds}$ | Standard deviation of the spectral displacement |
| $\phi$ | Standard normal cumulative distribution function |
| $S_D$ or $D_y$ | Spectral displacement |
| $S_A$ | Spectral acceleration |
| $h_e$ | Equivalent damping ratio |
| $LS_i$ | Limit State |

## LIST OF FIGURES

## LIST OF TABLES

# CHAPTER 1: INTRODUCTION

## 1.1 Background

Masonry is a type of construction that is made up of discrete pieces which are joined together with or without the use of a binding medium. A masonry structure is a non-homogeneous and anisotropic structural element, generally made up of two separate materials, masonry units and mortar. The properties of masonry units, mortar/binding material, workmanship, openings, unsupported height, loading eccentricities, age and the pattern in which the units are assembled highly affects the strength and durability of masonry structures. Masonry structures are strong in compression and weak in tension.

Masonry structures have been widely employed and are major construction practices all over the world since ages. We can see maximum of world's architectural historic heritages made up of masonry, which are still in existence. The prevailing geological formations and conditions in the given area has always influenced the choice of masonry materials. Because of locally available construction materials and relatively cheaper in construction, masonry structures are also typical construction practice in Nepal. We can see many of Malla and Rana architectures made of brick masonry bonded with lime, surkhi / mud mortars. The advantages of employing masonry as a building material include sound absorption, fire protection, low maintenance and durability. Generally, masonry units like stones, clay bricks and concrete blocks are used with mud, cement or lime mortar as binding material in Nepali societies. According to survey from UNDP and CBS (2017), most of the Nepalese houses have outer walls with mud bonded stone or bricks (37.6%) which is predominant in rural areas (49.3%) than in urban areas (20.4%). But, the percent of exterior walls of stone/brick masonry with cement bonded houses has increased from 33.4% in 2014/15 to 36.6% in 2015/16, and are in increasing number.

Most of the masonry buildings, susceptible of collapsing, are old structures which were not built according to the design guidelines or code requirements. Unreinforced masonry walls (URM) are generally load bearing structures and their stability is governed by their seismic weight. They undergo considerable stages of structural degradation with age, loadings and seismicity. Heavy weight, poor construction materials, brittleness, weak mortar joints, lack of adequate connections, rapid and

unmanaged development without proper engineering design and quality control has led to greater extent of damage in the recently occurred earthquake. Addition of extra storey in the existing building with increase in family size and financial support is pretty common in developing urban areas on Nepal. Even the construction technique and materials vary within these storey levels. Thus, it is necessary to assess the seismic performance of these structures in their current state and carry out necessary strengthening measures to control the risk of life and property.

The geological feature of Nepal is seismically active and records shows many losses of life and property due to past earthquakes. According to the NRA (2021), out of 1,047,261 damaged houses surveyed, 78.4% were of low strength masonry, 7.87% cement-mortared masonry and only 3.57% were reinforced concrete houses. Low strength masonry houses were greatly affected in comparison to other typologies in the recent Gorkha Earthquake in 2015.

It is obvious that additional research and development is required in this discipline, however there is a lack of data and research to evaluate its mechanical properties and structural performance. The masonry have various properties and thus the input parameters to define these properties vary at greater extent.

Present studies shows the advancement in RCC and steel structures globally. To characterize the non-linear structural behavior of these structures, a lot of research has been performed. However, little few researches have been made in masonry structures. Finite element modelling based on mechanical properties and geometry of the structural systems can be used to estimate model parameters of the system. There is presently no model that can adequately describe the nonlinear properties of these masonry structures. This could be due to the complexity of its modeling and the wide range of its attributes. There are also other several uncertainties involved in such modelling, like: rigidity of connection, supporting soil condition, etc. Simplified numerical micro-modelling, macro-modelling and discrete crack finite element approaches are proposed by researchers based on various assumptions. Recently, in the context of Nepal, after Gorkha earthquake, few papers have been published for retrofitting options for historically important temples and monuments, and a little few codal guidelines on residential houses.

In this thesis work, a case study on typical residential masonry buildings with clay bricks bonded with mud mortar (BMM) is only taken under considerations. A sample of 5 buildings is chosen in such a way that these buildings generally represent the present condition masonry buildings especially situated in urban settlements in Nepal. As larger openings in the lower stories are more susceptible of vulnerability to the whole building, these type of buildings are prioritized in the selection of buildings. The open space in the ground stories are usually used by the local shop vendors for running their business. Many of these buildings are later modified with addition of stories or replacing timber trussed roofs with RCC rigid slabs. As most of them are non-engineered buildings, seismic vulnerability assessment is required and necessary retrofitting measures are to be performed to ensure safety of life and property in future earthquakes. First of all, the visual assessment is performed and static analysis of the masonry building is done with 3D simplified macro modelling approach. Then, the non-linear multilinear plastic links are provided in possible rupture planes and pushover analysis is performed to study its non-linear behavior in the in-plane direction. Performance point is calculated from Capacity Spectrum Method (CSM) and fragility curves are generated to check seismic vulnerability levels. Thus, weakest points of failure are analyzed and possible retrofitting measures can be suggested.

The major aim of seismic capacity assessment is to quantify the seismic vulnerability of the structure to the given intensity of a ground motion. The study of fragility analysis determines the likelihood of earthquake damage to a specific structure type. Thus, study on masonry structures help to identify the inadequacies in earthquake resistance parameters and gives technical judgements for rehabilitation techniques of these structures.

### 1.2 Need of Research

Various study show that maximum of unreinforced load bearing buildings are susceptible of collapsing during earthquake. Rapid and unmanaged development in urban areas, addition of extra storey in existing building, random positioning of openings, irregularities in load path, and mixed construction materials has added to higher vulnerability level as these are completely non-engineered. Little few researches have been performed for these types of residential buildings. Thus, it is necessary to check the seismic performance of these buildings in their existing conditions and carry out necessary strengthening measures to control the risk of life and property. Hence,

building typology with larger openings in Ground level, and buildings with floor modifications for adding extra stories in the existing building, are taken as case study in the present thesis.

### 1.3 Objectives

The main objectives of the work are:

1. To generate capacity curve through pushover analysis using non-linear links
2. To quantify the vulnerability of the selected prototype residential buildings through fragility curves

### 1.4 Methodology

Figure 1.1 depicts the general methodological flowchart used in the present study.

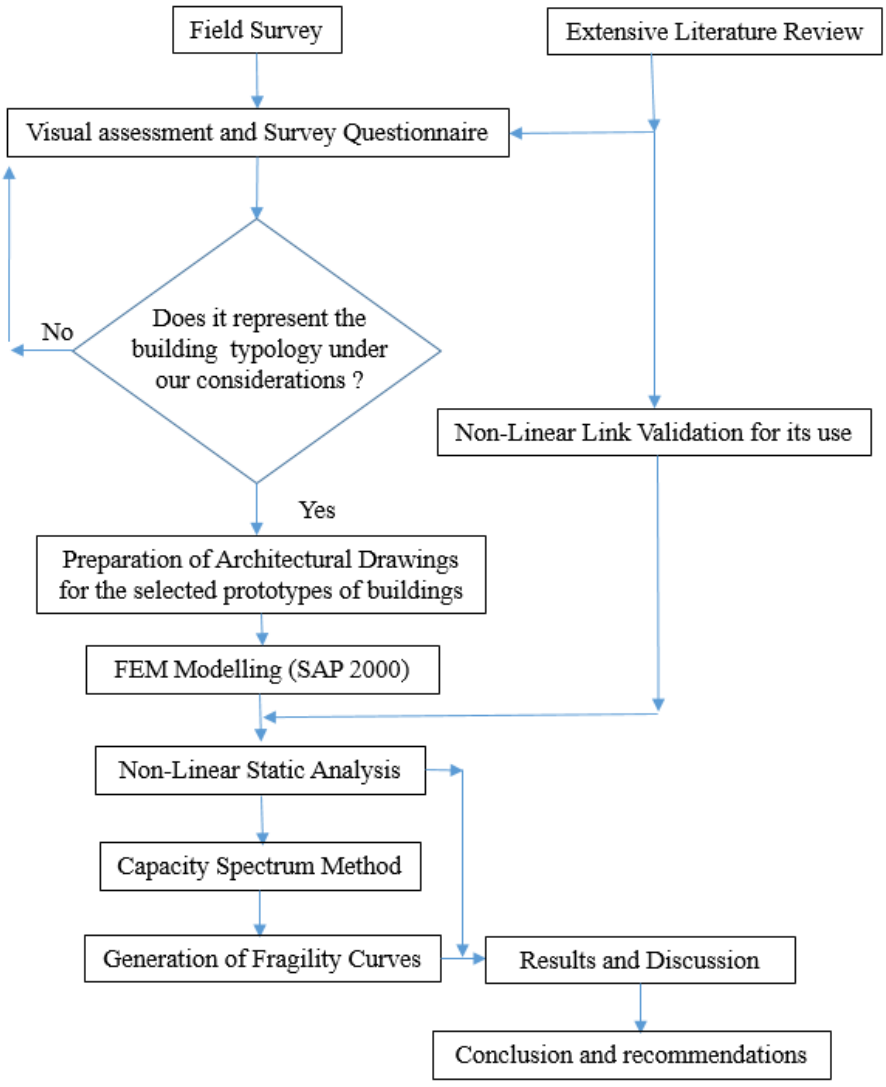


Figure 1.1 General Methodology flowchart adopted for present study

### 1.5 Scope of the work

1. The proposed study has direct implication towards strengthening of vulnerable residential buildings.

2. In general, this study also highlights the vulnerabilities of the existing typical URM residential buildings through a more detailed nonlinear push-over analysis.

3. The fragility curves developed will serve as an important tool to understand the effectiveness of proposed strengthening techniques over the existing structures.

### 1.6 Limitations

1. All nonlinearities are concentrated at NL links and their locations are defined by user based on the predefined conventional cracking patterns and stress concentrations. A more detailed micro-modeling approach or damage models could provide better representation of the failure patterns and capacity curves, a limitation for FE modeling using SAP2000.

2. Fragility curve generation is based on capacity spectrum method (CSM) from nonlinear pushover curves. Non-linear time history analysis could give more comprehensive results but would require input of more detailed dynamic characteristics of the structure, which are not available to the authors at present.

3. Foundation of structure is assumed to be fixed. More comprehensive analysis and knowledge is required to understand the subsoil conditions.

4. The mechanical properties of the masonry buildings are based on relevant previous researches. Because of lack of material testing equipments, lab based tests were beyond our scope.

### 1.7 Organization of the Chapters

The following five chapters make up the full thesis.

CHAPTER 1: presents an introductory parts of the present study with background, objective, methodology flowchart, scope, and limitations.

CHAPTER 2: presents the literature conducted for the present study. It includes the literature review about failure mechanisms of masonry buildings, modeling techniques of masonry walls and non-linear link elements. Nonlinear static analysis with Macro-Modelling approach, capacity spectrum and fragility curve generation are also

discussed under this chapter. Retrofit measures generally adopted in case of masonry buildings is presented in brief. And some researches on masonry structures in the context of Nepal are also presented.

CHAPTER 3: presents the methodology of present thesis work with techniques for the nonlinear modelling and analysis with a model validation. It includes the details of material properties, plasticity model, and methods used in each type of solution techniques.

CHAPTER 4: presents the analytical result obtained from modeling and discussion.

CHAPTER 5: presents the conclusion from present research works and recommendations for further future works.

# CHAPTER 2: LITERATURE REVIEW

## 2.1 Background

This chapter provides a critical summary of previous non-linear analytic research works on the masonry buildings. Initially the basic theories related to masonry structures is discussed and in later, various researches conducted by the researches in the context of Nepal is briefly presented. The introduction to unreinforced masonry structures, failure patterns, modelling techniques with nonlinear link elements and static pushover analysis is discussed below. Further, capacity spectrum method, generation of fragility functions are presented in detail.

## 2.2 Introduction to Unreinforced Masonry (URM)

Since ages, unreinforced masonry has been a widely used building material. Among them, solid clay brick unit masonry is the widely used masonry unit. Similarly, with clay brick unit masonry, other types like stone masonry, adobe, concrete masonry are mostly used in Nepal. These wall construction practice and laying patterns govern the stability and strength parameters. The properties of compressive, tensile, and shear strength vary greatly depending on the masonry unit and mortar used. These strength parameters decrease with age; old mortar joints are weaker than the masonry units. In older days, lime-surkhi and clay was used as mortar. However, later on, sand and cement are added to improve masonry strength, although brittle breaking along the masonry units can occur which results in lesser deformation capacity.

Unreinforced masonry is defined by FEMA 306 as masonry that has less than 25% of the minimum reinforcement prescribed by FEMA 273. It further sub divides URM components as Non – wall components (parapets, appendages, wall diaphragm ties) and Wall – components: URM1 (Solid cantilever walls), URM2 (weak pier in perforated wall), URM3 (weak spandrel in perforated wall), URM4 (strong spandrel in a weak pier-strong spandrel) and URM 5 (perforated wall with panel zone weak joints).

## 2.3 Behavior Failure Modes of Non-Wall URM Elements

Table 2. 1 Behavior Failure Modes of Non-Wall URM Elements (FEMA 306)

| Element | | Source of Deficiency | Behavior Mode | Intensity of Ground Shaking Usually Required to Produce Behavior Mode |
|---|---|---|---|---|
| Parapet | | Out-of-plane flexural tension | Parapet falls | Low-to-moderate |
| Appendages | | Connection failure | Falling hazard | Low-to-moderate |
| | | Missing headers or veneer ties | Veneer delamination | Moderate |
| | | Stiffness incompatibility | Cracking and spalling | Low-to-moderate |
| | | Pounding | Local spalling | Moderate |
| Wall-Diaphragm Ties | | | | |
| | Tension Ties | Inadequate or missing ties | Wall-diaphragm separation | Moderate |
| | Shear Ties | Diaphragm slides | Perpendicular walls punched out | Moderate |
| Diaphragms | | | | |
| | Rigid Concrete Slab | Not typically damaged | NA | NA |
| | Hollow Concrete Plank | Lack of interconnection | Incomplete load path, excessive deflection | Moderate-to-high |
| | HCT/Brick Arch on Steel Beams | Lack of tie rods between steel beams | Localized falling hazard as beams separate | Moderate-to-high |
| | Flexible | Inadequate strength/stiffness | Excessive deflection can cause wall damage | Moderate-to-high |

## 2.4 Typical Earthquake Failure Modes of URM Walls

URM components can collapse due to structural instability or overloading, dynamic disturbances, foundation settlements, in-plane or out-of-plane deformations. Walls oriented parallel in direction of earthquake are in-plane and in perpendicular to it are out-of-plane. Organizations such as TMS and FEMA have concluded that during earthquakes, URM wall failures cause more material damage and human death than any other type of structural element (Garbin, 2017). Generally, non-wall component cracks and damage often occurs before in-plane wall cracks becomes noticeable. Maximum of modes are related to in-plane damage, but out-of-plane damages are likely when in-plane damage is present (FEMA306).

The dominant failure mechanism is the mechanism that results in lower lateral resistance and it corresponds to the maximum lateral load. The following types of failure modes are generally encountered in unreinforced walls (FEMA273) as shown in figure 2.1.

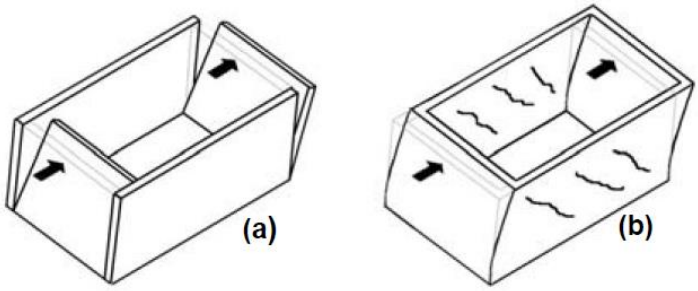


Figure 2.1 (a) Out-of-plane failure mechanism (b) In-plane failure mechanism

### 2.4.1 In-Plane Failure

According to Miha Tomazevic (1999), the seismic response of masonry walls which are subjected to in-plane earthquake loads is characterized as the following three categories (Figure 2.2) of mechanism and failure modes based on the output results of seismic damage analysis and subsequent investigations. The controlling mechanisms are the wall geometry (height/width ratio), masonry material quality, boundary restrictions, and stresses developed on these wall.

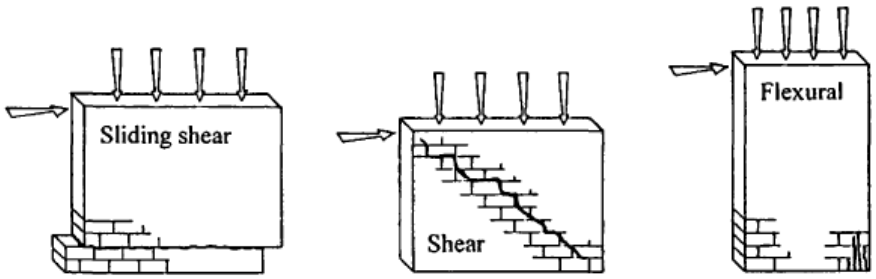


Figure 2.2 Typical Failure Modes of Masonry Walls subjected to In-Plane Seismic Load (Tomazevic, 1999)

**A. Horizontal sliding shear failure and bed joint sliding**

Sliding shear failure occurs when the vertical load is low or the mortar is of poor quality. Seismic forces split walls in two, with the upper section of the wall sliding over one of the horizontal mortar joints. Bed joint slippage is a defining feature of this condition. These walls usually have an aspect ratio of 1:1 or less. FEMA 273 gives the equation for shear capacity as:

$$V_{bjs} = v_{me}\, A_n = A_n\,[0.75(0.75v_{te}+P_{CE}/A_n)]/1.5 \qquad \text{Eq. 2.1}$$

**B. Shear failure / Diagonal shear failure**

The most likely failure mechanism on masonry walls is diagonal shear failure which occurs when principal tensile stress generated in the masonry wall as a result of a combination of horizontal and vertical stresses exceeds the tensile strength of the masonry materials. The wall develops a distinctive diagonal crack that follows the crack pattern through mortar joints, masonry units, or both. A single diagonal crack can produce a significant loss of strength and thus resulting brittle collapsing.

Diagonal Shear Strength,

$$Q_{CL} = V_{dt} = A_n f'_{dt} \frac{L}{h_{eff}} \sqrt{\frac{f_a}{f_{dt}} + 1} \qquad \text{Eq. 2.2}$$

**C. Flexural Cracking and Toe Crushing**

Either diagonal shear or bending failure occurs in masonry walls, if the vertical and axial compression loads are within normal limits. But, crushing of compressed zones at the ends of walls occurs when shear resistance and moment/shear ratio are high, indicating the flexural mechanism of failure. The toe-crushing failure on the lower side of the wall and/or an opening on the opposite side describe this failure. This type of behavior typically occurs in broad and sturdily built walls with $L/ h_{eff} > 1.25$ (FEMA306).

Rocking Strength,

$$Q_{CE} = V_r = 0.9\alpha P_E \frac{L}{h_{eff}} \qquad \text{Eq. 2.3}$$

Toe crushing strength

$$Q_{CL} = V_{tc} = \alpha P_L \frac{L}{h_{eff}} \left(1 - \frac{f_a}{0.7 f'_m}\right) \qquad \text{Eq. 2.4}$$

According to FEMA 273, Cl. 7.4.2.2, if their expected lateral strength which is constrained by the bed-joint sliding shear stress or rocking (the minimum of values from Equations 2.1 and 2.3) is less than the lower bound lateral strength which is limited by diagonal tension or toe compressive stress (the minimum of values from Equations

2.2 or 2.4). These components will be regarded force-controlled if they are not otherwise.

### 2.4.2 Out of Plane Failure and Foundation Rocking

This failure mechanism is characterized by foundation rocking about its base. Flexural rocking failure can occur at wider aspect ratios, greater than 2:1, and that to low vertical stresses rather than significant shear resistance. Out-of-plane mechanisms are generally disregarded in buildings' resistance assessment.

## 2.5 Analytical Modelling Techniques of Masonry

Masonry is characterized as discontinuous structural element whose bulky nature governs its deformations and failure mechanisms. As a result, isotopic elastic continuum-based models are ineffective for simulating the non-linear behavior of masonry walls under loads (Asteris, 2015).

The most difficult subject in engineering study and practice has always been structural modeling of masonry buildings. This complication is due to a large number of contributing factors, including brick dimension and anisotropy, joint width and arrangement of joints, brick and mortar material qualities, and craftsmanship quality. The modeling technique chosen is mostly determined by the application sector and the level of accuracy desired (Shrestha, 2011). Asteris et al. (2015) outlines the different analytical approaches used by different researchers as given in figure 2.3.

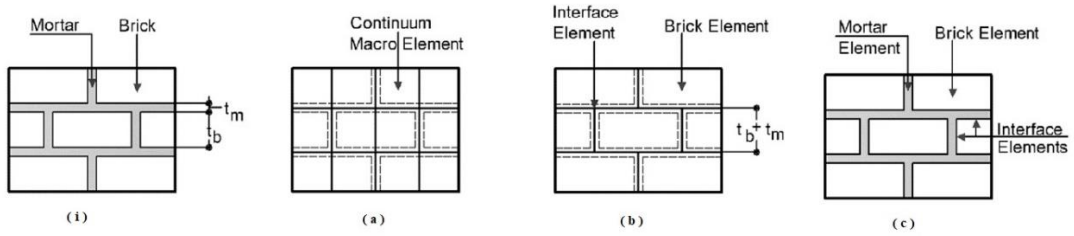


Figure 2.3 Masonry Modelling Strategies : (i) Masonry Sample, (a) One-Phase Macro Modelling, (b) Two-phase Micro Modelling, (c) Three-phase Micro Modelling (Asteris et.al., 2015)

a. Macro-Modelling : (Modelling masonry as one-phase material)

   A masonry element is described through the continuum homogenized model, commonly using the FEM approach, with the effects of mortar joints taken into account implicitly. The separate units and mortar joints are not distinguished.

It's suited to large-scale masonry structures, but it can't handle extensive stress analysis of smallest wall panels because of the difficulties in recording all of the probable failure mechanisms.

b. Simplified Micro – Modelling : (Modelling masonry as two-phase material)
   The brick elements are represented as fictional extended bricks using continuum components with the same dimensions as that of original bricks and the actual joint thickness in this technique. The mortar joint is also modeled as a zero-thickness interface. The interface stiffness is calculated using the stiffness of the real joints. The attributes of the mortar and the masonry unit interface are combined to a single element in this technique, and enlarged elements are employed for representing the brick units. This method reduces the computational complexity and generates a model that can be applied to a larger range of structures.
c. Detailed Micro – Modelling: (Modelling masonry as the three-phase material)
   The masonry unit and mortar interface is represented by dis-continuum elements in this technique, whereas the units and mortar in the joints are represented by continuum elements. While this modeling generates more accurate results, the level of refinement necessitates a computationally demanding evaluation, restricting its application to small scale laboratory specimens and structural details. Mechanical parameters such as Elastic modulus, poisson's ratio, and the inelastic properties for both brick units and mortar joints are considered because they are both represented through continuum elements.

As shown in Figure 2.4, these basic analytical modeling processes are further discretized into multiple numerical modeling approaches, with varying degrees of accuracy for the analysis of masonry structures.

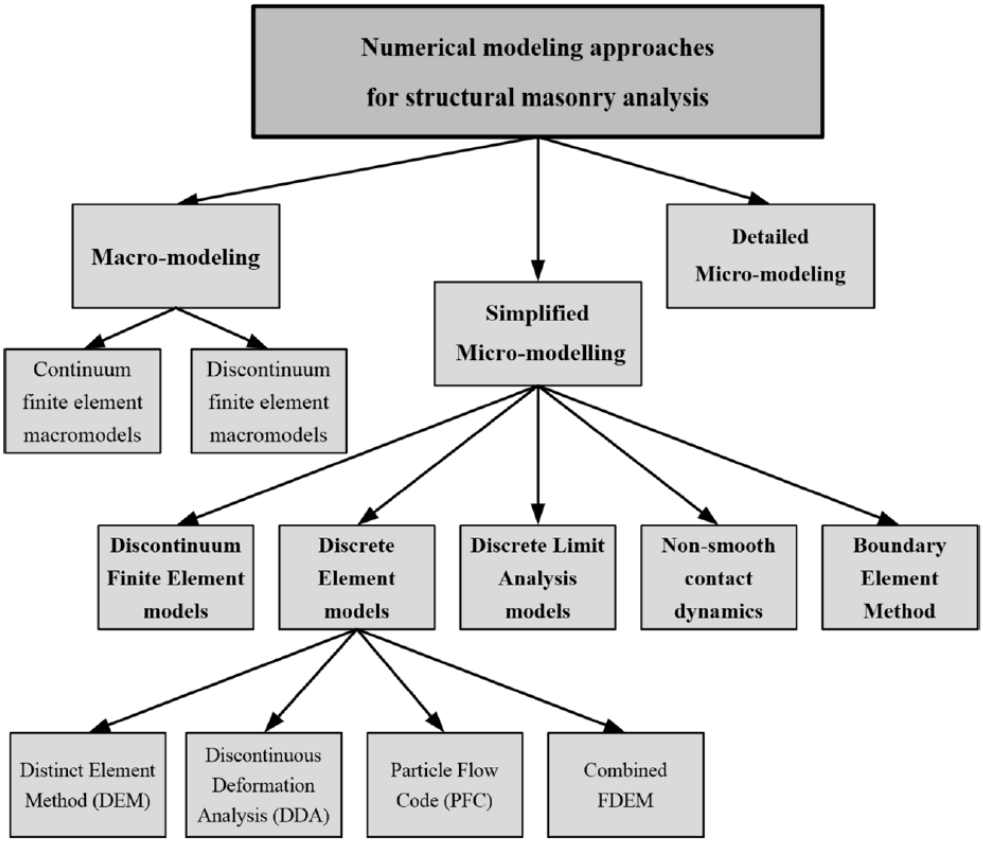


Figure 2.4 Different Numerical Approaches for Structural Masonry Analysis (Asteris, 2015)

## 2.6 Macro – Modelling

### A. Macro-Modelling Continuum Approach:

The masonry wall is treated as a homogeneous material in this method, with no differentiation made between individual masonry units and mortar in the joints.

### B. Macro-Modelling Dis-continuum Approach:

Using the technique of macro-element discretization, the in-plane nonlinear response of masonry walls is simulated by an equivalent discrete component. The corresponding macro-element is represented by an articulated quadrilateral / solid material with surrounding rigid edges, and failure mechanisms such as sliding shear, shear, and flexure behavior of masonry are represented by discrete distributions of springs / link components. The units are supposed to act elastically in this case, whereas the total nonlinear behavior is concentrated in the interface parts. This method is especially suitable for the analysis of smaller

masonry structures subjected to heterogeneous states of stress and strain due to the higher computational effort required.

### 2.7 Link Elements

A link is a two-joint connecting element. It can exhibit six degrees of freedom through which it can be deformed (axial, shear, torsion and bending). According to the types of attributes provided and analysis being performed, each Link or Support element can exhibit up to three different forms of behavior: linear, nonlinear, and frequency-dependent. The nonlinear force-deformation relationships are employed in nonlinear analysis at all degrees of freedom for which nonlinear features are given. CSI (2011) provides a full discussion of the link element's advanced features. The lateral load-displacement relations, failure mechanism, and crack patterns may all be anticipated quite well using the finite element technique (FEM), which models masonry units and mortar joints as discrete or continuous elements with links between them (Tomazevic 1999).

The Non-Linear (NL) link element is a unique kind of link element that permits user-defined force and deformation relations to be used to describe material nonlinearity. Nonlinear linkages are used to replace the area components that represent the interface of wall segments where yielding is expected to occur. Outside of the predicted yielding zones, linear elastic area elements with full gross section properties are used to represent the area elements.

Force-deformation relationships attributed to nonlinear links, to describe both axial and shear behavior, are defined as Multilinear Plastic link elements. The longitudinal orientation of link elements determines axial deformation, while the in-plane transverse direction determines shear behavior. The tributary area of wall elements represented by each of these nonlinear links influences the force vs deformation values. The flexural behavior of wall is directly controlled by the axial response parameters of the nonlinear links (Lepage and Sanchez, 2012).

In case of reinforced masonry walls, for simulating the axial response in compression by the nonlinear links, both the contributions from masonry and reinforcement elements is taken into account. However, the contribution of masonry is almost neglected in the tension. The tension quadrant in URM walls is thus defined by a horizontal straight line segment with an effectively zero force. In compression, the initial stiffness is

determined by the rigidity of the masonry and the length of the nonlinear link. Analogously, the initial stiffness in tension of reinforced masonry is determined by the rigidity of the steel reinforcement and the length of the nonlinear link. After attributing 0.9 f'm to the masonry in compression and fy to the reinforcing steel in tension and compression, peak forces are calculated. In tension and compression, the post-yield stiffness is set to zero. It is illustrated in figure 2.5.

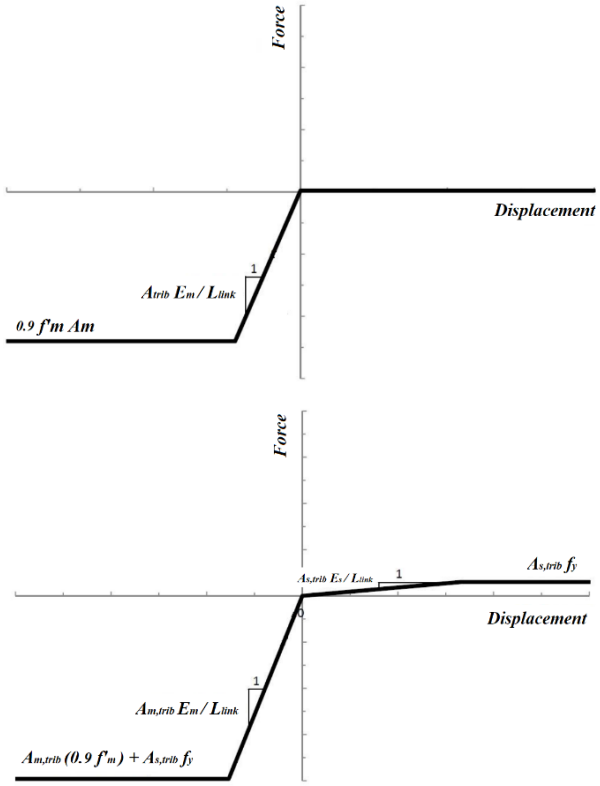


Figure 2.5 (a) Non - Linear Link Definition for URM Wall, Axial Direction (b) Non - Linear Link Definition for Reinforced Masonry Wall, Axial Direction

Similarly, the force-deformation (F-d) relationship provided to the nonlinear links is specified as bilinear and symmetrical to model the response under shear (Figure 2.6). The first linear line represents the stiffness of the wall segment based on gross section parameters, whereas the second line represents the nominal shear strength of the wall segment and is horizontal (constant force). The shear response links are defined in such a way that the shear carried by the link generates a secondary moment only at one end. A flexurally rigid line element is introduced to fully engage the wall cross sectional characteristics in order to adequately account for the effects of this moment. To deal with the secondary moment, special emphasis is given to the orientation of the link local axes.

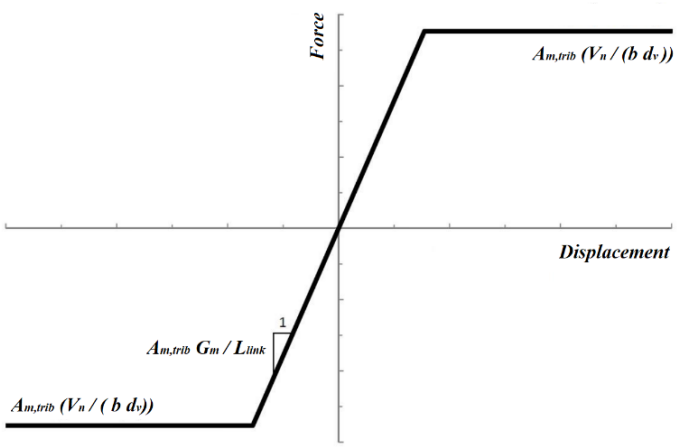


Figure 2.6 Non - Linear Link Definition, Shear Direction

After assigning nonlinear link elements, to establish the initial locations on the force-deformation curves of each nonlinear link, a nonlinear gravity load is defined. Then nonlinear static analysis is performed for the lateral loads.

### 2.8 Structural Analysis Procedures

Four analysis methodologies for seismic analysis of existing buildings are described in FEMA 273 and FEMA 356:

1. Linear Analysis:
    a. Linear static analysis is the simplest way of analysis. According to FEMA 356, linear static procedures are applicable to the buildings which do not have irregularities in mass and stiffness. The requirement states that the ratio of demand calculated by linear procedure to the strength (capacity) of component is less than two.
    b. Linear Dynamic analysis consider dynamic characteristics of the building to determine its overall behavior. It takes the peak model responses determined from the model's dynamic analysis.
2. Nonlinear Analysis:
    a. Nonlinear static analysis (Refer section 2.9)
    b. Nonlinear dynamic analysis calculates the response of structure through dynamic analysis using ground motion time histories. Basic modelling approaches and acceptance criteria are similar to non-linear static analysis.

## 2.9 Non-Linear Static Analysis / Pushover Analysis

Nonlinear static techniques calculate the structure's greatest global displacement due to shaking at its base (FEMA 306). The NSP is best for buildings that don't have a considerable significance of higher-mode response (FEMA 273). Capacity, demand, and performance are the three key elements that must be determined in a pushover analysis.

The building model integrating non-linear load-deformation features is subjected to monotonically increasing lateral loads, simulating inertial forces in an earthquake, up to the predefined value or state in nonlinear static analysis. According to Displacement Coefficient Method (DCM), proposed by FEMA 356, calculates this value as target displacement. The target displacement is supposed to give the largest displacement that might occur during design earthquake. ATC 40 defines Capacity Spectrum method (CSM) where at each stage, the load is increased and checked until the "Performance Point" condition is attained. In accordance to the distribution of inertia forces in the plane of each floor diaphragm, lateral loads are applied to the mathematical model. The control node is taken at the roof center, i.e. at centre of mass. For control node displacements ranging from zero to 150 percent of the target displacement, $\delta t$, a relationship between base shear and lateral roof displacement of the control node must be created (FEMA 356).

Structures redesign themselves during earthquakes (Khan, 2013). The pushover analysis replicates the phenomena in which particular structural components yield or fail, causing the building's dynamic forces to be redistributed to other components. The loads are applied until the weak link in the structure is discovered, after which the model is updated to account for the structural changes induced by the weak link. The redistribution of these loads is shown in a second iteration. After that, the structure is pushed again until the second weakest link is found. This approach is repeated until a yield pattern for the entire structure is found under seismic loading. Pushover analysis is commonly used to assess the seismic strength of existing structures, and it is mentioned in various present seismic retrofit design standards. It can also help with performance-based design of new buildings that rely on ductility or redundancy to withstand seismic effects. Penelis (2006) proposed a method for performing pushover analysis on unreinforced masonry structures that is both efficient and effective.

## 2.10 Capacity Spectrum Method (CSM)

The CSM is a performance based seismic analysis method that can be implemented as a nonlinear time history analysis alternative, which was first used in the HAZUS (Figure 2.7) earthquake loss estimating approach (Borzi, 2008). The intersection of an acceleration and displacement spectrum (demand curve) representing ground motion and a capacity curve representing the horizontal displacement of the structure under increasing lateral load gives the performance point of a building type under a specific ground-shaking scenario (or PESH). Capacity curve is the pushover curve converted to plots of spectral acceleration ($S_A$) versus spectral displacement ($S_D$). For this, capacity curve and response spectra must both be transformed into a spectral acceleration - displacement graph. The global structure is reduced to a single degree of freedom structure as a result of this transformation. The performance point, which specifies the spectral displacement of the building due to the given earthquake, is estimated using a trial and error technique.

The Capacity Spectrum Method is widely used for a variety of applications, including rapid evaluation of a large inventory of buildings, design verification for new building construction, evaluation of an existing structure to identify damage states, and correlation of building damage states to various ground motion amplitudes. From the 1970s until the present, Sigmund A. Freeman (2004) summarizes the evolution of the CSM and includes discussion, modification and recommendation by various researchers in his paper.

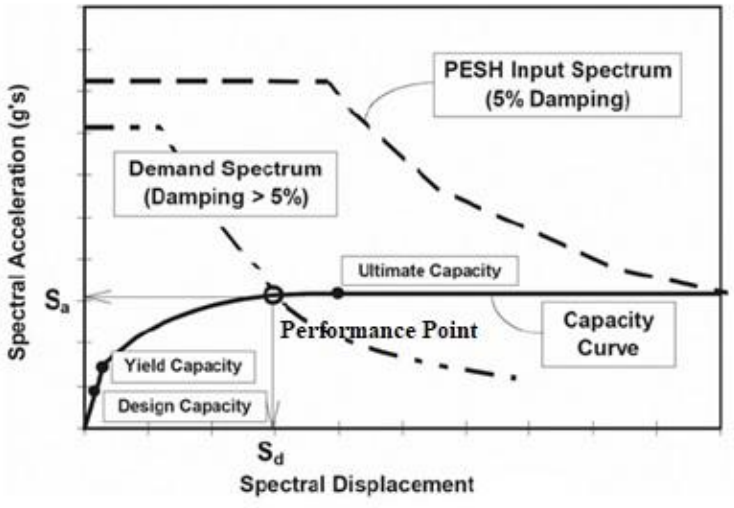


Figure 2.7 Capacity Spectrum Method as applied in HAZUS

## 2.11 Fragility Analysis

Seismic vulnerability is a measure of how vulnerable a structure is to damage when the ground shakes severely. The two most largely utilized formulations to describe the vulnerability are damage probability matrices and vulnerability/ fragility curves (Borzi, 2008). The probabilistic chance of reaching a predetermined limit state in correspondence with a certain value of the chosen seismic intensity parameter is the seismic fragility of a structure (Pasticier, 2008). In discrete terminology, the same probability is a component of a damage probability matrix.

A lognormal probability distribution governs fragility curves, which is determined by two key parameters: the mean spectral displacement $\bar{S}_{d,ds}$ the standard deviation $\beta_{ds}$ . For a given damage condition $d_s$, the fragility curve is given by:

$$P[d_s/S_d] = \Phi[\frac{1}{\beta_{ds}} \ln(\frac{S_d}{\bar{S}_{d,ds}}) ] \qquad \text{Eq. 2.5}$$

Seismic fragility curves are expressed in multiple formats for use in wide variety of loss-assessment applications (Remki, 2017). Fragility curves can be derived by analytical, heuristic, empirical and hybrid approaches (Gautam, 2018). When there is a lack of data in the field, fragility curves can also be developed analytically through simulation. Fragility curves divide damage into four physical damage stages, as shown in figure 2.8, for a given level of structure response: slight, moderate, extensive, and complete (HAZUS-MH 2.1). Based on these damage states, FEMA 273 assigns four building performance levels: operational, immediate occupancy (IO), life safety (LS), and collapse prevention (CP).

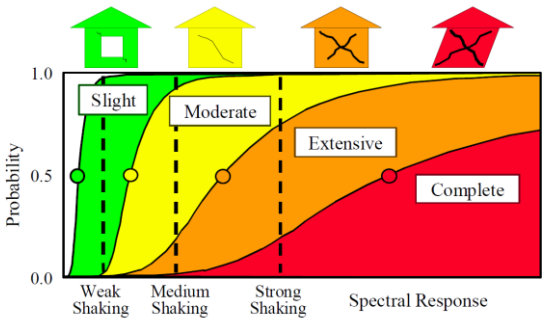


Figure 2.8 Example of Fragility Curves for Slight, Moderate, Extensive and Complete Damage, (HAZUS-MH2.1)

## 2.12 Retrofitting Strategies for Masonry Buildings

Retrofit is the quantified implementation of seismic strengthening measures to reduce seismic deficiencies. There are various alternatives for retrofitting of load bearing masonry buildings, but a method which makes use of locally available resources can be implemented well and can be scaled up in later phase. According to the Gorkha Earthquake 2015 data from the National Reconstruction Authority (NRA), about 299,588 houses were destroyed and 269,107 were partially damaged. And the enlisted beneficiaries who have partially damaged houses were suitable for receiving retrofitting grant of one lakh. These beneficiaries, however, due to lack of adequate knowledge and skill in retrofitting have not been able to retrofit their houses (NSET, 2019). Few of the NGOs provide 51 days mason training on the job (OJT) for masons. And for the engineers, Ministry of Urban Development (2016) has published the manual on "seismic retrofitting guidelines of buildings in Nepal". Similarly, NRA (2017) also has published the "repair and retrofitting manual for masonry structures" under the housing reconstruction programme, and "ready to use manual for repair and retrofitting of masonry structures" in March 2021.

**Concepts of Repair, Restoration and Retrofit**

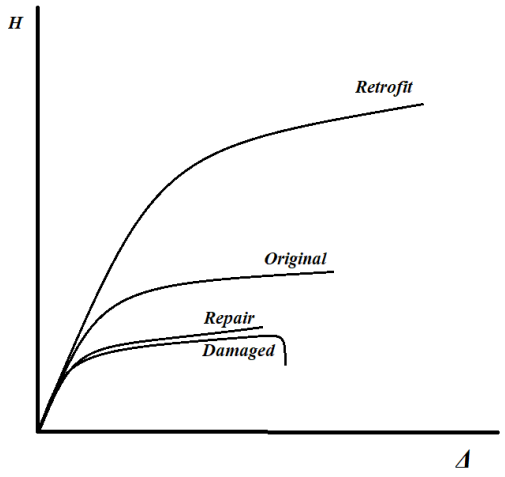


Figure 2.9 Concepts of Repair, Restoration and Retrofit

Repair: is carried out in order to restore all of its prior functions as well as its architectural shape. The structural strength of a damaged building is not considerably improved through repair.

Restoration: is performed when it is expected that the damaging phenomenon will not occur again, and the original strength provides an appropriate level of safety.

Retrofit: is done when the strength available before the damage was insufficient and restoration alone will not be adequate in the future earthquakes.

A good retrofit scheme is the combination of three distinctive features of a structure:

a. Improvement of regularity: improvement of geometry, stiffness, resistance and mass distribution in plan and elevation such that regularity in the overall structure is created. It includes breakdown of complex configurations like C-type, T-type, U- Type into simple configurations, addition of rigid slabs to increase stiffness and resistance, and addition or relocation of walls for correcting load paths and uniformity of mass distribution.
b. Increasing Strength: through introduction of new building elements, use of seismic isolation or energy dissipation devices, or reducing the height or seismic weight of the structure. Strength of the existing structural elements increases the resistance and stiffness of the structure, however, deformation capacity is practically unchanged.
c. Increasing Ductility: by reinforced strips or reinforcement jacketing of the entire brittle masonry wall. The entire deformation capacity is increased while the ultimate resistance and stiffness is only slightly increased.

**Considerations:**

The available intervention strategies should be chosen depending on the building's typology and predicted performance after retrofitting. Direct / indirect cost implication, compatibility of the solution with functional requirements, availability of construction techniques (materials, workmanship and equipments), aesthetic view of building, environmental aspects, etc. need to be considered while selecting the best retrofit strategy.

**Basic approaches of retrofit for masonry buildings:**

a. Jacketing: of steel meshes or GI wires are adopted on low strength masonry buildings especially heavier in weight, weakest in strength, and having brittleness. It improves shear strength, ductility, building integrity and deformability.

b. Splint and Bandage: as the economic version of jacketing where Reinforcing bars are only provided at the most essential points where stress concentrations can be developed. Splints are vertical elements installed at opening jambs, corners, and wall intersections. The goal is to maintain integrity in the vertical direction. The bandages, on the other hand, are horizontal elements that run around all of the walls, sills, lintels, and eaves levels to connect the various walls together, avoiding out-of-plane collapse and the initiation and widening of cracks from their corners.
c. Bolting/ Pre-stressing: improves shear strength of in-plane walls and connections between orthogonal walls, but is far inferior in terms of improving safety to jacketing or split and bandage.
d. Base Isolation: by inserting a flexible layer between the structure and the ground, the superstructure is supposedly strengthened and isolated from ground motion. It is used for historic structures and important facilities, and it is highly costly when compared to other procedures.
e. Use of FRP (Fiber Reinforced Polymer: is a new technology that involves applying thin films of glass or carbon FRP to the exterior surface of masonry walls to improve their flexural and shear capacity. Although the materials used in FRP are more expensive than traditional strengthening materials like steel and concrete; the labor, equipment, and building expenses are frequently lower.

## 2.13 Researches in the context of Nepal

Some of the works done by researchers in this field, in the context of Nepal are described briefly in the following:

Hari Ram Parajuli (2012) performed various testing methods to determine the mechanical properties of brick masonry buildings used in old heritages around Patan Durbar Square. A two storey building was selected. Elastic wave tomography at existing walls was performed to determine properties of brick and wall elements like density, Poisson's ratio, elastic modulus, shear modulus, shear wave velocity, etc. Sample brick wallets were prepared and destructive tests in compression, shear, combined horizontal and vertical loading were performed in the lab as it was not possible to extract core samples from existing building. To assess the dynamic features of the building, such as fundamental periods, modes, and damping, ground micro

tremor measurements and ambient vibration tests were used. The data suggested in this paper are also taken in our present thesis work.

Prem Nath Maskey (Rits-DMUCH, 2012) has described the present condition of traditional and old masonry buildings in Jhatpol, Patan, where a considerable number of them have been intervened with RCC slabs and extension of stories, which has exacerbated the seismic vulnerability with significantly greater height and smaller plan dimensions. They discovered that the majority of the structures are three or four stories tall, with floor heights ranging from 1.8 to 2.4 meters, and rectangular plans with a depth of around 6 meters and lengths ranging from 3 to 10 meters, with a length to breadth ratio of not more than 2. Because the building's center of mass and center of stiffness coincide, these simple and symmetric plan configurations have made it more stable and caused no excessive torsion. The average wall thickness on the bottom floor is 45 cm or more, with the thickness decreasing as the floor levels rise. A shallow base is built of stones or bricks, with a superstructure made of locally available burnt clay bricks and mud-mortar. Three walls, two outside walls, and one spine wall in the center were discovered to support the entire construction, which was sometimes replaced with a timber frame system to produce a bigger continuous room. Floor to be timber framed with 50 x 100 mm timber joists closely spaced at 200 to 300 mm spacing and a layer of terra cotta tiles or wooden planks. Wooden pegs are used to link all of the wooden parts together properly. The *Dalan* is located on the ground level, with columns that range in size from 100 x 100 mm to 150 x 150 mm in cross section, and are spaced 100 to 150 cm apart. At the corners, there are vertical posts that act as vertical tensile reinforcement. They also show that further stories with wider openings are added to these buildings, and traditional roofs are replaced with corrugated galvanized iron sheets. The addition of balconies with a concrete slab projecting from the masonry wall without sufficient support has made the buildings even more vulnerable. These adjustments have had a significant impact on the initially anticipated lateral load resisting characteristics in terms of stiffness and strength, with some structures being unable to withstand gravity loads.

Aiko Furukawa et.al. (2017) compared dynamic features before (in 2009) and after (in 2016) the Gorkha Earthquake (2015) to assess the damage to historic masonry buildings in Nepal. A two storey masonry building in Patan Durbar Square, 300 years old, was taken into consideration and finite element models corresponding to pre and post-

earthquake were prepared. The ground motion parameters in Gorkha earthquake were taken as inputs and structural response was observed. The vibrational features, such as natural frequencies and damping ratios, were compared, and structural damage was identified. The natural frequencies of the lowest 8 modes were found to have reduced by 3.46 to 11.86 percent, indicating structural deterioration. On the ground and first floors, several cracks were discovered, indicating a loss of rigidity. Stiffness was found to be reduced by factors ranging from 8 to 13.8 percent.

Shrestha et.al. (2017) performed a case study on damage of Jagannath Temple located in Durbar Square of Kathmandu. Ambient vibration and in-situ tests on masonry walls were conducted using the pendulum hammer, rebound hammer, and in-place push. In SAP 2000, a 3D numerical modelling of the temple was created, and the linear static analysis was performed. The principal causes of the damage were discussed based on the observational cracks and the conclusions gained from numerical model analysis output. Furthermore, generalization of damage patterns were found to be difficult, because of highly diversified aspects in old heritage structures with similar architecture. Wooden bands in horizontal and vertical directions were tested for use in the temple's restoration and to improve the resistance of walls to shear and out-of-plane deformation. According to their findings, wooden bands would be efficient in relieving stress in masonry walls.

Dais et.al. (2019) investigated restoration and seismic enhancement solutions for the three tired Jaisedewal Temple after the Gorkha Earthquake. A 3D macro modelling approach was developed in FEM software ABAQUS and static nonlinear and time-history analyses were performed. They discovered that World Heritage brick masonry multi-tiered Nepalese Pagodas had sustained considerable damage, with several of these temples collapsing. And, Though many research has been done to determine the seismic vulnerabilities of historic temples, less has been done to determine the efficacy of low-cost seismic retrofit and repair methods. They suggest that in order to obtain a realistic simulation of seismic activity, the presence of flexible connections along the structure should be taken into account during modeling. It was found that the pushover analysis failed to capture the failure mechanism of the top part of the Nepalese temple under investigation. Therefore, time-history analysis was performed to accurately reproduce the response of the structure during a seismic excitation. Finally, the seismic retrofit of the structure was highlighted, and its impact on the structure's seismic

behavior was investigated. Their suggested interventions reduced the time period about 30% and box type behavior of the structure was obtained limiting the effects of local failure modes. The major core drift and out of plane deformations at the periphery wall were decreased when the structure was retrofitted. The wooden pillars' participation in carrying horizontal loads was enhanced, resulting in additional stresses being transmitted to the foundation.

Meera Chikanbanjar (2019) performed the non-linear static analysis of unreinforced masonry building using two different modelling approaches: equivalent frame model in SAP 2000 and macro element approach in 3Muri software. Three masonry building made up of brick in cement mortar masonry of same plan configuration but different number of storey were taken into consideration and each of these buildings were analyzed considering flexible floor (wooden floor with mud covering) and rigid floor (concrete slab) separately. It was observed that URM with rigid floor has high capacity, as it creates box effect such that all the walls behave as one, in comparison to flexible floor where walls tend to act individually. Appropriate modeling strategy should be chosen based on the deep knowledge of structure and modeling strategy and analysis requirement. In the analysis, it was found that equivalent frame method in SAP2000 can well represent the non-linear behavior of masonry buildings. It is easy and fast method and it is efficient and suitable for practitioners.

In Nepal, Jaishi et.al. (2003) published a paper on the dynamic and seismic performance of historic multi-tiered temples. To assess the time period of Nepalese temples, an empirical formula is proposed. 10 typical multi-tiered temples were selected and dynamic properties were obtained by using FEM. To validate these models, three of these models were tested through ambient vibration method and fundamental time period measured was found to be less than 0.6 s for these masonry temples in Nepal. And the damping ratio was between 1 to 6%. The important sections of Nepalese temples were discovered to be the piers that run between the openings located at the base level, with tensile and compressive loads accounting for the majority of failure patterns.

Paudel et.al. (2021) performed a case study on renovation and strengthening of a masonry institutional building of Pulchowk Campus. It was constructed in 1970 and was largely damaged from the Gorkha earthquake in 2015. It was developed and

implemented a procedure for strengthening damaged classrooms that was efficient, low-cost, and efficient. In SAP 2000, a macro-modeling method was used, with the structure set at the plinth level and the area element as a non-linear shell element. RC jacketing modeled using layered links was found to be efficient method of retrofitting the masonry structures after four possible retrofit options were identified, modelled and analyzed. The new option developed in this paper is the RC columns combined with brick piers via shear-keys, which are modeled through independent hook elements available in FEM software SAP2000. Pushover analyses were performed to compare the increment of performance level of masonry building with various retrofitting options. Retrofitting the ground level alone with RC columns and brick piers was chosen for the final implementation.

For URM school buildings in Nepal, Giordano et.al. (2019) derived the fragility curves using a Monte Carlo simulation. They pointed out the high level of vulnerability of school buildings in Nepal and more than 20% of classrooms were damaged or collapsed during earthquake. The majority of Nepal's overall building typologies are URM, which are marked by several construction flaws like: insufficient wall-to-wall or wall-to-floor connections, which have resulted in numerous out-of-plane collapses. Thus, in their paper, a spectral-based technique for deriving fragility curves for Nepalese URM school buildings exposed to out-of-plane damage is explored, and a technique is applied to the case of typical brick mud-mortar (BMM) URM Nepalese structures, considering construction techniques, material properties, and failure mechanisms that are identified after the buildings are subjected to out-of-plane damage. The key assumptions were that failure modes are out of plane, walls behave independently, and the building's vulnerability is determined by the wall with the worst seismic performance, which was computed using well-consolidated spectral-based approaches. Their findings demonstrate that the 50th percentiles of analytical fragilities are in good agreement with those from observational fragilities of Nepalese URMs in the literature.

Motra et.al. (2020) performed the structural condition assessment and retrofitting of Shital Niwas building, a 96 years old Rana-era building mixed with Malla architecture, European Palladian / neoclassical style and a central courtyard system, which was significantly damaged during Gorkha Earthquake. Seismic weaknesses were analyzed, including mud mortar masonry's low strength, the heavy weight of the walls and floors, the presence of long unsupported walls under flexible diaphragms, a high ratio of

openings, and the lack of earthquake-resistant elements. A 3D FEM modeling was prepared using ETABS assuming homogenized wall material. Structural masonry walls which are hinged at the plinth level are modeled as thick shell elements. The floor girders, joists, and bottom chords of the roof truss were modelled using two node frame elements. Girders or rafters are used to model floors and roofs. A macro-element approach is used to carry out pushover analysis. Steel plates and carbon fiber reinforced polymer (CFRP) bands were chosen as a retrofitting approach after comprehensive analysis and design.

Tiwari et.al. (2020) performed the multiple analytical approaches on seismic retrofit design of URM buildings in Nepal. A two storey URM building made up of Brick in Cement Mortar was taken into consideration. Static analysis was performed in SAP2000 in which wall and slab elements are modelled as shell elements and nonlinear pushover analysis was performed on TRIMURI. Initial assessment was done based on visual observations, non-destructive and in situ testing. Addition of internal walls was found to be effective for improving the seismic performance of the building. RCC splint and bandage were provided in the inner and outer walls to enhance the tensile capacity of building. It was observed that the time period decreases, base shear increases, ductility increases and displacement demand capacity decreases after retrofitting. The linear retrofitting design from SAP2000 gave more conservative results than nonlinear based design from TRIMURI.

Gautam et.al. (2018) proposed a new damage data for deriving fragility functions for RC buildings, and masonry buildings made up of bricks and stones. For the residential buildings, using over a million damage data points, this research builds empirical fragility functions, i.e. from the 1934 Bihar-Nepal earthquake (M8.4), 1980 Chainpur earthquake (M6.5), 1988 Eastern Nepal earthquake (M6.8), 2011 Eastern Nepal earthquake (M 6.9), and 2015 Gorkha earthquake (M 7.8). It suggests that because to differences in building materials and technology, fragility functions designed for any one type of structure/component, region, or context cannot be used to represent other scenario. As a result, these fragility functions can only be used in a given location. The fragility functions presented from the study reveal significant information about the lesser damage of inferior reinforced concrete buildings in Nepal, as well as the likelihood of substantial damage in the case of masonry buildings made up of stones and brick. The findings suggest that the majority of Nepal's rural residential stone and

brick masonry constructions are highly vulnerable to severe earthquakes, with a high risk of extensive damage and collapse.

# CHAPTER 3: METHODOLOGY

## 3.1 Introduction

This chapter includes the methods implemented for modelling and analysis of the masonry buildings. The general methodology adopted for the current study is illustrated in Figure 1.1. The present thesis work primary focuses on unreinforced masonry walls situated in urban settlements. The building typology selected represents features of non-engineered masonry buildings with Clay-Brick masonry bonded with Mud Mortar (BMM). Selected building typologies have larger openings in the base levels, which are used by local shop vendors. Few of these buildings are modified with CGI roofs and RCC slabs by the house owners. Thus buildings taken into consideration also represent flexible or rigid floor diaphragms, and some of them both. First of all, a detail visual assessment was done and a detail survey based on the contextual assessment framework was also performed. Then 5 residential buildings which represent these typology were selected with different plans, varying elevations and number of stories, for the present thesis work.

There are various modelling techniques for masonry structures depending upon the level of accuracy and computational cost. Because of its simplicity and wide ranges of its application, Macro – Modelling FEM technique is implemented in this present study. The masonry buildings are modelled in finite element software SAP 2000 v23.1.0. It allows the users to define link elements to impart non-linearity in the building models. Links are provided along in-plane direction and static non-linear analysis is performed along this direction. The nonlinear static analysis outputs of the model is then further assessed to obtain fragility curves under different earthquake scenarios. From the analysis, seismic vulnerability of these buildings is studied.

## 3.2 Case Study Models

The building prototypes selected in the present thesis represent the typical urban URM buildings made up of masonry walls of clay brick in mud mortar, especially with larger openings in front face and in ground floor. These buildings were modified by the house owners on the later phase with addition of extra stories and replacement of wooden floor and roof with RCC slabs. The important parameters required for analyzing the vulnerability of the building are measured and recorded from the visual assessment and

survey questionnaire. Photographs are also used as cross reference for preparing the architectural drawings and to access damages incurred in the latest earthquake.

Figure 3.1 URM houses in urban areas with openings in Front Elevation

### 3.2.1 Visual Assessment and Survey Questionnaires

A comprehensive examination of the seismic risk in existing structures is required in order to identify the most critical places and prioritize retrofit operations (Pasticier, 2007). First of all, reconnaissance survey of different aspects of the buildings was visually examined. Accessible parts of the building were measured and recorded. Further details of the building were assessed through questionnaire with the house owner. Existing damages from recent earthquakes and seismically vulnerable structural elements were carefully observed.

### 3.2.2 General Building Descriptions

These collected data were then referred to prepare the building plans, elevations, sections; and a complete drawing was developed in Auto-CAD software which provided the basis for finite element modelling. Buildings A, B, and D are four storied buildings, C three storied and E two storied. Building D is slender in comparison to other buildings. Building A is square in plan. Similarly, Building E has wider aspect ratio. All these buildings have larger openings in their ground floor levels. Some of their floor levels are modified with RC Slabs. Detail description of these buildings taken under the considerations for present thesis work is presented in APPENDIX A.

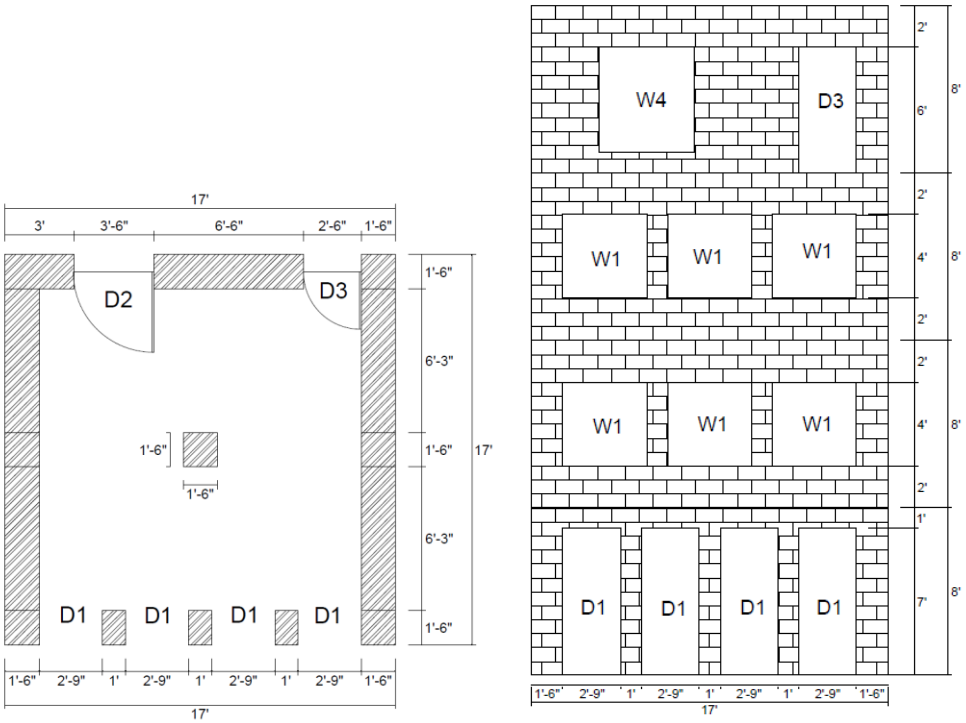


Figure 3.2 (a) Ground Floor Plan (b) Front Elevation (Building- A)

The different aspects taken into consideration during modelling are discussed below:

### 3.2.3 Design Loads

DEAD LOADS :

| | |
|---|---|
| Self-Weight : | |
| Masonry Walls (BMM): | 17.68 kN/ $m^3$ |
| RCC Slab/Beams: | 25 KN/$m^3$ |
| Timber: | 8 KN/ $m^3$ |
| Floor Finish: | 1 KN/$m^2$ |

LIVE LOADS:

| | |
|---|---|
| On Floor : | 2 KN/$m^2$ |
| On accessible RCC Roof : | 2 KN/$m^2$ |
| On inaccessible flexible Roof : | 0 kN/$m^2$ |

### 3.2.4 Material Properties

Because of lack of material testing data and equipment, the mechanical material properties of brick masonry and timber structures are taken into consideration from relevant literatures. Although a lot of researches are made for Brick bonded with Cement Mortar, material testing on Brick in Mud Mortar masonry walls for residential buildings is very rare. Few of the researches in the context of Nepal are done for monumental buildings and the input variables are also defined based on these probabilistic distributions, especially in: elastic modulus of masonry ($E_m$), its compressive strength ($f_m$), and weight ($\gamma_m$). *Hari Ram Parajuli in 2012 performed the tests on masonry prisms in Pulchowk campus lab for the old residential building from Patan, whose values are taken as reference in our present study; as it nearly resembles low strength URM residential buildings under considerations in the same/similar urban areas.

| | *Hari Ram Parajuli (2012) | Chhabi Mishra (2019) | Giordano et.al. (2019) (Reference from Parajuli) | Motra et.al. (2021) (Special Case: Presidential Palace) |
|---|---|---|---|---|
| **Masonry : (BMM)** | | | | |
| Modulus of Elasticity E ($N/mm^2$) | 509 | 310 *(Cov. = 0.13)* | 537.25 *(Cov.=0.469)* | 542 *(Cov.= 0.22)* |
| Modulus of Rigidity G ($N/mm^2$) | 204 | | | |
| Poisson's Ratio (ν) | 0.25 | | | |
| Density $\gamma_m$ ($kN/m^3$) | 17.68 | | 17.68 *(Cov.=0.05)* | |
| Compressive Strength of masonry $f_k$ ($N/mm^2$) | 1.82 | 1.7 *(Cov.= 0.047)* | | 0.96 *(Cov = 0.22)* |
| ***Brick :*** *Compressive strength $f_b$* ($N/mm^2$) | *11.03* | *5.05 (Cov.=0.505)* | *11.03 (Cov.=0.51)* | |
| ***Mortar :*** *Compressive strength $f_m$ ($N/mm^2$)* | *1.58* | *1.40 (Cov.= 0.164)* | | |
| Shear Strength of masonry ($N/mm^2$) | 0.15 | 0.054 | | 0.206 *(Cov. = 0.3)* |
| Ultimate Shear Strain | 0.00646 | | | |

Similarly, the experimental works performed by Phaiju and Pradhan (2018) also suggested the compressive strength of bricks to be 11.12 N/mm$^2$ ($E_b$ = 3357.9 N/mm$^2$) for the samples particularly available around Kathmandu region.

The mechanical properties of the timber like: weight density ($\gamma$) = 800 kg/m$^3$, Young's modulus (E) = 12500 MPa, poisson's ratio ($\nu$) = 0.12 and modulus of rigidity (G) = 1500 MPa is taken in the present study (Shrestha et.al., 2017). Concrete is assumed to have grade of 15 MPa, with elasticity modulus (E) of 19.36 GPa and with poisson's ratio ($\nu$) 0.2.

### 3.3 Development of Numerical Models

The case study buildings are modelled in Finite Element Software, SAP 2000 v23.1.0. A 3D macro-modelling approach is adopted to model the buildings at present conditions. The wall components are modelled as thick shell area elements and the slab floors as thin shell area elements. The storey floor levels made up of RCC slab is assigned to be rigid diaphragm and timber floor level in first storey to be semi-rigid. All timber members are modelled as frame elements, with wooden joists and rafters considered to be pinned. Roof coverings are CGI sheets and their loads are ignored in the modelling. The structural members of the model may include different thickness of wall elements. Meshing is done at 6" x 6" to increase accuracy. Due to a lack of actual field data and material testing, all mechanical properties of building materials were obtained from relevant previous literatures, which accounted for the current study. The foundation is supposed to be rigidly fixed at ground level.

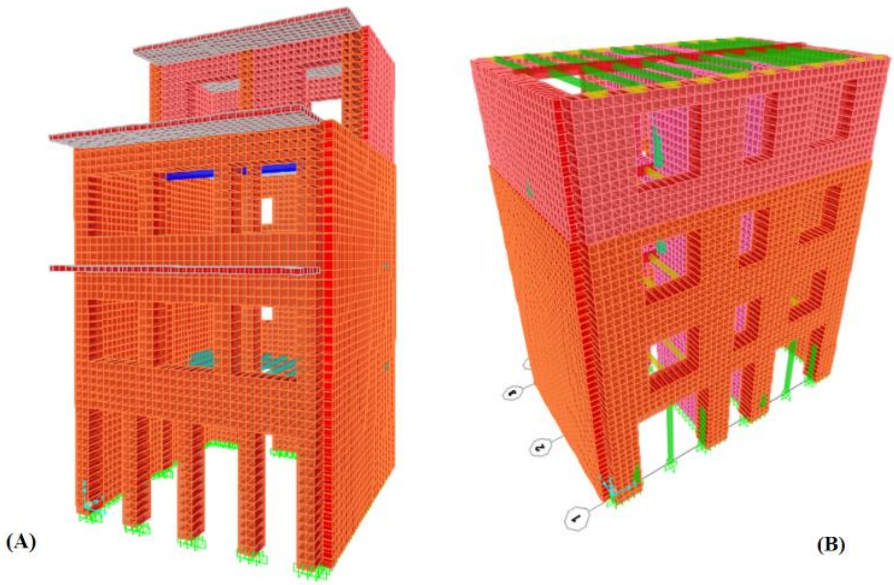

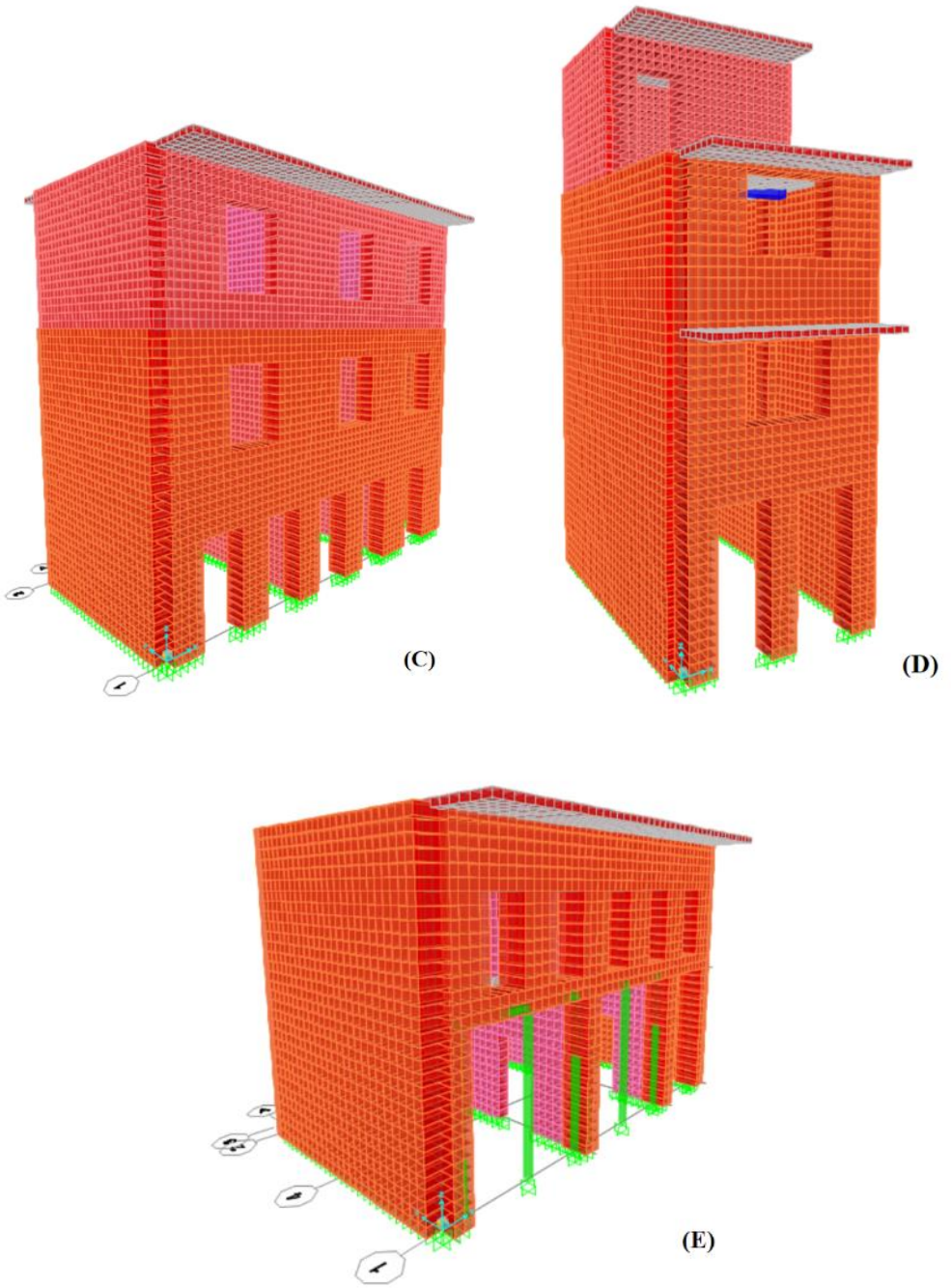


Figure 3.3 The 3D FEM Models taken under considerations, SAP2000

### 3.4 Model Validation for the use of NL-Links

Andres Lepage and Reynaldo E. Sanchez (2012) proposed two modelling techniques: Non Linear Layer Model and Non Linear Link Model, for practical nonlinear static analysis; which were imposed to aid in the development and implementation of a revised limit design technique for special reinforced masonry shear walls. The area elements at potential critical yielding sections in the Nonlinear Layer model are adjusted with particular layer definitions that account for material nonlinearity. In the Nonlinear Link model, nonlinear connections are used to modify the area elements at potential critical yielding sections. In their paper, the proposed simplified models are described through their application to a 2D one-story masonry wall with two wide openings as shown in Figure 3.4.

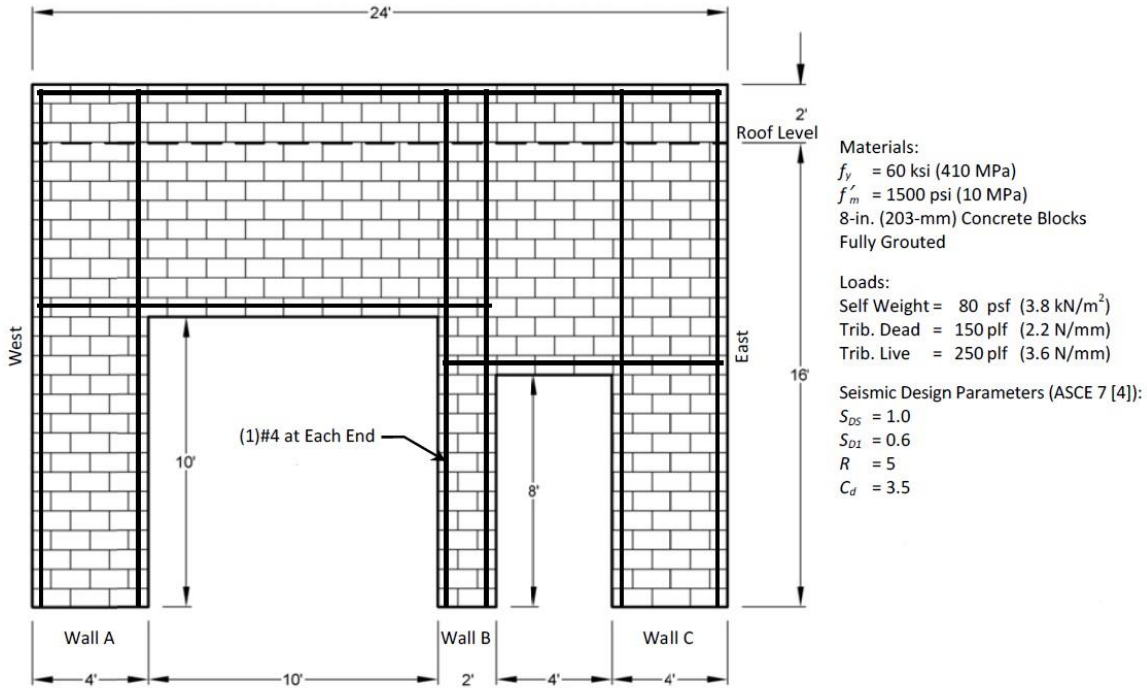


Figure 3.4 Description of Wall Considered, Lepage and Sanchez (2012)

The model consists of three vertical wall segments with three joint segments coupled by two horizontal wall segments. The perforated wall configuration assumes roof level to be rigid diaphragm which is located at 2'-0" (610 mm) below the top of the wall segment. Potential hinge locations are identified as the ends of vertical and horizontal wall segments.

This present thesis mainly focuses on the methodology proposed by Lepage and Sanchez in their second method. In the Non Linear link model proposed in the paper, the area elements representing the interface of wall segments, where yielding is anticipated to occur, are replaced with nonlinear links which are defined as Multilinear plastic (Figure 3.5). The user-defined force-deformation relationship is assigned to present both axial and in-plane shear behavior of the yielding wall segments. Outside of the predicted yielding zones, linear-elastic area elements with full gross section properties are used to simulate the area elements. A gravity load scenario is described as a pre-load condition in nonlinear static analysis to establish the beginning points on the force-deformation curves of each nonlinear link.

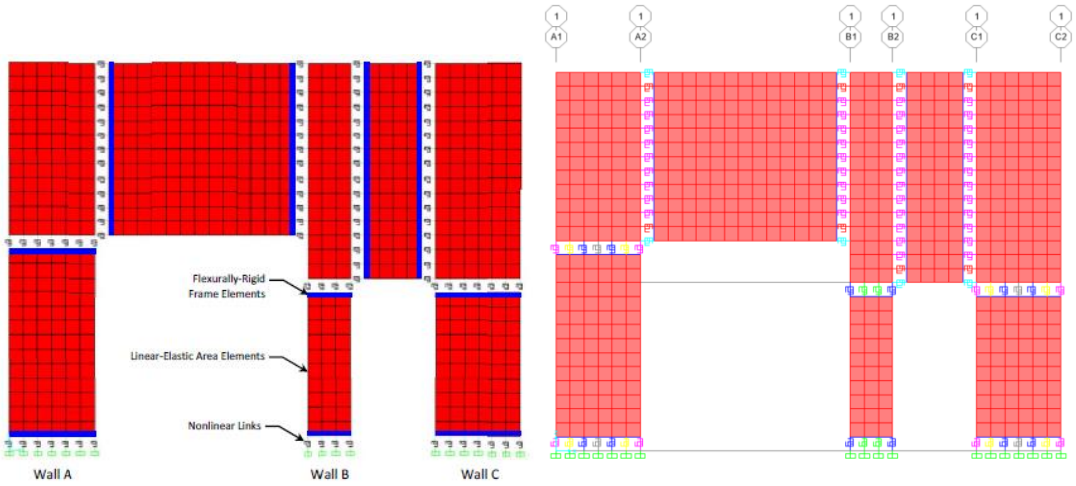


Figure 3.5 (a) Non-Linear Link Positioning as Suggested by Lepage and Sanchez (2012), (b) Model Prepared in SAP2000 v23

In comparison to the relevant output data of proposed nonlinear static analysis from Lepage and Sanchez to that of output from a refined computational model, SAP2000 v23, indicate that the proposed models were sufficiently accurate. This comparison helps us to better understand the use of Non-Linear Multi Plastic Link Elements. This suggest us to use nonlinear links in our model, which would replace the area elements just like in the Reynaldo and Sanchez model. The introduction would be based on the visual assessment of the building under study and in accordance with the observed crack patterns in the actual structure.

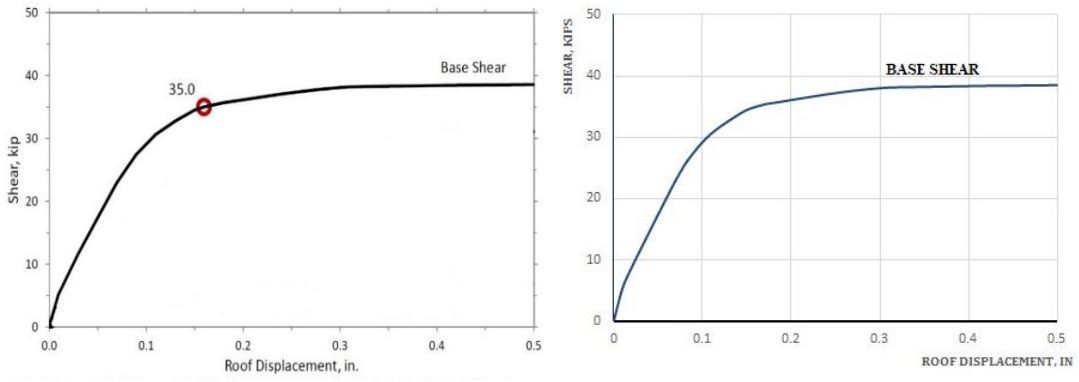


Figure 3.6 (a) Shear vs. Roof Displacement for Nonlinear Link Model, Eastward Loading, Lepage et al. (2012), (b) Pushover Curve (Shear vs Roof displacement) obtained from SAP 2000 v23

## 3.5 Link Parameters

### 3.5.1 Stress-Strain Curve

For simplifying the analysis and design, the values of sectional forces, stress and strain parameters are generally determined based on gross cross-sectional geometrical characteristics of the masonry walls, and assuming the elastic, homogeneous and isotropic global parameters (Tomazevic, 1999). These assumptions suggest the equations which are based on theory of elasticity and can be implemented for seismic vulnerability assessment. Although these equations seem simplified, they reflect the actual failure mechanisms. An idealized bi- or tri-linear resistance envelope can be used to simulate the actual hysteretic behavior of a masonry wall that is subjected to a combination of constant vertical load and a sequence of lateral load reversals.

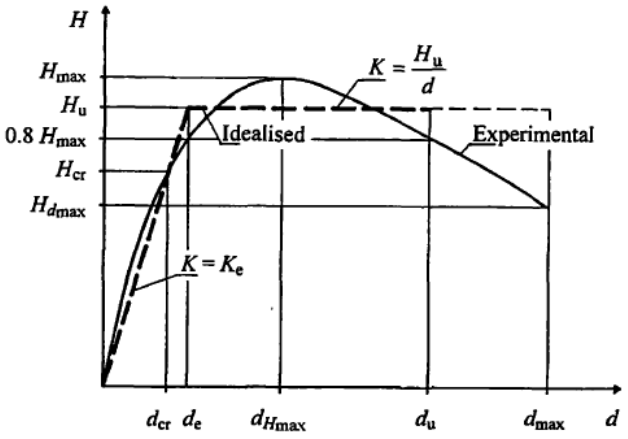


Figure 3.7 Idealization of experimental resistance envelope with bilinear relationship (Tomazevic, 1999)

Tomazevic suggests the average value ratio of $H_u/H_{max}$ ratio to be 0.9 i.e. $H_u = 0.9\ H_{max}$ and ultimate ductility factor $\mu_u$ = 2.0-3.0 for the case of plain masonry walls (taken value = 2).

Thus, this gives us the bi-linearized stress-strain curve for Brick Masonry (Clay Bricks in Mud Mortar) used in our present work as shown in Figure 3.8. The tensile strength of masonry is taken to be zero. Similarly, the shear value to be 0.15Mpa.

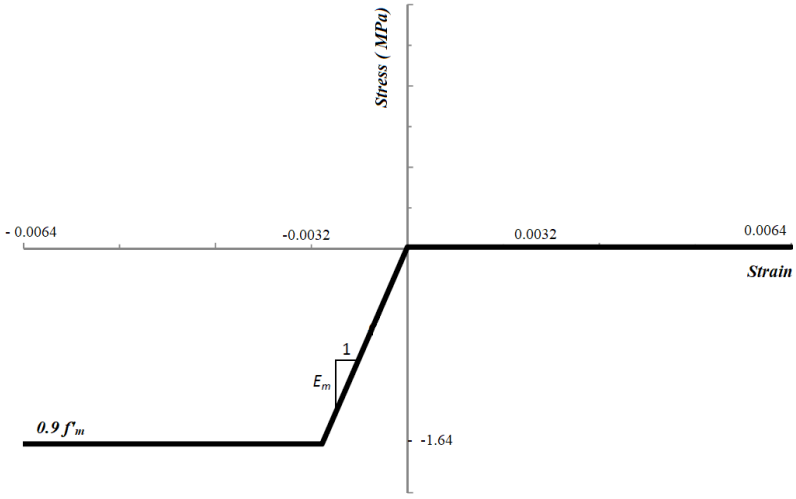


Figure 3.8 Axial stress-strain bi-linearized curve

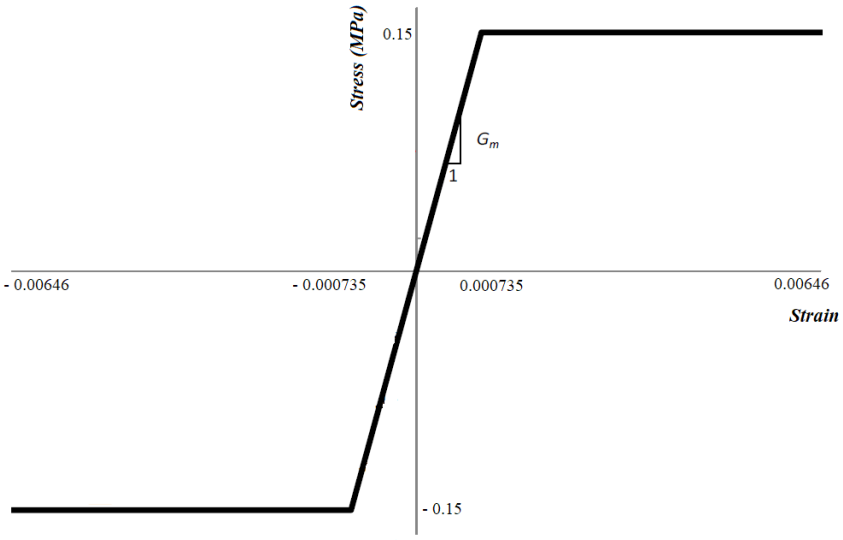


Figure 3.9 Shear stress-strain bi-linearized curve

### 3.5.2 Calculation of Link Parameters

The initial stiffness, given in table 3.1, was obtained through linear-elastic response using gross-section properties of wall materials. The force-deformation curve is taken to be bi-linear plot. The tensile stress of masonry is taken to be zero. Different link types were defined based on material sectional properties, tributary areas and their positioning on centres and ends. For simplicity and accuracy all the wall meshing is done at 6" x 6" (0.1524m x 0.1524m) sizes, so that minimum number of links can be defined. End links are provided at nodal ends of the cracks origination and centre links at central nodes of meshed wall.

Table 3.1 Initial stiffness values for NL-Link (kN/m)

| **Link Properties** | **Axial Direction (U1)** | **Shear Direction (U2 and U3)** |
|---|---|---|
| BMM – 9" Thick wall - Centres | 117070 | 46920 |
| BMM – 9" Thick wall - Ends | 58535 | 23460 |
| BMM – 14" Thick wall - Centres | 183240 | 73440 |
| BMM – 14" Thick wall - Ends | 91620 | 36720 |
| BMM – 18" Thick wall - Centres | 234140 | 93840 |
| BMM – 18" Thick wall - Ends | 117070 | 46920 |

The force – displacement plot for link elements are obtained as below:

A. <u>BMM – 9" Thick wall – Centres:</u>

Size of mesh:

| | |
|---|---|
| L = | 6" (0.1524m) |
| Ht. = | 6" (0.1524m) |

Thickness of wall:

| | |
|---|---|
| B = | 9" ( 0.23m) |

Thus, Length of link for both horizontal and vertical placement ($l_{link}$) = 0.1524m

Tributary cross section area of each mesh ($A_{trib}$) = 0.035052$m^2$

Now, the strain parameter multiplied by length of link gives displacement and stress values multiplied by the tributary areas give the force – deformation plot for the link component.

Axial Force - Displacement Plot: Bilinear (U1):

| Displacement(m) | Force(kN) |
|---|---|
| -0.00098 | -57.42 |
| -0.00049 | -57.42 |
| 0 | 0 |
| 0.00098 | 0.00 |

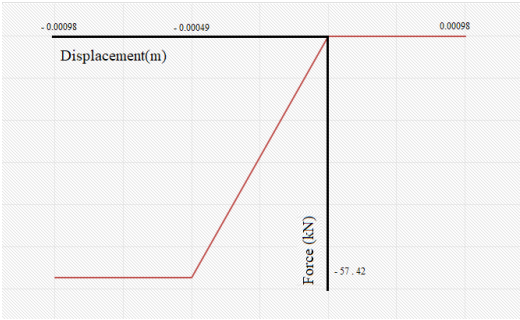


In the similar way, we get the plot for

Shear Force – Displacement Bilinear Plot (U2) and (U3):

| Displacement(m) | Force(kN) |
|---|---|
| -0.00098 | -5.26 |
| -0.00011 | -5.26 |
| 0 | 0 |
| 0.00011 | 5.26 |
| 0.00098 | 5.26 |

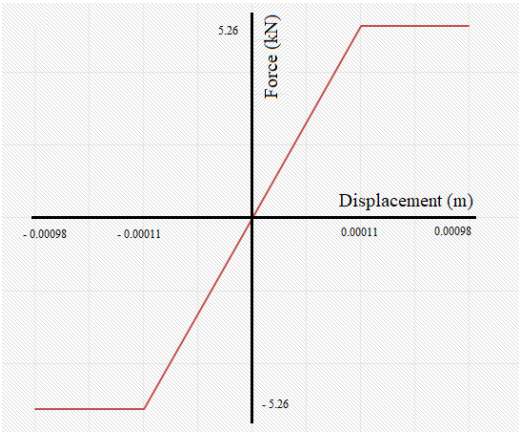


B. <u>BMM – 9” Thick wall – Ends:</u>

Size of mesh:

| | |
|---|---|
| L = | 6” (0.1524m) |
| Ht. = | 6” (0.1524m) |

Thickness of wall:

| | |
|---|---|
| B = | 9” ( 0.23m) |

Thus, Length of link for both horizontal and vertical placement ($l_{link}$) = 0.1524m

Tributary cross section area of each mesh ($A_{trib}$) = 0.017526$m^2$

Now, the strain parameter multiplied by length of link gives displacement and stress values multiplied by the tributary areas give the force – deformation plot for the link component.

Axial Force - Displacement Plot: Bilinear (U1):

| Displacement(m) | Force(kN) |
|---|---|
| -0.00098 | -28.71 |
| -0.00049 | -28.71 |
| 0 | 0 |
| 0.00098 | 0.00 |

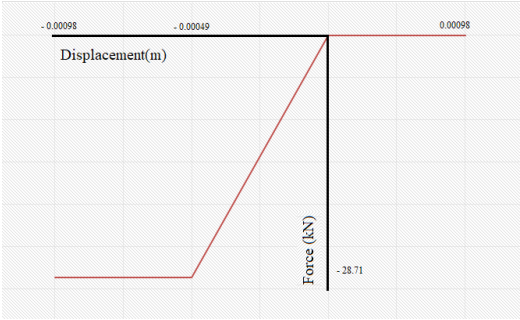


In the similar way, we get the plot for

Shear Force – Displacement Bilinear Plot (U2) and (U3):

| Displacement(m) | Force(kN) |
|---|---|
| -0.00098 | -2.63 |
| -0.00011 | -2.63 |
| 0 | 0 |
| 0.00011 | 2.63 |
| 0.00098 | 2.63 |

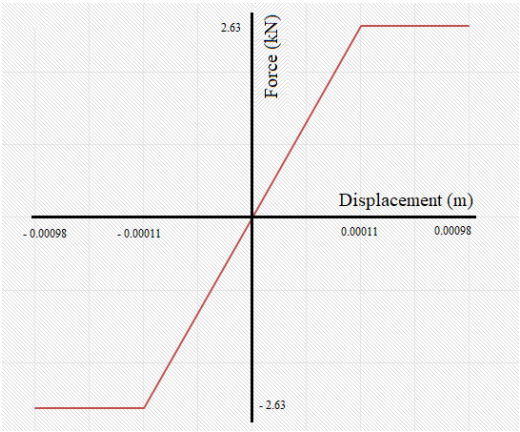


C. <u>BMM – 14” Thick wall – Centres:</u>

Size of mesh:

| | |
|---|---|
| L = | 6” (0.1524m) |
| Ht. = | 6” (0.1524m) |

Thickness of wall:

| | |
|---|---|
| B = | 14” ( 0.36m) |

Thus, Length of link for both horizontal and vertical placement ($l_{link}$) = 0.1524m

Tributary cross section area of each mesh ($A_{trib}$) = 0.054864$m^2$

Now, the strain parameter multiplied by length of link gives displacement and stress values multiplied by the tributary areas give the force – deformation plot for the link component.

Axial Force - Displacement Plot: Bilinear (U1):

| Displacement(m) | Force(kN) |
|---|---|
| -0.00098 | -89.87 |
| -0.00049 | -89.87 |
| 0 | 0 |
| 0.00098 | 0.00 |

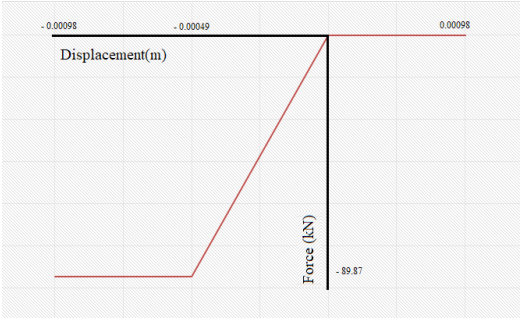


In the similar way, we get the plot for

Shear Force – Displacement Bilinear Plot (U2) and (U3):

| Displacement(m) | Force(kN) |
|---|---|
| -0.00098 | -8.23 |
| -0.00011 | -8.23 |
| 0 | 0 |
| 0.00011 | 8.23 |
| 0.00098 | 8.23 |

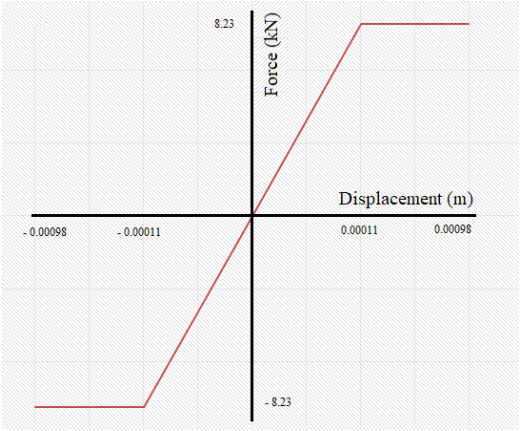


D. <u>BMM – 14” Thick wall – Ends:</u>

Size of mesh:

| | |
|---|---|
| L = | 6” (0.1524m) |
| Ht. = | 6” (0.1524m) |

Thickness of wall:

| | |
|---|---|
| B = | 14” ( 0.36m) |

Thus, Length of link for both horizontal and vertical placement ($l_{link}$) = 0.1524m

Tributary cross section area of each mesh ($A_{trib}$) = 0.027432$m^2$

Now, the strain parameter multiplied by length of link gives displacement and stress values multiplied by the tributary areas give the force – deformation plot for the link component.

Axial Force - Displacement Plot: Bilinear (U1):

| Displacement(m) | Force(kN) |
|---|---|
| -0.00098 | -44.93 |
| -0.00049 | -44.93 |
| 0 | 0 |
| 0.00098 | 0.00 |

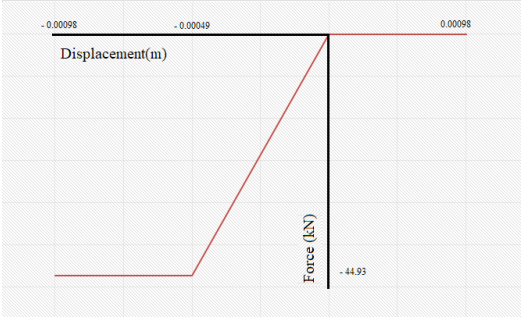


In the similar way, we get the plot for

Shear Force – Displacement Bilinear Plot (U2) and (U3):

| Displacement(m) | Force(kN) |
|---|---|
| -0.00098 | -4.11 |
| -0.00011 | -4.11 |
| 0 | 0 |
| 0.00011 | 4.11 |
| 0.00098 | 4.11 |

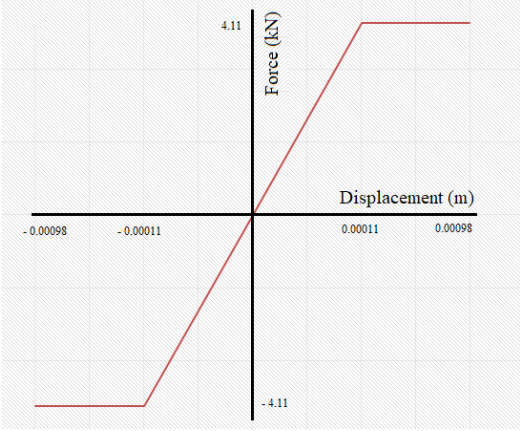


E. <u>BMM – 18” Thick wall – Centres:</u>

Size of mesh:

| | |
|---|---|
| L = | 6” (0.1524m) |
| Ht. = | 6” (0.1524m) |

Thickness of wall:

| | |
|---|---|
| B = | 18” ( 0.46m) |

Thus, Length of link for both horizontal and vertical placement ($l_{link}$) = 0.1524m

Tributary cross section area of each mesh ($A_{trib}$) = 0.070104$m^2$

Now, the strain parameter multiplied by length of link gives displacement and stress values multiplied by the tributary areas give the force – deformation plot for the link component.

Axial Force - Displacement Plot: Bilinear (U1):

| Displacement(m) | Force(kN) |
|---|---|
| -0.00098 | -114.83 |
| -0.00049 | -114.83 |
| 0 | 0 |
| 0.00098 | 0.00 |

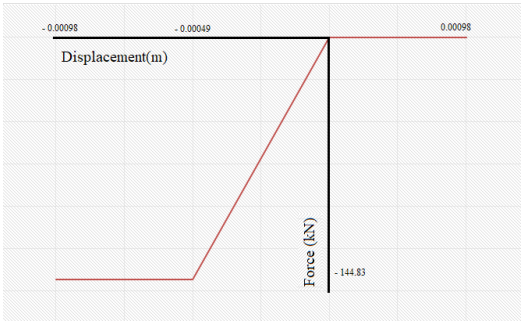


In the similar way, we get the plot for

Shear Force – Displacement Bilinear Plot (U2) and (U3):

| Displacement(m) | Force(kN) |
|---|---|
| -0.00098 | -10.52 |
| -0.00011 | -10.52 |
| 0 | 0 |
| 0.00011 | 10.52 |
| 0.00098 | 10.52 |

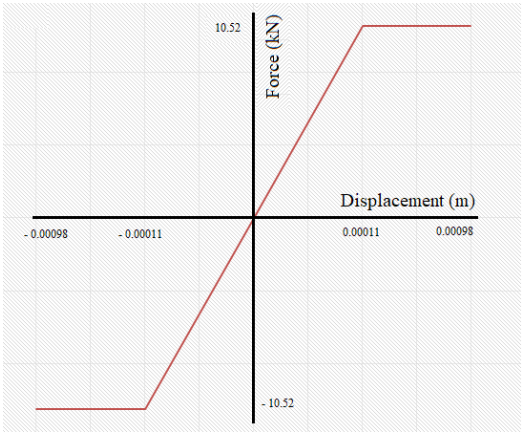


F. <u>BMM – 18” Thick wall – Ends:</u>

Size of mesh:

| | |
|---|---|
| L = | 6” (0.1524m) |
| Ht. = | 6” (0.1524m) |

Thickness of wall:

| | |
|---|---|
| B = | 18” ( 0.36m) |

Thus, Length of link for both horizontal and vertical placement ($l_{link}$) = 0.1524m

Tributary cross section area of each mesh ($A_{trib}$) = 0.035052$m^2$

Now, the strain parameter multiplied by length of link gives displacement and stress values multiplied by the tributary areas give the force – deformation plot for the link component.

Axial Force - Displacement Plot: Bilinear (U1):

| Displacement(m) | Force(kN) |
|---|---|
| -0.00098 | -57.42 |
| -0.00049 | -57.42 |
| 0 | 0 |
| 0.00098 | 0.00 |

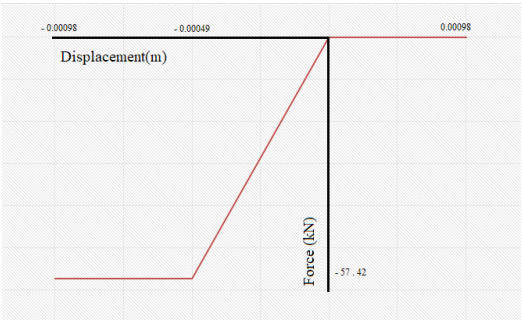


In the similar way, we get the plot for

Shear Force – Displacement Bilinear Plot (U2) and (U3):

| Displacement(m) | Force(kN) |
|---|---|
| -0.00098 | -5.26 |
| -0.00011 | -5.26 |
| 0 | 0 |
| 0.00011 | 5.26 |
| 0.00098 | 5.26 |

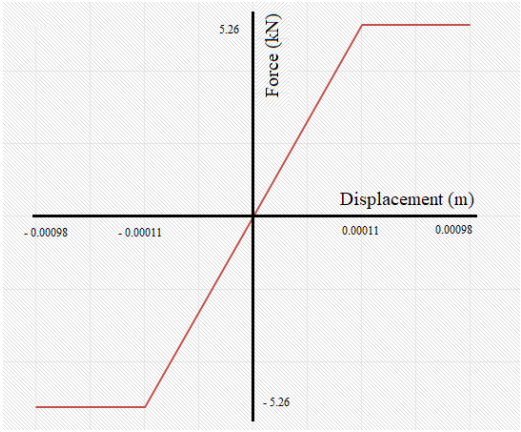


The calculated link properties are provided as SAP2000 inputs; steps followed is described in APPENDIX B.

### 3.5.3 Effect of Openings

The material parameters taken into considerations by Lepage and Sanchez were changed to the material parameters that of unreinforced Brick in Mud Mortar of 18" thickness and link properties were also assigned as calculated above. The positioning of links was done to the same position as suggested, i.e. at critical potential hinge regions. Various literatures and field observation show that the corners of openings have the high stress concentration and cracks originate from these corners. The calculated parameters were analyzed in the same 2D Planer structure taken under consideration by Lepage and Sanchez. Upon comparison of results, the nature of capacity curve was found to be similar to that suggested in the literature.

Similarly, the effect of base opening and without opening was compared. On comparison, base shear was found to be far too low for the structure with openings. The capacity curve of base shear versus roof displacement is lower for the wall with openings. The positioning of links in the wall without opening is assumed to represent potential foundation sliding and diagonal shear cracks.

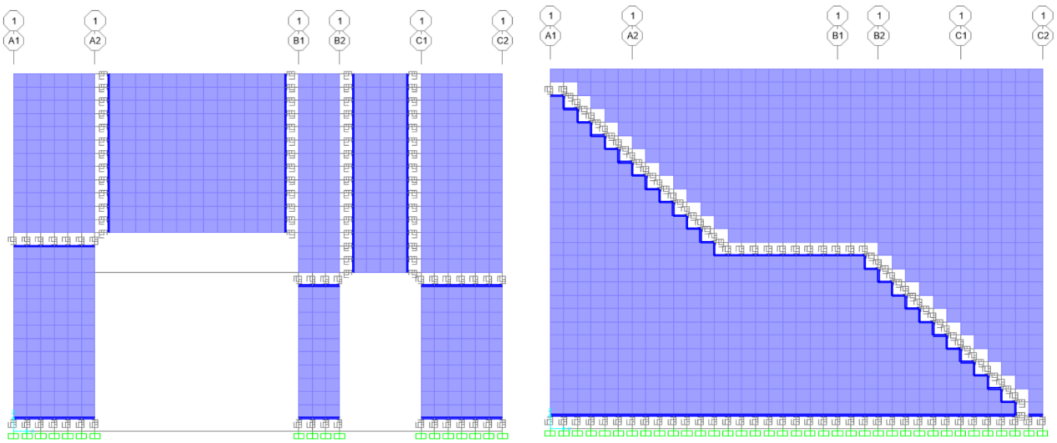

Figure 3.10 18" BMM wall (a) With Openings (b) Without Openings

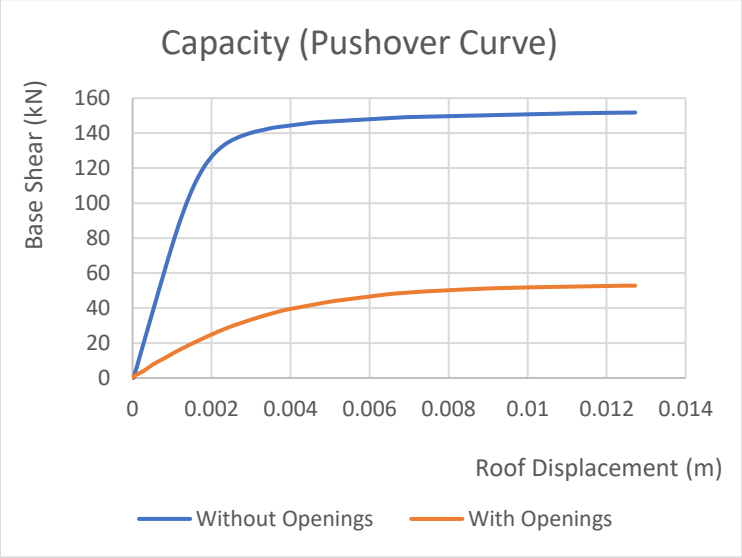


Figure 3.11 Comparison of Capacity Curves with and without openings

### 3.5.4 Positioning of NL-Links:

The positioning of NL-Links is based on the visual assessment of the building under study, literatures (Lepage and Sanchez, 2012) and in accordance with the observed crack patterns in the actual structure. Different trails were performed and the best critical positioning that perfectly describes the building non-linearity was chosen. Comparison of different link positioning and their analysis output comparison is also shown in APPENDIX C.

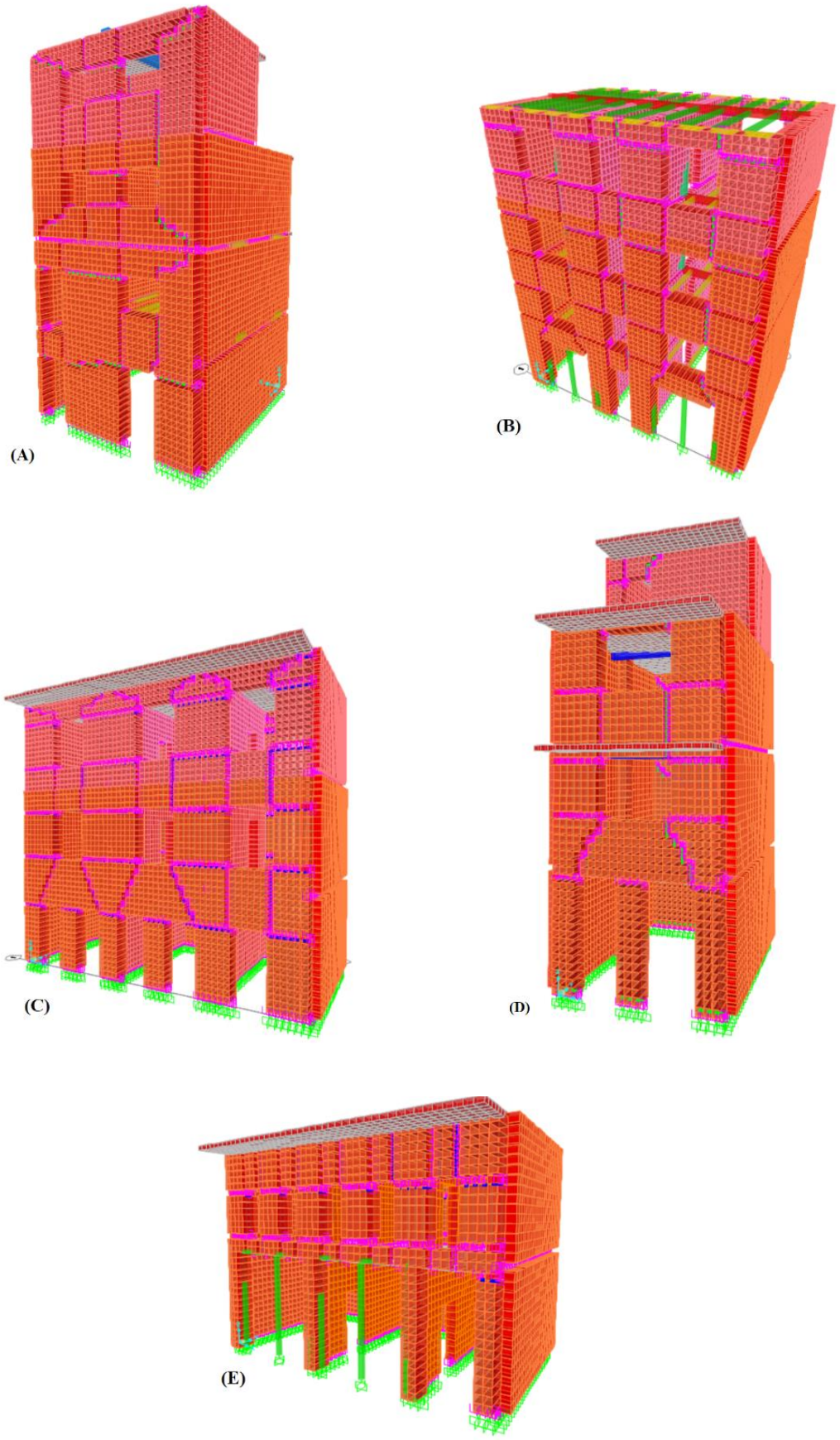


Figure 3.12 The 3D FEM Models with Non-Linear Links, SAP2000

### 3.6 Pushover Analysis

The building model is subjected to nonlinear static pushover analysis. For brevity and simplicity, pushover in only one direction (along X – Axis) is presented in this thesis. The direction represents the weaker side of the building with presence of majority of openings along the in-plane loaded walls. Steps followed for performing the analysis is described in APPENDIX D.

### 3.7 Capacity Spectrum Method (CSM)

After obtaining the Pushover curve, it is converted to the capacity spectrum of $S_A$ Vs $S_D$ relationship represented by an Equivalent Single Degree of Freedom (ESDOF) System.

$$S_A(T) = \frac{V_B}{M} \qquad \text{Eq. 3.1}$$

Where, $V_B$ represents the seismic base shear, and M is the effective modal mass given by:

$$M = \frac{L_n^2}{M_n} = \frac{(\sum m_i\{\delta_{i1}\})^2}{\sum m_i\{\delta_{i1}\}^2} \qquad \text{Eq. 3.2}$$

Also,

$$S_D(T) = \frac{D_R}{\beta} = \frac{(\delta_{1i})^T [m] (\delta_{1i})}{(\delta_{1i})^T [m] (1)} \qquad \text{Eq. 3.3}$$

Where, displacement vector of first mode is given by: $\{\delta\}_1 = \{\Phi\}_1 \beta_1 S_D(T)$ Eq. 3.4

And, [m] is the lumped floor mass matrix.

Similarly, the input response spectrum curves in $S_A$ - T, resulting from input parameters of certain earthquake intensity, is converted to Acceleration-Displacement Response Spectrum (ADRS) i.e. $S_A$ - $S_D$ plot by the relation:

$$S_D(T) = \left(\frac{T}{2\Pi}\right)^2 S_A(T) \qquad \text{Eq. 3.5}$$

With the demand spectrum and capacity curve in the same domain of spectral acceleration and spectral displacement (ADRS format), the CSM analysis follows the following stepwise procedures as proposed by Otani et. al.(2000):

1. We decide the first yield point of the structure under consideration. In this study, the yield point corresponds to the spectral displacement ($D_y$) when the storey drift ratio reaches 0.1%.
2. Assume, the ductility, $\mu$ = 1, tangential to the spectral displacement axis on the capacity spectrum for the decided first yield point.
3. Now, we draw the line of equivalent stiffness, passing through the origin and this point.
4. The first plot of the performance point is find out, which is the point of intersection of the demand spectrum and the line of equivalent stiffness, $\mu$ = 1.
5. Now, changing the ductility factor, $\mu$ = 1.5, we locate the second point on the capacity curve, equivalent to multiplying factor times (n) to the first yield displacement ($D_y$). The multiplying factor corresponds to the ductility factor, which describes the limit states of the structure.
6. We draw the second line of equivalent stiffness which passes through the origin to the second point.
7. The equivalent damping ratio, $h_e$ , is calculated from the following empirical formula:

$$h_e = 0.25 \left( 1-\frac{1}{\sqrt{\mu}}\right)+ 0.05 \qquad \text{Eq. 3.6}$$

   $h_e$ for first mode is assumed as 0.05 for the damage-initiation limit state because structure behavior remains elastic at this stage.
8. Up to the damage initiation limit state, the demand spectra are prepared with a damping ratio of 5%, and at the life safety limit state, the demand spectra are prepared with an identical damping ratio. The response reduction factor of the demand spectrum, $F_h$ , is derived from the following formula:

$$F_h = \frac{1.5}{1+10\ h_e} \qquad \text{Eq. 3.7}$$

9. Now we draw the reduced demand spectrum by multiplying both parameters by $S_A$ and $S_D$ by $F_h$.
10. Now, we find the second performance point which is the point of interaction of the demand spectrum and line of equivalent stiffness, $\mu$ =1.5.
11. We repeat the steps 5 to 10, and collect all the performance point with different ductility factors which gives the demand curve.

12. The interaction of the obtained demand curve and the capacity curves provides the final performance points.

A single performance point is obtained for one PGA level of the particular earthquake spectrum. A similar procedure is followed to obtain performance points for different PGA levels of earthquake response spectra. The programming was performed in MATLAB.

A sample example for the determination of performance point with PGA 0.1g of NBC 105:2020 for hard soil response spectrum is shown in Figure 3.13.

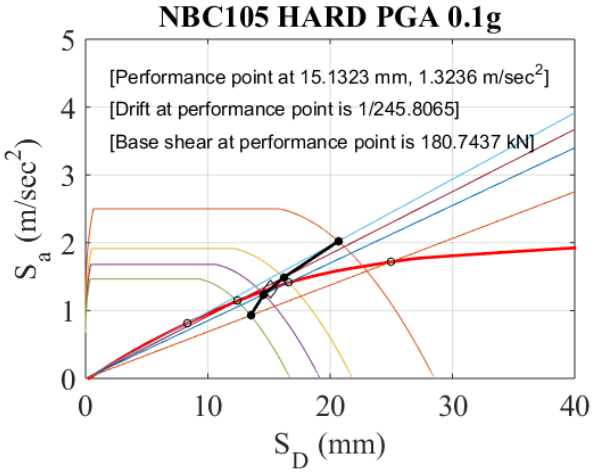


Figure 3.13 Determination of performance point using CSM for PGA of 0.1g of NBC 105:2020 (Building A)

### 3.8 Fragility Curve

The CSM analysis for various ground motion parameters gives us a set of different values of performance point. These results can be correlated to a damage state, expressing the vulnerability of a structure to a user-defined intensity measure, as a graphical function of capacity curve. This fragility curve expresses the probability of exceedance of a specified damage stage as a function of input earthquake intensity parameters like: PGA, PGV, $S_A$, etc.

Three categories of limit states of: Immediate Occupancy (IO), Life safety (LS) and collapse prevention (CP) is defined for the generation of fragility curves. The different threshold values are assigned for the target structure from the structural capacity viewpoint at:

- Immediate Occupancy (IO) = $^{1}/_{750}$ (i.e. 0.13%)

- Life safety (LS) = $^{1}/_{500}$ (i.e. 0.2%)

- Collapse Prevention (CP) = $^{1}/_{250}$ (i.e. 0.4%)

For present study, methodology proposed by Wen et.al. (2004) is used for the generation of fragility curves. The probability that the structure exceeds the limit-damage state for the given ground motion intensity is provided by:

$$P(LS_i/GMI) = 1 - \emptyset \left(\frac{\lambda^{i}_{CL} - \lambda_{D/GMI}}{\beta_{D/GMI}}\right) \quad \text{Eq. 3.8}$$

Where the mean and standard deviation parameters are defined by:

$$\lambda_{D/GMI} = \ln(a_1) + a_2 \ln(GMI) \quad \text{Eq. 3.9}$$

$$\beta_{D/GMI} = \sqrt{\frac{\sum_{k=1}^{n} [LN(GMI_k) - \lambda_{GMI}(GMI_k)]^2}{n-2}} \quad \text{Eq. 3.10}$$

The constants $a_1$ and $a_2$ are obtained through linear regression analysis as the logarithmic plot of storey drift and Ground Motion Intensity (GMI) parameters in terms of PGA.

A series of input parameters from different earthquake scenarios are provided, to obtain the linear plot, which gives us the threshold value. The fragility curves plots the probability of exceeding this threshold value corresponding to the categories of user-defined limit states.

# CHAPTER 4: RESULTS AND DISCUSSIONS

## 4.1 Static Analysis

The buildings were modelled in SAP2000 software and analyzed first in static method. Results on comparison show higher base shear for the building models with heavier mass and greater number of stories. All the buildings have their first mode of oscillation along X-direction. The fundamental time period before and after the introduction of link elements were found within the closer range, though slightly increased after the introduction of non-linear links. Stress analysis shows the greater concentration of tensile and compressive stresses in the corners of the openings. The output results from static analysis is shown in APPENDIX E.

## 4.2 Force-Displacement Curve

The non-linear links provided on the potential crack developing regions impart the non-linearity in the building model. Pushover in only one direction, i.e. along X-axis as the in plane direction, was considered in the analysis. The pushover curve obtained from the software were compared and analyzed for the building samples taken under consideration. The pushover curves obtained for different buildings is shown in Figure 4.1. As we can clearly see these curve follow the linear path which later on breaks into the curve with low to zero slope representing non-linearity in the structure.

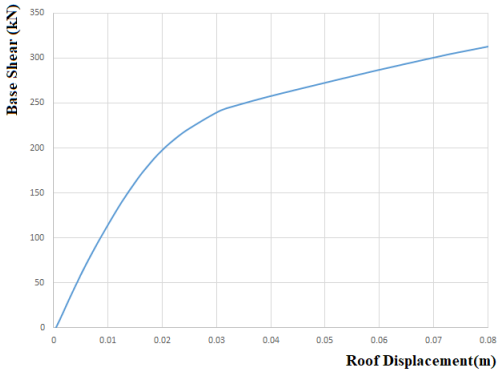


**Building- "A"**

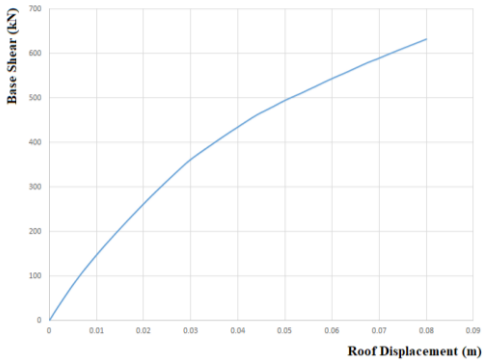


**Building- "B"**

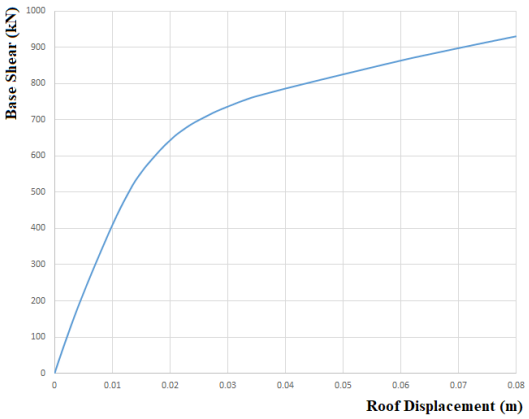


**Building- "C"**

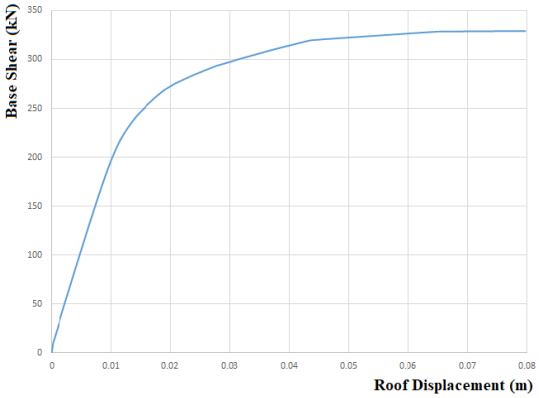


**Building- "D"**

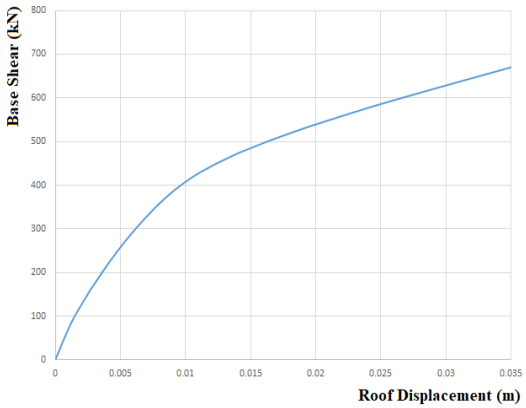


**Building- "E"**

Figure 4.1 Pushover Capacity Curves for different buildings

### 4.3 Determination of Performance Point

After obtaining the Pushover curve, it is converted to the capacity spectrum of Spectral Acceleration "$S_A$" versus Spectral Displacement "$S_D$" relationship. Similarly, the input response spectrum curves in $S_A$ - T, resulting from input parameters of NBC 105:2020 spectrum intensity, is converted to Acceleration-Displacement Response Spectrum (ADRS). The steps were followed according to Otani et.al. (2000) and programming was performed in MATLAB.

Determination of performance point using CSM for different PGA levels of earthquake spectra from NBC 105:2020, for building A is shown below, graphs for all other buildings are shown in APPENDIX F.

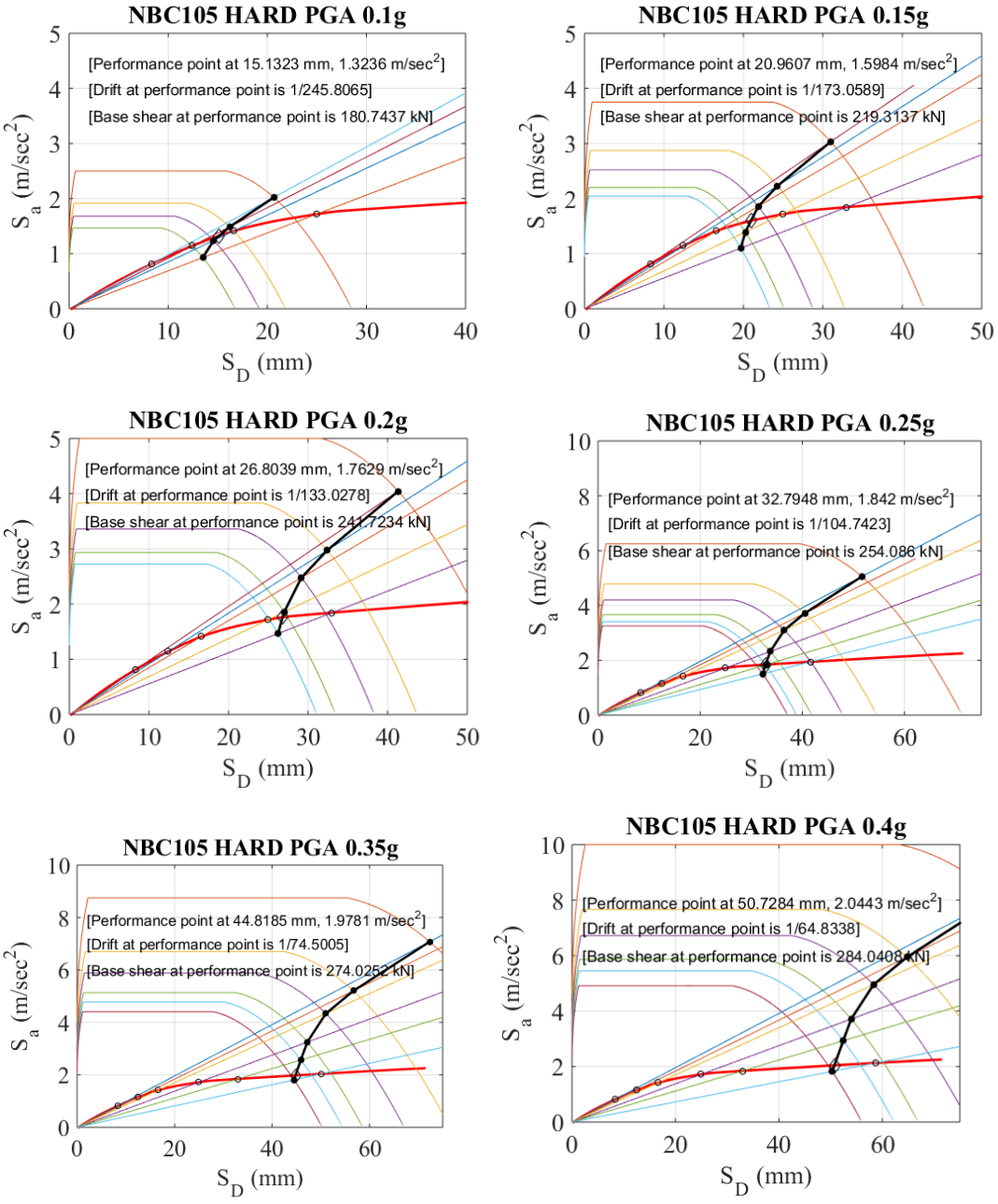


Figure 4.2 Determination of Performance point through Capacity Spectrum Method (Building A)

For Building A, the performance point for 0.1g PGA is at spectral displacement of 15.13mm and acceleration of 1.3236 m/sec$^2$. The drift at performance point is at 1/245.8, with base shear corresponding to performance point is 180.74kN. In the similar

way, performance point is obtained through trial and error method for higher values of PGA, and the performance point obtained is shown in Figure 4.2, with drift and base shear values corresponding to these levels. For higher values of PGA, the performance point shifts right representing greater value of spectral displacement, higher value of drift and base shear. The performance point obtained for other buildings, B, C, D and E, with their corresponding drift and base shear values is shown in APPENDIX F.

### 4.4 Fragility Curve

The CSM analysis for various ground motion parameters gives us a set of different values of performance point. These results can be correlated to a damage state, expressing the vulnerability of a structure to a user-defined intensity measure, as a graphical function of capacity curve.

The logarithmic regression plot of obtained performance points in terms of drift and PGA levels is shown in Figure 4.3.

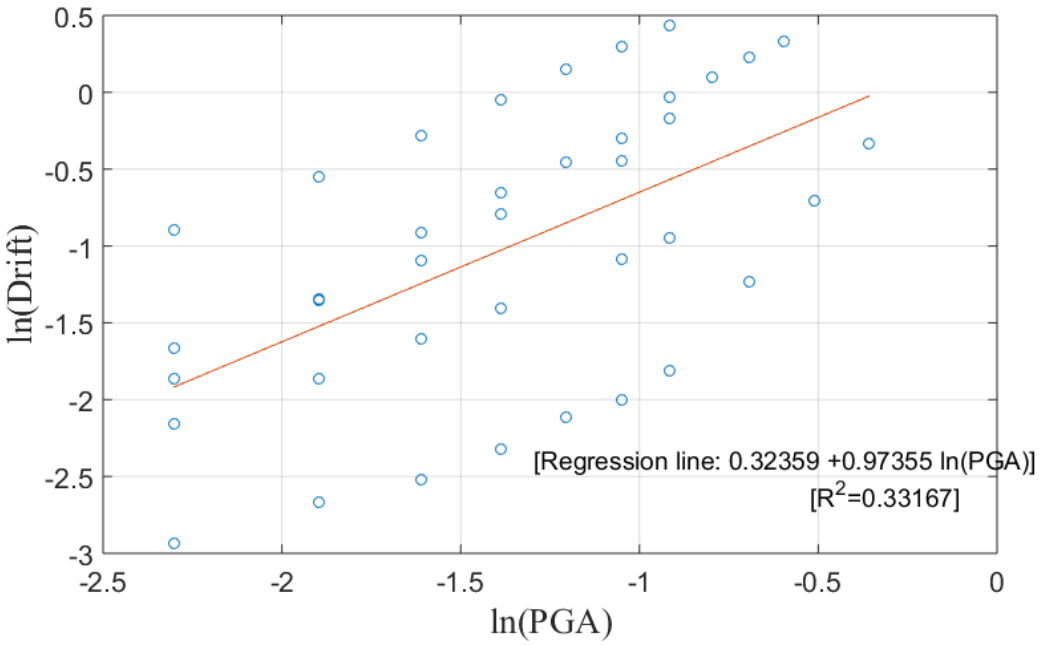


Figure 4.3 Regression Plot

The regression plot is obtained in the form of equation:

$$\lambda_{D/GMI} = 0.32359 + 0.97355 \ln(PGA) \qquad \text{Eq. 4.1}$$

Three categories of limit states of: Immediate Occupancy (IO) at 0.13% drift, Life Safety (LS) at 0.2% drift and Collapse Prevention (CP) at 0.4% drift is defined for generating the fragility curves. The obtained fragility curve is shown in Figure 4.4.

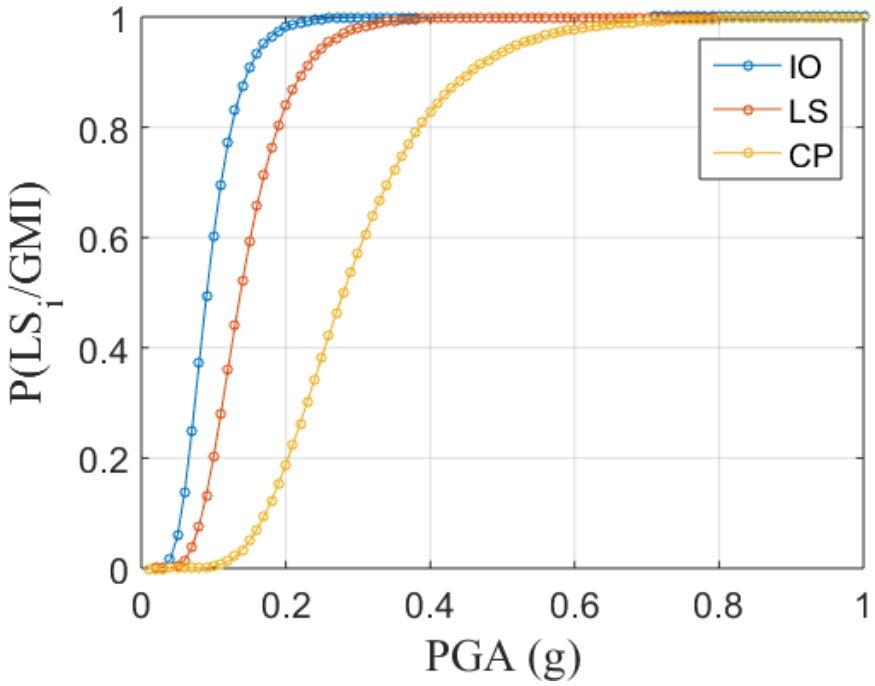


Figure 4.4 Fragility Curve

From Figure 4.4, we can observe, at 0.2g PGA, buildings have nearly 100% probability of exceedance of the Immediate Occupancy level (IO), 80% probability of exceedance of the Life safety level, and 20% probability of exceedance of the Collapse Prevention level (CP). For 0.35g PGA, that corresponds to the peak seismic zoning factor of 0.35g with return period of 475 years for any area as defined by NBC 105: 2020, the probability of exceeding the IO, LS and the CP limit states is 100%,100% and about 75%. And at 0.4g PGA, the probability of exceedance of Collapse prevention level reaches more that 80%. It is thus evident that the buildings taken into consideration are in risk for life safety.

# CHAPTER 5: CONCLUSIONS AND RECOMMENDATION

## 5.1 Introduction

In this chapter, the conclusion drawn from the research work and recommendation for further study has been presented. A different simplified approach of vulnerability assessment of masonry buildings with Non-Linear link elements have been researched. The result for the non-linear force-displacement relation along with the determination of performance points from Capacity Spectrum Method (CSM) are shown in the result section. Based on the result, a conclusion of the research work was developed.

## 5.2 Conclusions

The major objective of the present thesis work is to assess the seismic vulnerability of URM masonry buildings through a simplified technique of using link elements for non-linear analysis/ pushover analysis of the masonry walls. In this thesis, we have taken five masonry buildings that represent the buildings situated in urban settlements. The analysis of five masonry residential buildings have resulted in better understanding of their seismic behavior and vulnerability. Instead of time history analysis, a completely new approach was used for generating the fragility curves, from the building capacity curves and response spectra, following the method proposed by Otani et.al. (2000). All these programming in MATLAB helped us to better understand the generation of fragility functions.

The major findings that we obtained after this research are:

- The non-linear behavior of masonry walls can be captured using non-linear tensile and compressive properties along with shear friction and cohesion coefficients and generate a bilinear plot for the non-linear analysis, which reduces computational effort in comparison to simplified micro-modeling technique or layered shell macro-element analysis with approximately similar precision. However, these analyses need to be validated using experiments and improved modeling based on detailed knowledge.
- The fragility analyses of these structures revealed that these buildings with lowest strength, high slenderness ratio, heavy weight and greater number of stories showed high probabilities of collapse under the design earthquake. For the PGA value of 0.35g, these buildings have 100% probability of exceeding

the immediate occupancy and life safety level, and 75% probability of exceedance of collapse state. This suggests that the performance of these buildings needs to be enhanced by improving the properties of the URM walls using suitable retrofitting techniques.

### 5.3 Recommendations

The present study focuses on the nonlinear static analysis of masonry buildings along the in-plane direction only. For the current thesis work, limited parameters from literatures have been considered to find the influences in the crack pattern in the masonry walls. A detailed material testing should be performed to study the actual mechanical properties of the masonry structures. Similarly, positioning of link elements can be further optimized with high knowledge of excellence and analysis. There are some limitations in the present study which can be incorporated in future as follow:

- The seismic vulnerability of these buildings can be checked with various possible retrofitting strategies, as presented in section 2.12.
- All nonlinearities are concentrated at NL links and their locations are defined by user based on the predefined conventional cracking patterns and stress concentrations. A more detailed micro-modeling approach or damage models could provide better representation of these failure patterns and capacity curves.
- The link positions can be replaced with non-linear layer parameters.
- A larger data of the sample buildings gives the better representation of the seismic vulnerability level.

## REFERENCES


Asteris, P.G., Sarhosis, V., Mohebkhah, A., and V. Plevris, 2015, "Numerical Modeling of Historic Masonry Structures, Chapter 7", A volume in the Advances in Civil and Industrial Engineering (ACIE) Book Series.

ATC 40, 1996, "Seismic Evaluation and Retrofit of Concrete Buildings", Seismic Safety Commission.

Borzi, B., Pinho, R., and H. Crowley, 2008, "Simplified Pushover-Based Vulnerability Analysis for Large Scale Assessment of RC Buildings", Engineering Structures 30, 804-820.

Chhabi, Mishra, 2019, "Mechanical Properties of Components of Nepalese Historical Masonry Buildings", proceedings of International Exchange and Innovation Conference on Engineering & Sciences (IEICES). 4, pp.118-123, 2018-10-18.

Chikanbanjar,M., Motra, G.B., and D.K. Maharjan, 2019, "Non-Linear Analysis of Unreinforced Masonry Building", Proceedings of IOE Graduate Conference,Volume 6.

CSI Analysis Reference Manual, 2017, "Structural Analysis and Design", Computers and structures Inc.

Dais, D., Sarhosis, V., Smyrou, E. and L.E. Bal, 2019, "Investigations on the Restoration and Seismic Enhancement Options for the Jaisedewal Temple after the Gorkha Earthquake in Nepal", Earthquake Risk and Engineering towards a Resilient World, SECED.

FEMA 306, 1998, "Evaluation of Earthquake Damaged Concrete and Masonry Wall Buildings", ATC-43 Project.

FEMA 273, 1997, "NEHRP Guidelines for the Seismic Rehabilitation of Buildings", ATC–33 Project.

FEMA 356, 2020, "Pre-standard and Commentary for the Seismic Rehabilitation of Buildings".

Freeman, S.A., 2004, "Review of the Development of the Capacity Spectrum Method", ISET Journal of Earthquake Technology, Paper No. 438, Volume 41.

Furukawa, A., Kiyono, J., Parajuli, R.R., Parajuli, H.R., and K. Toki, 2017, "Evaluation of Damage to a Historic Masonry Building in Nepal through Comparison of Dynamic Characteristics before and after the 2015 Gorkha Earthquake", Frontiers in Built Environment.

Garbin, E., Galati, N., Nanni, A., Modena, C. and M.R. Valluzi, 2007, "Provisional Design Guidelines for the Strengthening of Masonry Structures Subject to In-Plane Loading", 10th North American Masonry Conference.

Gautam, D., Fabbrocino, G., and F.S. de Magistris, 2018, "Derive Empirical Fragility Functions for Nepali Residential Buildings, Engineering Structures", Volume 171, Pages 617-628.

Giordano,N., Luca, F.D., Sextos, A. and P.N. Maskey, 2019, "Derivation of Fragility Curves for URM School Buildings in Nepal", 13th International Conference on Applications of Statistics and Probability in Civil Engineering, ICASP13, Seoul, South Korea.

HAZUS – MH 2.1., "Earthquake Loss Estimation Methodology", Department of Homeland Security, FEMA.

Jaishi, B., Ren, W.X., Zong, Z.H., and P.N. Maskey, 2003, "Dynamic and Seismic Performance of Old Multi-Tired Temples in Nepal", Engineering Structures 25(14):1827-1839.

Kaushik, H.B., Rai, D. C., and S. K. Jain, 2007, "Stress-Strain Characteristics of Clay Brick Masonry under Uniaxial Compression", Journal of Materials in Civil Engineering 19(9).

Khan, M., 2013, "Earthquake Resistant Structures", Elsevier Inc. *ISBN: 978-1-85617-501-2*

Lepage, A., and R. E. Sanchez, 2012, "Practical Nonlinear Analysis for Limit Design of Reinforced Masonry Walls", The open Civil Engineering Journal, 107-118.

Motra, G.B. and S. Paudel, 2021, "Performance Evaluation of Strengthening Options for Institutional Brick Masonry Buildings: A case study of Pulchowk Campus", Progress in Disaster Science 10(9).

Motra, G.B., Sah, B.K., and P. Jha, 2021, "Structural Condition Assessment and Retrofitting of Shital Niwas Building (presidential palace)", Progress in Disaster Science 10(1):100174.

National Reconstruction Authority (NRA), 2021, "A Journal of Development", Vol-I.

Parajuli, H.R., 2012, "Determination of Mechanical Properties of the Kathmandu World Heritage Brick Masonry Buildings", 15th World Conference of Earthquake Engineering (WCEE).

Pasticier, L., Amadio, C., and M. Fragiacomo, 2008, "Non-Linear Seismic Analysis and Vulnerability Evaluation of a Masonry Building by means of the SAP2000 V10

Code", Earthquake Engineering and Structural Dynamics, 37:467–485. *DOI: 10.1002/eqe.770*

Penelis, Gr. G., 2006, "An Efficient Approach for Pushover Analysis of Unreniforced Masonry (URM) Structures", Journal of Earthquake Engineering, 10:3, 359-379.

Phaiju, S., and Pradhan, P., 2018, "Experimental Work for Mechanical Properties of Brick and Masonry Panel", Journal of Science and Engineering 5, 51-57.

Remki, M., and F. Kehila, 2017, "Analytically Derived Fragility Curves and Damage Assessment of Masonry Buildings", National Center of Applied Research in Earthquake Engineering CGS, Scottsdale, USA, pp 42-54.

Rits-DMUCH (Research Center for Disaster Mitigation of Urban Cultural Heritage), 2012, "Disaster Risk Management for the Historic City of Patan", Nepal. Kyoto, Japan.

Shrestha, K.C., 2011, "Development of Seismic Retrofitting Techniques for Historical Masonry Structures with Application of High Performance Materials", Department of Architecture and Architectural Engineering, Kyoto University.

Shrestha, S., Shrestha, B., Shakya, M., and P.N. Maskey, 2017, "Damage assessment of cultural heritage structures in Nepal after 2015 Gorkha Earthquake: A Case Study of Jagannath Temple", Sage Journals, Volume: 33 issue: 1_suppl, page(s): 363-376.

Tiwari, K., Guragain, R., and H. Shrestha, 2020, "Multiple Analytical Approaches on Seismic Retrofit Design of Unreinforced Masonry Buildings in Nepal", 17th World Conference on Earthquake Engineering, 17th WCEE, Sendai, Japan.

Tomazevic, M., 1999, "Earthquake Resistant Design of Masonry Buildings", Series on Innovation in Structures and Construction – Vol. 1, Imperial College Press. *ISBN 1-86094-066-8*.

UNDP, and CBS – Nepal, 2016, "Annual Household Survey 2015/2016", United Nations Development Programme. *https://reliefweb.int/country/np*

Wen, Y., Ellingwood, B., and J. Bracci, 2004, "Vulnerability Function Framework for Consequence-based Engineering".

## APPENDIX: A

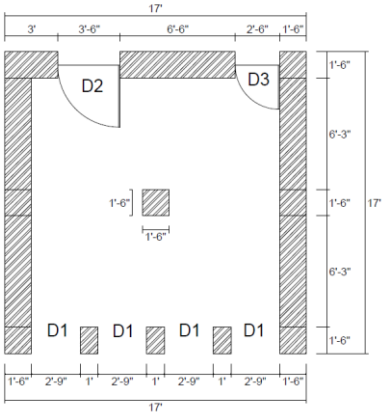


GROUND FLOOR PLAN

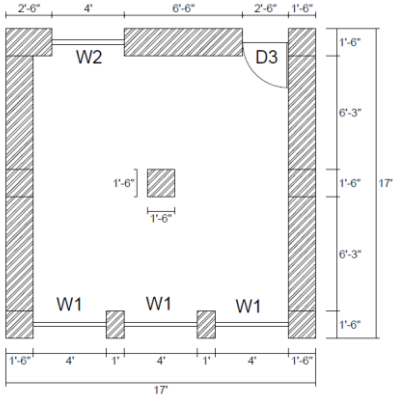


FIRST FLOOR PLAN

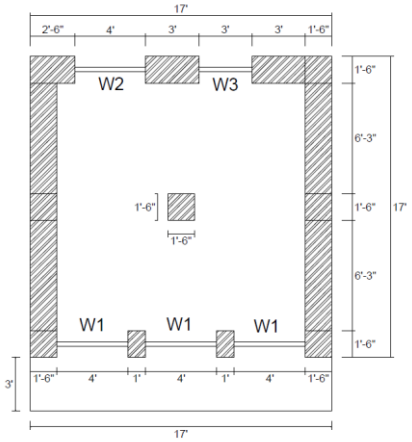


SECOND FLOOR PLAN

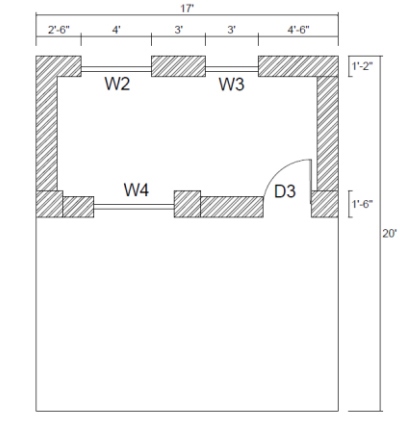


THIRD FLOOR PLAN

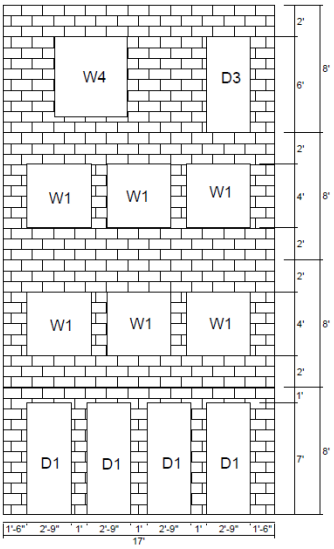


FRONT VIEW

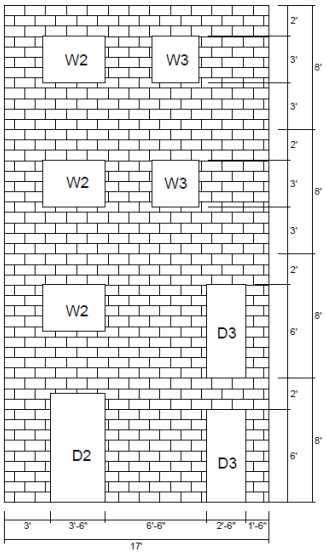


BACK SIDE VIEW

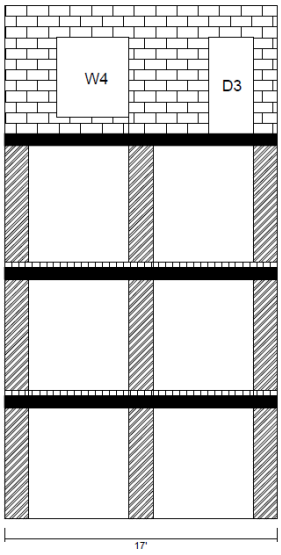


SECTIONAL VIEW

Floor Diaphragm:
4th Floor and 3rd Floor:
RCC Slab = 0.1m
RCC Beam = 0.23m X 0.3m
2nd Floor and 1st Floor :
RCC Beam = 0.23m X 0.23m
Floor Joists = 0.1m X 0.125m @ 1' 6" c/c

**Building: (A)**

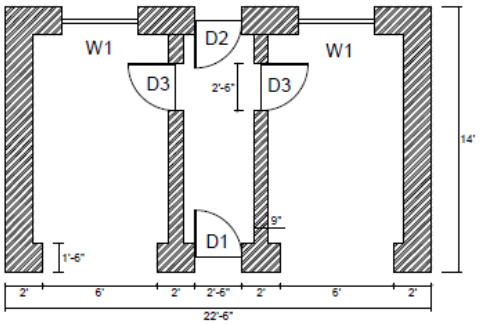


GROUND FLOOR PLAN

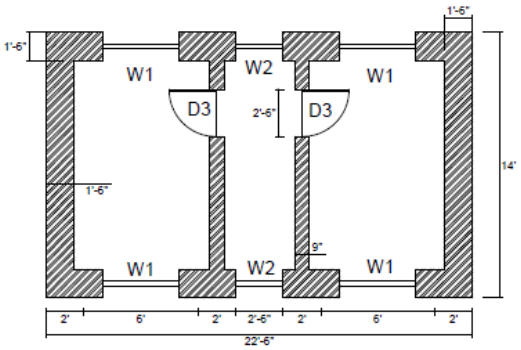


FIRST AND SECOND FLOOR PLAN

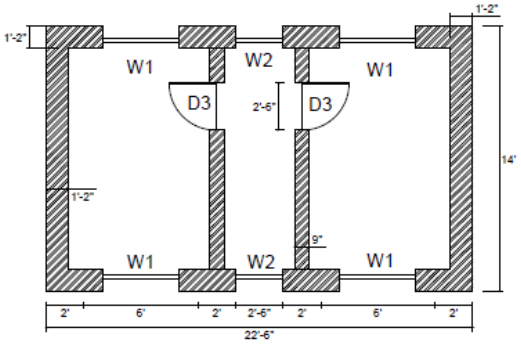


THIRD FLOOR PLAN

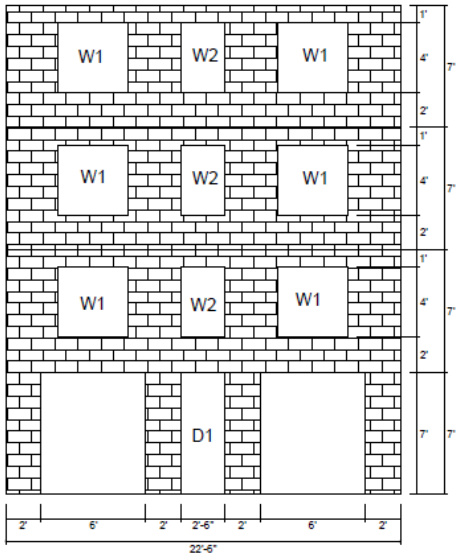


Front View

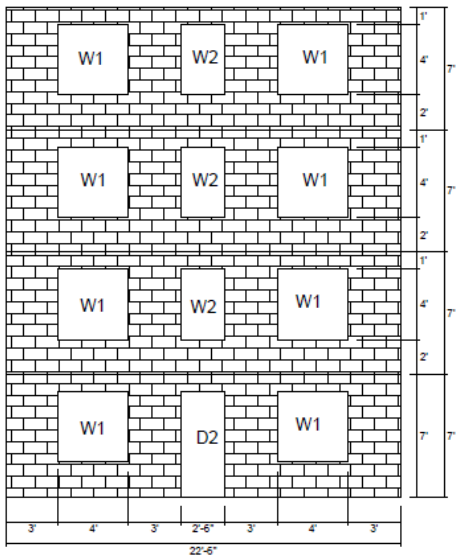


Back Side View

Floor Diaphragm:

Fourth, Third, Second and First Floor :

- Timber Beam = 0.15m x 0.175m
- Timber Post = 0.15m x 0.15m
- Floor Joists = 0.075m x 0.125m @ 2' c/c
- Roof Joists = 0.075m x 0.1m @ 2' c/c
- Wall Plate at Roof Level = 0.1m x 0.075m
- Beam above door level = 0.1m x 0.1 m
- Door Column Posts = 0.1m x 0.1m

## BUILDING: (B)

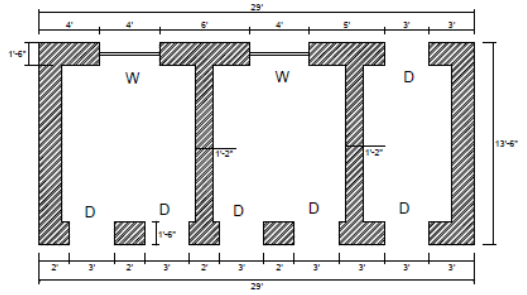


GROUND FLOOR PLAN

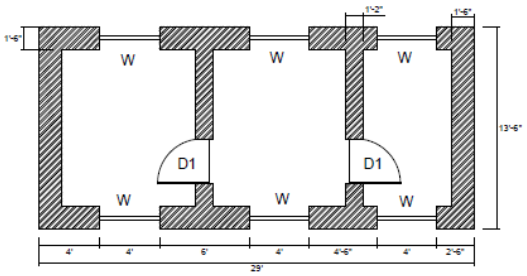


FIRST FLOOR PLAN

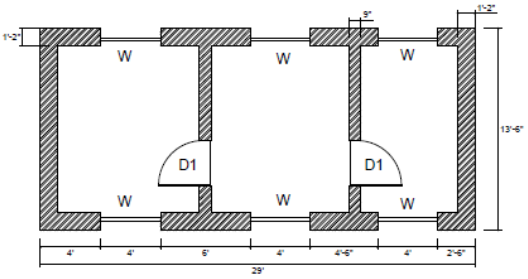


SECOND FLOOR PLAN

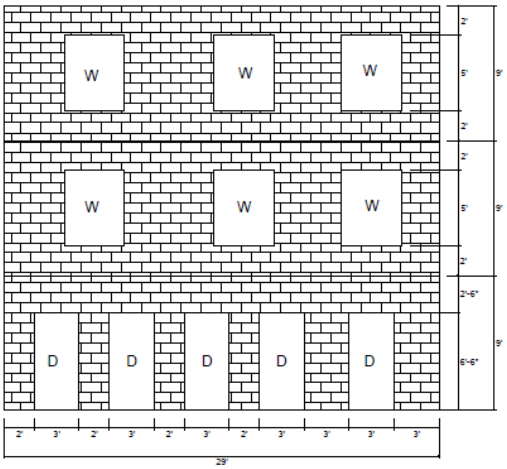


FRONT VIEW

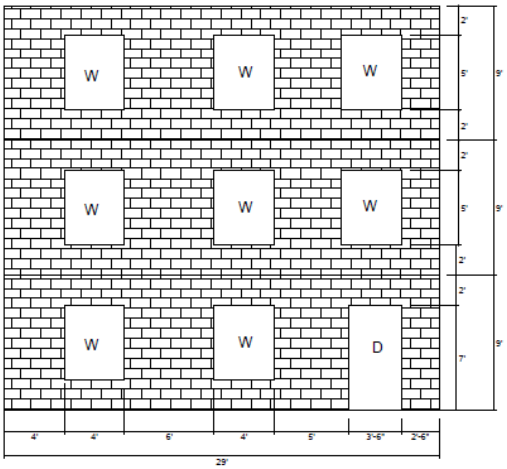


BACK SIDE VIEW

Floor Diaphragm:
3rd Floor = RCC (4")
2nd Floor = RCC (4")
1st Floor :
Timber Beam = 0.15m X 0.2m
Floor Joists = 0.075m X 0.125m @ 1' 6" c/c

## BUILDING: (C)

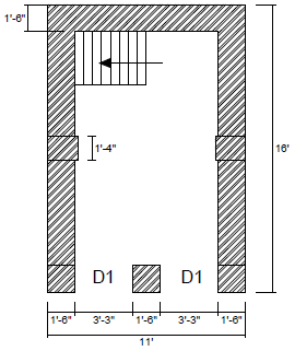


GROUND FLOOR PLAN

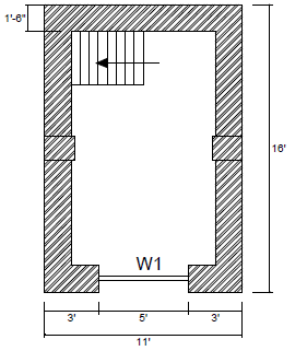


FIRST FLOOR PLAN

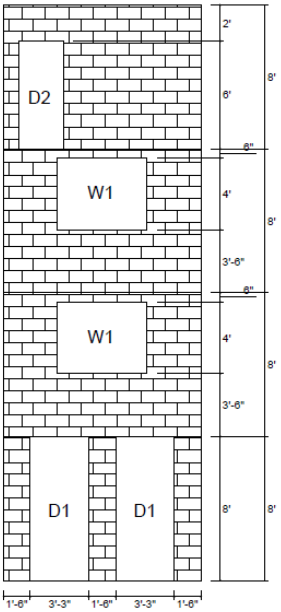


FRONT VIEW

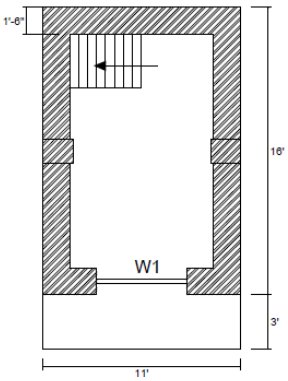


SECOND FLOOR PLAN

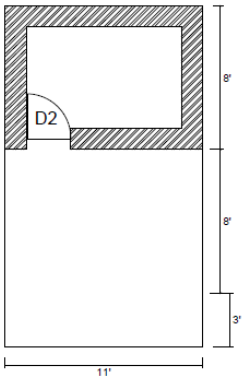


THIRD FLOOR PLAN

Floor Diaphragm:
Fourth, Third, Second and First Floor : RCC Slab (4")

## BUILDING: (D)

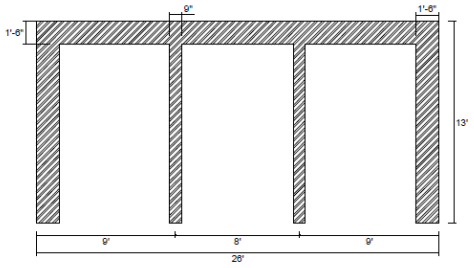


GROUND FLOOR PLAN

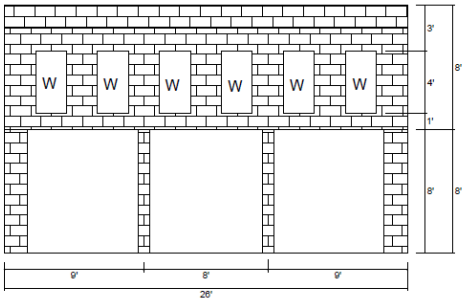


FRONT VIEW

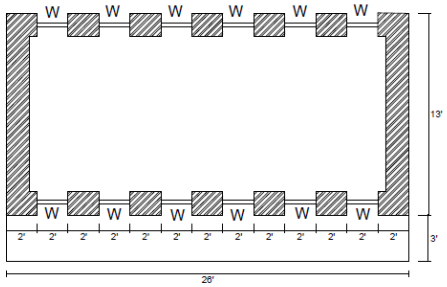


FIRST FLOOR PLAN

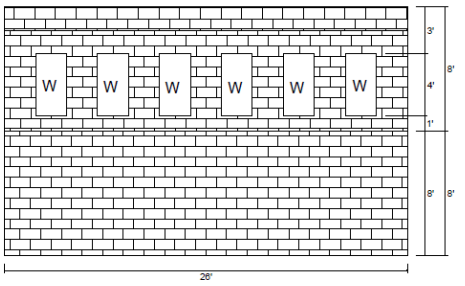


BACK VIEW

Floor Diaphragm:
Second and First Floor : RCC Slab (4")

## BUILDING: (E)

**APPENDIX: B**

The calculated link parameters are provided in SAP2000 FEM Software in the following step described below:

**Steps:**

Define/Sections Properties
Link/Support Properties
Click to: Add New Property
Link/Support Type: Multilinear Plastic
Property Name: **BMM – 9" Thick Walls - Centres**
Total Mass and Weight
Mass: 0.009444523
Weight: 0.09444523
Rotational Inertia 1: 0
Rotational Inertia 2: 0
Rotational Inertia 3: 0
Factors for Line, Area and Solid Springs
Property is defined for This Length in a Line Spring: 1
Property is defined for This Area in Area and Solid Springs: 1

Directional Properties
Select Direction **U1** and check Nonlinear
Properties: Modify/Show for U1
Properties Used for Linear Analysis Cases
Effective Stiffness: 117070 KN/m
Effective Damping: 0
Hysteresis Type and Parameters
Hysteresis Type: Kinematic
Multi-Linear Force-Deformation Definition

| Displacement(m) | Force(kN) |
|---|---|
| -0.00098 | -57.42 |
| -0.00049 | -57.42 |
| 0 | 0 |
| 0.00098 | 0 |

Select Direction **U2** and check Nonlinear
Properties: Modify/Show for U2
Properties Used for Linear Analysis Cases
Effective Stiffness: 46920 KN/m
Effective Damping: 0
Shear Deformation Location
Distance from End-J: 0
Hysteresis Type and Parameters
Hysteresis Type: Kinematic
Multi-Linear Force-Deformation Definition

| Displacement (m) | Force(kN) |
|---|---|
| -0.00098 | -5.56 |
| -0.00011 | -5.56 |
| 0 | 0 |

| | |
|---|---|
| 0.00011 | 5.56 |
| 0.00098 | 5.56 |

Select Direction **U3** and check Nonlinear
Properties: Modify/Show for U2
Properties Used for Linear Analysis Cases
Effective Stiffness: 46920 KN/m
Effective Damping: 0
Shear Deformation Location
Distance from End-J: 0
Hysteresis Type and Parameters
Hysteresis Type: Kinematic
Multi-Linear Force-Deformation Definition

| Displacement(m) | Force(kN) |
|---|---|
| -0.00098 | -5.56 |
| -0.00011 | -5.56 |
| 0 | 0 |
| 0.00011 | 5.56 |
| 0.00098 | 5.56 |

In the similar way, we carry out the repeated steps for all other link properties.

**APPENDIX: C**

As a trail and learning process the links were provided at different positions for the in-plane loading condition (along X-axis) and the output results were analyzed. This suggest us even the best positioning and minimum number of link parameters can also represent the non-linearity of the building within closer range. Thus, link parameters used in our building models are limited as minimum as possible for simplicity and runtime minimization.

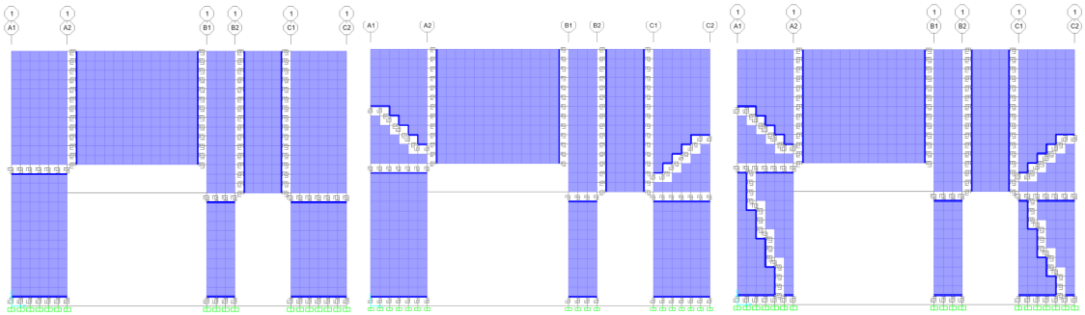

*Position 1* *Position 2* *Position 3*

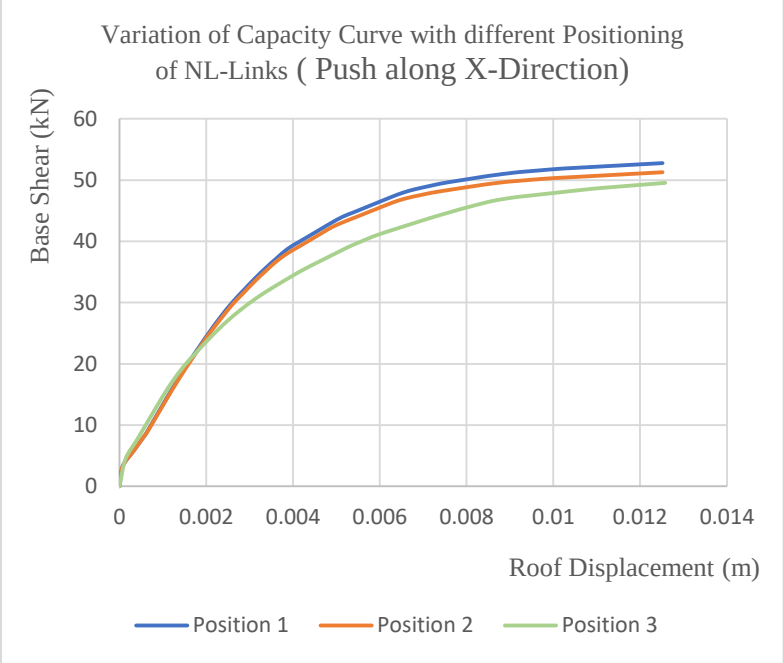

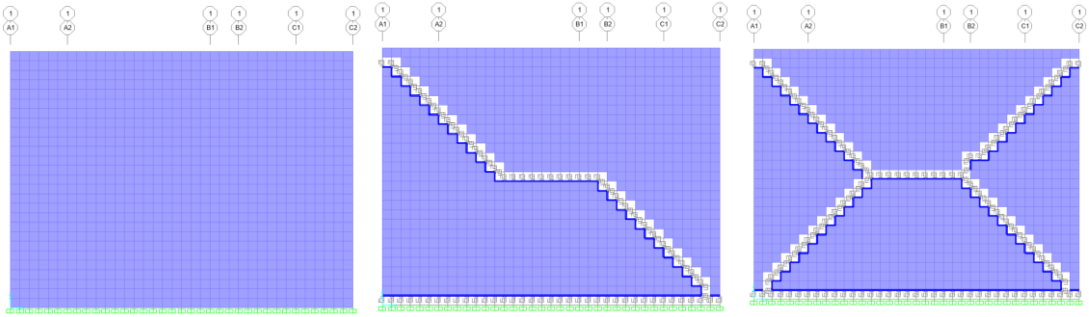

*No Links* *Position 1* *Position 2*

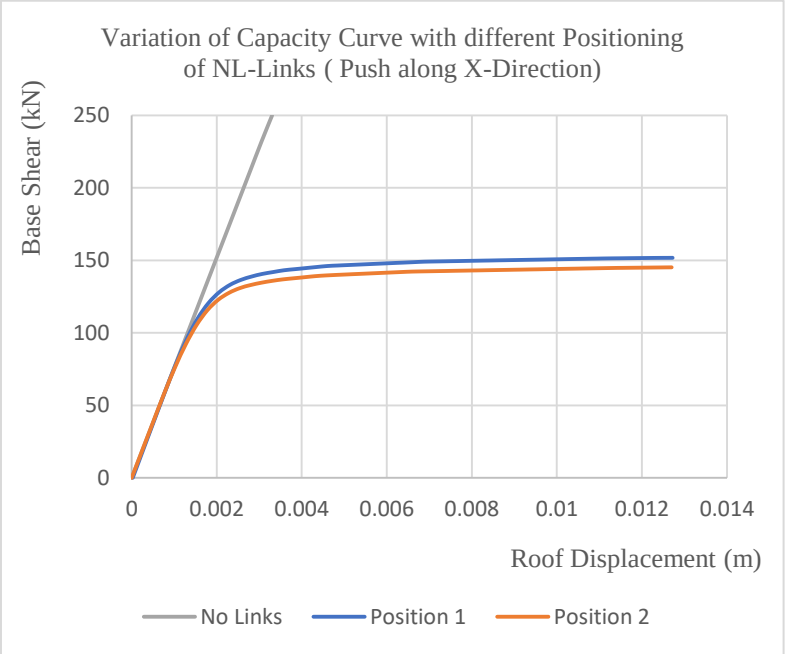

**APPENDIX: D**

Steps followed for Pushover analysis:

| Load Case | Remarks |
|---|---|
| Nonlinear Gravity | "Load Case Type: **Static**<br>Analysis Type: **Non linear**<br>Initial Conditions: Zero Initial Conditions-Start from Unstressed State<br>Modal Load Case: All Modal Loads Applied Use Modes from Case-**Modal**<br>**Loads applied**<br>Load Type: Load Pattern<br>Load Name: Dead<br>Scale Factor : 1<br>Load Type: Load Pattern22<br>Load Name: Live<br>Scale Factor : 0.25<br>Load Type: Load Pattern<br>Load Name: Floor Finish<br>Scale Factor : 1<br>**Geometric Nonlinearity parameters**-None<br>**Other Parameters**<br>Load application: Full Load<br>Results Saved: Final State Only<br>Nonlinear parameters: Default" |
| PSX | "Load Case Type: **Static**<br>Analysis Type: **Non linear**<br>Initial Conditions: Continue from State at End of Nonlinear Case – **Gravity**<br>Modal Load Case: All Modal Loads Applied Use Modes from Case-**Modal**<br>**Loads applied**<br>Load Type: Load Pattern<br>Load Name: EQX<br>Scale Factor : 1<br>**Geometric Nonlinearity Parameters:** None<br>**Other Parameters**<br>Load application<br>• Load Application Control- Displacement Control<br>• Control Displacement- Use Monitored Displacement- Load to a Monitored Displacement Magnitude of **0.08 m**<br>• Monitored Displacement- DOF **U1** at Joint **10522**<br>Results Saved<br>• Results Saved- Multiple States<br>• For Each Stage<br>Minimum Number of Saved States-150<br>Maximum Number of Saved States-200<br>Save positive Displacement increments only<br>Nonlinear Parameters: Default" |

## APPENDIX: E

| TABLE A1: Base Reactions (Building A : without links) | | | | | | | |
|---|---|---|---|---|---|---|---|
| **Output Case** | **Step** | **Global FX** | **Global FY** | **Global FZ** | **Global MX** | **Global MY** | **Global MZ** |
| Text | | KN | KN | KN | KN-m | KN-m | KN-m |
| DEAD | | -2.5E-11 | 3.1E-11 | 1488.626 | 4267.1426 | -3643.532 | 5.294E-10 |
| MODAL | 1 | -960.652 | -3.757 | 3.455 | 31.819 | -5612.811 | 1946.2849 |
| MODAL | 2 | 30.336 | -0.416 | -0.4 | -3.1809 | 218.5066 | -83.0166 |
| MODAL | 3 | 1871.442 | -7.262 | -7.314 | -15.6431 | 11788.94 | -4318.23 |
| MODAL | 4 | 28.052 | 36.062 | 122.172 | -232.2858 | 21.7697 | 11.0509 |
| MODAL | 5 | -12.521 | -23.14 | -70.409 | 161.4866 | -105.4916 | -7.9279 |
| MODAL | 6 | -79.807 | 5648.254 | -46.832 | -40116.69 | -232.722 | 14695.477 |
| MODAL | 7 | 1473.274 | 248.856 | 17.547 | -2397.834 | 21124.103 | -31315.47 |
| MODAL | 8 | -6149.80 | -294.156 | -168.569 | 1819.2477 | 4419.0183 | 30228.925 |
| MODAL | 9 | 1994.392 | 4841.528 | -262.975 | -4129.779 | -13193.64 | 12902.994 |
| MODAL | 10 | 426.192 | -16402.9 | 3629.616 | 18904.002 | -17530.96 | -37720.91 |
| MODAL | 11 | -681.586 | 3405.976 | 34485 | 97500.64 | -102642.3 | 8369.284 |
| MODAL | 12 | 1020.89 | -74.084 | 26905.86 | 81538.20 | -37098.52 | 2971.4726 |
| LIVE | | -5.43E-12 | 5.49E-11 | 192.338 | 494.6958 | -457.7854 | 3.007E-10 |
| FLOOR FINISH | | -2.89E-12 | 2.27E-11 | 46.022 | 117.9954 | -111.1113 | 5.084E-11 |
| EQx | | -471.887 | -2.9E-10 | 9.1E-11 | 3.394E-09 | -3406.805 | 1488.2139 |
| EQy | | -4.71E-11 | -471.887 | 1.75E-10 | 3406.8051 | -1.11E-09 | -1193.227 |

| TABLE A2: Base Reactions (Building A : with links) | | | | | | | |
|---|---|---|---|---|---|---|---|
| **Output Case** | **Step** | **Global FX** | **Global FY** | **Global FZ** | **Global MX** | **Global MY** | **Global MZ** |
| Text | | KN | KN | KN | KN-m | KN-m | KN-m |
| DEAD | | 0.00002 | 2.26E-11 | 1486.31 | 4255.546 | -3638.48 | -0.000044 |
| MODAL | 1 | -1755.05 | 3.144 | 5.692 | 7.4528 | -10407.68 | 3846.0027 |
| MODAL | 2 | 22.818 | -6.393 | -0.539 | 16.2116 | 221.9557 | -113.4088 |
| MODAL | 3 | -321.719 | 20.954 | 1.34 | -66.1172 | -2314.056 | 980.4965 |
| MODAL | 4 | 9.667 | 19.546 | 135.441 | -116.7099 | -59.6013 | 14.2044 |
| MODAL | 5 | 4.482 | 2.802 | -5.462 | 7.5965 | -69.668 | 1.0687 |
| MODAL | 6 | -72.218 | 5640.085 | -52.199 | -39559.08 | -283.9016 | 14836.52 |
| MODAL | 7 | 903.458 | 239.319 | -0.603 | -2703.68 | 20918.872 | -23579.58 |
| MODAL | 8 | -4608.54 | -694.321 | -119.59 | 1806.6001 | 1341.3461 | 29881.31 |
| MODAL | 9 | 533.404 | -5462.32 | 86.718 | -2364.89 | -1876.403 | -17216.40 |
| MODAL | 10 | 91.114 | 1094.562 | -456.642 | -884.4301 | 16252.315 | -6481.069 |
| MODAL | 11 | 3442.525 | -898.956 | -575.737 | -152.3789 | 9950.1708 | -3410.652 |
| MODAL | 12 | -89.445 | 10501.33 | -10484.2 | -36910.24 | 28043.834 | 23083.416 |
| LIVE | | 0.000004 | 5.61E-11 | 192.338 | 494.6958 | -457.7854 | -0.000009 |
| FLOOR FINISH | | 7.21E-07 | 2.23E-11 | 46.022 | 117.9954 | -111.1113 | -0.000001 |
| EQx | | -471.189 | -4.0E-10 | -1.5E-08 | -5.74E-07 | -3403.001 | 1485.0812 |
| EQy | | 0.000022 | -471.192 | -8.2E-07 | 3403.0239 | 0.0001784 | -1191.109 |

| TABLE A3: Modal Participating Mass Ratios (Building A : without links) | | | | | | |
|---|---|---|---|---|---|---|
| **StepType** | **StepNum** | **Period** | **UX** | **UY** | **SumUX** | **SumUY** |
| Text | Unitless | Sec | Unitless | Unitless | Unitless | Unitless |
| Mode | 1 | 0.467681 | 0.17661 | 0.000002701 | 0.17661 | 0.000002701 |
| Mode | 2 | 0.46515 | 0.00017 | 3.243E-08 | 0.17678 | 0.000002733 |
| Mode | 3 | 0.454721 | 0.59898 | 0.000009021 | 0.77577 | 0.00001175 |
| Mode | 4 | 0.37981 | 0.0000655 | 0.00011 | 0.77583 | 0.00012 |
| Mode | 5 | 0.374389 | 0.00001232 | 0.00004208 | 0.77584 | 0.00016 |
| Mode | 6 | 0.270028 | 0.00014 | 0.6785 | 0.77598 | 0.67866 |
| Mode | 7 | 0.201723 | 0.01438 | 0.00041 | 0.79036 | 0.67907 |
| Mode | 8 | 0.156924 | 0.09174 | 0.00021 | 0.8821 | 0.67928 |
| Mode | 9 | 0.10956 | 0.00229 | 0.01351 | 0.88439 | 0.69279 |
| Mode | 10 | 0.10819 | 0.00009955 | 0.14746 | 0.88449 | 0.84025 |
| Mode | 11 | 0.093208 | 0.00014 | 0.0035 | 0.88463 | 0.84375 |
| Mode | 12 | 0.091596 | 0.00029 | 0.000001546 | 0.88492 | 0.84375 |

| TABLE A4: Modal Participating Mass Ratios (Building A : with links) | | | | | | |
|---|---|---|---|---|---|---|
| **StepType** | **StepNum** | **Period** | **UX** | **UY** | **SumUX** | **SumUY** |
| Text | Unitless | Sec | Unitless | Unitless | Unitless | Unitless |
| Mode | 1 | 0.503553 | 0.7934 | 0.000002545 | 0.7934 | 0.000002545 |
| Mode | 2 | 0.465596 | 0.00009802 | 0.000007693 | 0.7935 | 0.00001024 |
| Mode | 3 | 0.464712 | 0.01934 | 0.00008204 | 0.81283 | 0.00009228 |
| Mode | 4 | 0.386924 | 0.000008392 | 0.00003431 | 0.81284 | 0.00013 |
| Mode | 5 | 0.377318 | 0.000001631 | 6.377E-07 | 0.81284 | 0.00013 |
| Mode | 6 | 0.271867 | 0.00011 | 0.69618 | 0.81296 | 0.69631 |
| Mode | 7 | 0.216091 | 0.00713 | 0.0005 | 0.82009 | 0.69681 |
| Mode | 8 | 0.17782 | 0.08507 | 0.00193 | 0.90516 | 0.69874 |
| Mode | 9 | 0.153365 | 0.00063 | 0.06613 | 0.90579 | 0.76486 |
| Mode | 10 | 0.118448 | 0.000006543 | 0.00094 | 0.9058 | 0.76581 |
| Mode | 11 | 0.113199 | 0.0078 | 0.00053 | 0.91359 | 0.76634 |
| Mode | 12 | 0.101758 | 0.000003438 | 0.04737 | 0.91359 | 0.81371 |

| TABLE B1: Base Reactions (Building B : without links) | | | | | | | |
|---|---|---|---|---|---|---|---|
| **Output Case** | **Step** | **Global FX** | **Global FY** | **Global FZ** | **Global MX** | **Global MY** | **Global MZ** |
| Text | | KN | KN | KN | KN-m | KN-m | KN-m |
| DEAD | | 2.79E-12 | 1.97E-12 | 1451.59 | 3158.781 | -4977.57 | -3.1E-12 |
| MODAL | 1 | -4348.54 | -0.147 | -0.11 | 0.7854 | -24041.4 | 7982.616 |
| MODAL | 2 | -0.023 | 7260.369 | 26.05 | -43977.4 | -88.2538 | 24906.68 |
| MODAL | 3 | 1189.161 | -8.678 | 0.326 | 56.0346 | 7947.561 | -3457.75 |
| MODAL | 4 | -965.499 | -3.657 | 0.58 | 27.8915 | -8145.97 | 45537.27 |
| MODAL | 5 | -15.541 | -4941.69 | 542.062 | 35517.46 | -1865.23 | -16904.9 |
| MODAL | 6 | 9670.715 | -12.255 | 1.96 | 79.4508 | -14306.8 | -28572.8 |
| MODAL | 7 | -1769.02 | -13.108 | 2.421 | -35.3259 | -32398.6 | 7627.903 |
| MODAL | 8 | 1270.16 | 85.607 | -9.849 | -63.5072 | -4544.33 | 4690.371 |
| MODAL | 9 | -1447.12 | 303.755 | -27.803 | -125.782 | -12129.2 | -31061.2 |
| MODAL | 10 | 19.718 | 29704.28 | -2666.9 | -12520.9 | 9265.518 | 102276.1 |
| MODAL | 11 | 14265.1 | -28.722 | -3.414 | -45.3346 | 11379.65 | -25155.7 |
| MODAL | 12 | 1137.123 | -137.097 | 8.587 | -87.4392 | -46607.3 | 74963.17 |
| LIVE | | 5.64E-13 | 7.76E-13 | 138.257 | 278.5976 | -475.255 | 6.13E-12 |
| FLOOR FINISH | | 3.02E-13 | 4.16E-13 | 74.083 | 149.2819 | -254.657 | 3.27E-12 |
| EQx | | -464.174 | 1.3E-12 | -4.3E-11 | -1.5E-10 | -2896.07 | 997.9028 |
| EQy | | 7.41E-13 | -464.174 | 5.8E-12 | 2896.066 | -6.2E-13 | -1617.46 |

| TABLE B2: Base Reactions (Building B : with links) | | | | | | | |
|---|---|---|---|---|---|---|---|
| **Output Case** | **Step** | **Global FX** | **Global FY** | **Global FZ** | **Global MX** | **Global MY** | **Global MZ** |
| Text | | KN | KN | KN | KN-m | KN-m | KN-m |
| DEAD | | 2.4E-09 | 2.86E-12 | 1451.809 | 3168.126 | -4978.55 | -2.8E-09 |
| MODAL | 1 | 3970.565 | 0.424 | 0.138 | -1.7925 | 21517.54 | -7296 |
| MODAL | 2 | -6.2 | 6914.764 | 37.773 | -41679 | -165.972 | 23725.85 |
| MODAL | 3 | 1329.544 | 34.227 | -0.863 | -205.956 | 8544.815 | -3942.06 |
| MODAL | 4 | -741.733 | 21.195 | -2.794 | -123.6 | -7041.16 | 40792.36 |
| MODAL | 5 | 9.631 | 5398.92 | -335.426 | -35723.6 | 1166.382 | 18319.61 |
| MODAL | 6 | -6479.61 | 16.505 | -8.757 | -61.7517 | 14744.18 | 12019.25 |
| MODAL | 7 | -4355.54 | -15.959 | 18.93 | -12.0928 | 2391.129 | 29805.06 |
| MODAL | 8 | 3435.237 | -63.629 | 20.329 | 67.2447 | 27222.58 | -12396.7 |
| MODAL | 9 | -5943.78 | -100.335 | 16.084 | 102.468 | -1668.22 | 22455.27 |
| MODAL | 10 | -5381.36 | 308.54 | -34.729 | -25.2708 | -14434.8 | -15731.4 |
| MODAL | 11 | -68.37 | -26553 | 1561.302 | 5736.709 | -5791.15 | -91421.8 |
| MODAL | 12 | 944.755 | 715.97 | -126.69 | -1050.14 | -22762.2 | 51587.59 |
| LIVE | | -2E-10 | 5.45E-13 | 138.257 | 278.5976 | -475.255 | 1.16E-09 |
| FLOOR FINISH | | -1.1E-10 | 2.92E-13 | 74.083 | 149.2819 | -254.657 | 6.21E-10 |
| EQx | | -464.332 | -7E-13 | 8.31E-08 | 3.33E-08 | -2891.6 | 984.1575 |
| EQy | | 7.23E-09 | -464.332 | -7.6E-08 | 2891.605 | 7E-07 | -1592.48 |

| TABLE B3: Modal Participating Mass Ratios (Building B : without links) | | | | | | |
|---|---|---|---|---|---|---|
| **StepType** | **Step** | **Period** | **UX** | **UY** | **SumUX** | **SumUY** |
| Text | | Sec | Unitless | Unitless | Unitless | Unitless |
| Mode | 1 | 0.316575 | 0.77238 | 8.86E-10 | 0.77238 | 8.86E-10 |
| Mode | 2 | 0.234376 | 5.82E-12 | 0.64686 | 0.77238 | 0.64686 |
| Mode | 3 | 0.204732 | 0.0101 | 5.38E-07 | 0.78249 | 0.64686 |
| Mode | 4 | 0.170943 | 0.00324 | 4.63E-08 | 0.78573 | 0.64686 |
| Mode | 5 | 0.137412 | 3.5E-07 | 0.03541 | 0.78573 | 0.68227 |
| Mode | 6 | 0.118886 | 0.07598 | 1.22E-07 | 0.8617 | 0.68227 |
| Mode | 7 | 0.091245 | 0.00088 | 4.83E-08 | 0.86258 | 0.68227 |
| Mode | 8 | 0.088431 | 0.0004 | 1.82E-06 | 0.86298 | 0.68227 |
| Mode | 9 | 0.081369 | 0.00037 | 1.64E-05 | 0.86336 | 0.68229 |
| Mode | 10 | 0.080824 | 6.75E-08 | 0.15312 | 0.86336 | 0.83541 |
| Mode | 11 | 0.075122 | 0.02636 | 1.07E-07 | 0.88971 | 0.83541 |
| Mode | 12 | 0.067085 | 0.00011 | 1.55E-06 | 0.88982 | 0.83541 |

| TABLE B4: Modal Participating Mass Ratios (Building B : with links) | | | | | | |
|---|---|---|---|---|---|---|
| **StepType** | **Step** | **Period** | **UX** | **UY** | **SumUX** | **SumUY** |
| Text | | Sec | Unitless | Unitless | Unitless | Unitless |
| Mode | 1 | 0.33238 | 0.78224 | 8.93E-09 | 0.78224 | 8.93E-09 |
| Mode | 2 | 0.236838 | 4.92E-07 | 0.61158 | 0.78224 | 0.61158 |
| Mode | 3 | 0.226733 | 0.01899 | 1.26E-05 | 0.80123 | 0.61159 |
| Mode | 4 | 0.177136 | 0.0022 | 1.8E-06 | 0.80343 | 0.6116 |
| Mode | 5 | 0.157793 | 2.34E-07 | 0.07346 | 0.80343 | 0.68506 |
| Mode | 6 | 0.132274 | 0.05225 | 3.39E-07 | 0.85568 | 0.68506 |
| Mode | 7 | 0.128901 | 0.02129 | 2.86E-07 | 0.87698 | 0.68506 |
| Mode | 8 | 0.09847 | 0.00451 | 1.55E-06 | 0.88149 | 0.68506 |
| Mode | 9 | 0.090983 | 0.00984 | 2.8E-06 | 0.89133 | 0.68506 |
| Mode | 10 | 0.088098 | 0.00709 | 2.33E-05 | 0.89842 | 0.68509 |
| Mode | 11 | 0.083257 | 9.13E-07 | 0.13772 | 0.89842 | 0.82281 |
| Mode | 12 | 0.073691 | 0.00011 | 6.14E-05 | 0.89853 | 0.82287 |

| TABLE C1: Base Reactions (Building C : without links) | | | | | | | |
|---|---|---|---|---|---|---|---|
| **Output Case** | **Step** | **Global FX** | **Global FY** | **Global FZ** | **Global MX** | **Global MY** | **Global MZ** |
| Text | | KN | KN | KN | KN-m | KN-m | KN-m |
| DEAD | | 9.2E-12 | -1.5E-10 | 1905.873 | 3963.835 | -8521.12 | 2.03E-09 |
| MODAL | 1 | 6697.483 | -67.506 | -2.029 | 415.1945 | 39010.3 | -10708.2 |
| MODAL | 2 | -94.116 | -7522.09 | -71.633 | 48413.44 | -467.52 | -32826.5 |
| MODAL | 3 | -1837.59 | 200.197 | -71.971 | -1691.32 | -16022.1 | 60371.55 |
| MODAL | 4 | -15508.3 | -392.883 | -121.908 | 1099.177 | 47671.77 | 42525.5 |
| MODAL | 5 | 551.172 | -38587.3 | -1342.3 | 18067.97 | 7416.914 | -162306 |
| MODAL | 6 | -528.662 | -1496.67 | 83165.99 | 170851 | -345533 | -1985.27 |
| MODAL | 7 | 913.833 | 439.695 | -6628.11 | -11286.5 | 180211.2 | -2277 |
| MODAL | 8 | -2174.47 | -4657.08 | -3764.68 | -4775.41 | 9523.246 | -71037.3 |
| MODAL | 9 | -2180.71 | -6881.75 | 1462.877 | 7623.958 | 5618.702 | -118647 |
| MODAL | 10 | 7393.869 | -821.773 | 8375.723 | 20952.53 | -97662.8 | -106337 |
| MODAL | 11 | 423.558 | 93.891 | -13278.5 | -26979.8 | 259870.2 | -18359.2 |
| MODAL | 12 | -446.253 | 3571.343 | -3688.28 | -34957.8 | 11655.01 | -35973.2 |
| LIVE | | 5.21E-12 | 1.11E-11 | 245.958 | 506.033 | -1083.57 | 4.11E-10 |
| FLOOR FINISH | | 2.59E-12 | 5.97E-12 | 125.941 | 259.1119 | -554.729 | 2.12E-10 |
| EQx | | -747.631 | 4.81E-11 | -2.8E-11 | -5.9E-10 | -4334.68 | 1598.476 |
| EQy | | 5.69E-11 | -747.631 | 2.89E-11 | 4334.681 | 7.18E-10 | -3440.21 |

| TABLE C2: Base Reactions (Building C : with links) | | | | | | | |
|---|---|---|---|---|---|---|---|
| **Output Case** | **Step** | **Global FX** | **Global FY** | **Global FZ** | **Global MX** | **Global MY** | **Global MZ** |
| Text | | KN | KN | KN | KN-m | KN-m | KN-m |
| DEAD | | 1.5E-07 | 5.87E-11 | 1915.796 | 3989.2 | -8566.31 | -4.9E-06 |
| MODAL | 1 | 6610.376 | -49.863 | -2.45 | 318.6739 | 37288.27 | -9530.66 |
| MODAL | 2 | -84.667 | -7543.09 | -73.345 | 48371.38 | -468.637 | -32813.1 |
| MODAL | 3 | 2902.512 | -263.01 | 108.679 | 2407.319 | 22174.04 | -65119.4 |
| MODAL | 4 | -9700.09 | -442.749 | 76.203 | 1608.576 | 41634.4 | 27141.44 |
| MODAL | 5 | -1152.08 | 26218.67 | 363.007 | -12679 | -8053.09 | 90792.76 |
| MODAL | 6 | 562.778 | 22222.8 | 135.946 | -14570.8 | 4952.299 | 124968.6 |
| MODAL | 7 | -6604.37 | 909.259 | 10332.72 | 24300.68 | 70985.58 | 17434.53 |
| MODAL | 8 | -1901.32 | 445.937 | -61917.3 | -125349 | 279209.7 | -523.558 |
| MODAL | 9 | -1669.04 | -1522.52 | 51917.31 | 105933.8 | -225265 | -2797.73 |
| MODAL | 10 | -952.236 | -4292.37 | -656.114 | 31.3603 | 21577.56 | -33091 |
| MODAL | 11 | 3856.556 | 12797.19 | 5469.62 | 13562.29 | -40489.5 | 101500.1 |
| MODAL | 12 | 612.401 | -1284.88 | 13678.9 | 28328.14 | -140261 | -26306.3 |
| LIVE | | 4.01E-07 | -3.5E-12 | 245.958 | 506.033 | -1083.57 | -2E-06 |
| FLOOR FINISH | | 1.99E-07 | -1.9E-12 | 125.941 | 259.1119 | -554.729 | -9.9E-07 |
| EQx | | -625.717 | 6.53E-11 | -3.8E-08 | -2.9E-07 | -4083.91 | 1350.769 |
| EQy | | 1.29E-05 | -625.719 | -8.6E-09 | 4083.925 | 0.000109 | -2892.81 |

| TABLE C3: Modal Participating Mass Ratios (Building C : without links) | | | | | | |
|---|---|---|---|---|---|---|
| **StepType** | **Step** | **Period** | **UX** | **UY** | **SumUX** | **SumUY** |
| Text | | Sec | Unitless | Unitless | Unitless | Unitless |
| Mode | 1 | 0.276139 | 0.79022 | 8.03E-05 | 0.79022 | 8.03E-05 |
| Mode | 2 | 0.249542 | 0.0001 | 0.66477 | 0.79032 | 0.66485 |
| Mode | 3 | 0.173643 | 0.0093 | 0.00011 | 0.79962 | 0.66496 |
| Mode | 4 | 0.104198 | 0.0859 | 5.51E-05 | 0.88552 | 0.66501 |
| Mode | 5 | 0.081426 | 4.05E-05 | 0.19832 | 0.88556 | 0.86333 |
| Mode | 6 | 0.07679 | 2.94E-05 | 0.00024 | 0.88559 | 0.86357 |
| Mode | 7 | 0.071876 | 6.75E-05 | 1.56E-05 | 0.88566 | 0.86358 |
| Mode | 8 | 0.068847 | 0.00032 | 0.00148 | 0.88598 | 0.86506 |
| Mode | 9 | 0.068173 | 0.00031 | 0.0031 | 0.88629 | 0.86816 |
| Mode | 10 | 0.064685 | 0.0029 | 3.58E-05 | 0.88919 | 0.86819 |
| Mode | 11 | 0.06299 | 8.56E-06 | 4.2E-07 | 0.8892 | 0.86819 |
| Mode | 12 | 0.061284 | 8.51E-06 | 0.00055 | 0.88921 | 0.86874 |

| TABLE C4: Modal Participating Mass Ratios (Building C : with links) | | | | | | |
|---|---|---|---|---|---|---|
| **StepType** | **Step** | **Period** | **UX** | **UY** | **SumUX** | **SumUY** |
| Text | | Sec | Unitless | Unitless | Unitless | Unitless |
| Mode | 1 | 0.280116 | 0.81162 | 4.62E-05 | 0.81162 | 4.62E-05 |
| Mode | 2 | 0.24976 | 8.42E-05 | 0.66793 | 0.8117 | 0.66798 |
| Mode | 3 | 0.170471 | 0.02146 | 0.00018 | 0.83316 | 0.66816 |
| Mode | 4 | 0.117808 | 0.05468 | 0.00011 | 0.88784 | 0.66827 |
| Mode | 5 | 0.088123 | 0.00024 | 0.12506 | 0.88808 | 0.79333 |
| Mode | 6 | 0.082074 | 4.34E-05 | 0.0676 | 0.88812 | 0.86093 |
| Mode | 7 | 0.079335 | 0.00521 | 9.88E-05 | 0.89334 | 0.86103 |
| Mode | 8 | 0.077817 | 0.0004 | 2.2E-05 | 0.89374 | 0.86106 |
| Mode | 9 | 0.076407 | 0.00029 | 0.00024 | 0.89402 | 0.86129 |
| Mode | 10 | 0.070719 | 6.84E-05 | 0.00139 | 0.89409 | 0.86268 |
| Mode | 11 | 0.070446 | 0.00111 | 0.01217 | 0.8952 | 0.87485 |
| Mode | 12 | 0.068968 | 2.56E-05 | 0.00011 | 0.89522 | 0.87496 |

| TABLE D1: Base Reactions (Building D : without links) | | | | | | | |
|---|---|---|---|---|---|---|---|
| **Output Case** | **Step** | **Global FX** | **Global FY** | **Global FZ** | **Global MX** | **Global MY** | **Global MZ** |
| Text | | KN | KN | KN | KN-m | KN-m | KN-m |
| DEAD | | 1.41E-11 | 3.06E-11 | 1314.299 | 3570.479 | -2211.39 | 4.3E-10 |
| MODAL | 1 | -3299.23 | -7.162 | -5.046 | 41.1038 | -20683.2 | 7830.502 |
| MODAL | 2 | 18.648 | -6257.61 | -59.465 | 43028.72 | 260.7041 | -10687 |
| MODAL | 3 | -936.996 | 93.18 | 51.223 | -399.785 | 17722.16 | -29832.3 |
| MODAL | 4 | -15087.1 | -397.04 | 1692.966 | 5418.131 | -10014 | 70424 |
| MODAL | 5 | 1237.269 | -25298.3 | 10279.16 | 50582.75 | -18169.4 | -47737.4 |
| MODAL | 6 | 2696.951 | 8684.326 | 63182.14 | 168578.1 | -108344 | 4225.758 |
| MODAL | 7 | -14385.6 | -3959.83 | 18441.08 | 49906.56 | -45017 | 10667.56 |
| MODAL | 8 | -3119.08 | -25931.6 | 31833.95 | 73342.03 | -27358 | 1085.897 |
| MODAL | 9 | -14243.4 | 19188.71 | -69.245 | 12907.39 | 35575.91 | 131327.5 |
| MODAL | 10 | -18962.4 | -7943.2 | -11761 | -44177.3 | 57930.61 | 19539.08 |
| MODAL | 11 | -10852.3 | -8324.24 | -12312.7 | -57759.1 | -54761.4 | 83332.85 |
| MODAL | 12 | 1993.494 | 17295.44 | -387.707 | -54989.2 | 7841.788 | 13621.44 |
| LIVE | | -2.7E-13 | 2.38E-11 | 132.851 | 305.5671 | -222.712 | 2.05E-10 |
| FLOOR FINISH | | -1.4E-13 | 1.19E-11 | 66.426 | 152.7835 | -111.356 | 1.03E-10 |
| EQx | | -421.319 | 7.29E-10 | 6.21E-11 | -5.3E-09 | -2965.71 | 1254.712 |
| EQy | | 4.25E-10 | -421.319 | -2.7E-11 | 2965.706 | 3.01E-09 | -734.877 |

| TABLE D2: Base Reactions (Building D : with links) | | | | | | | |
|---|---|---|---|---|---|---|---|
| **Output Case** | **Step** | **Global FX** | **Global FY** | **Global FZ** | **Global MX** | **Global MY** | **Global MZ** |
| Text | | KN | KN | KN | KN-m | KN-m | KN-m |
| DEAD | | 2.6E-07 | 1.86E-11 | 1313.849 | 3569.38 | -2210.43 | -9.5E-07 |
| MODAL | 1 | 3233.62 | 18.461 | 4.559 | -120.712 | 20021.2 | -7472.33 |
| MODAL | 2 | -45.306 | 6168.606 | 23.459 | -42518.6 | -364.319 | 10607.31 |
| MODAL | 3 | 823.037 | -97.53 | -55.473 | 397.591 | -19330.4 | 28136.59 |
| MODAL | 4 | 14830.62 | 408.097 | -1704.56 | -5486.35 | 11302.11 | -71466.6 |
| MODAL | 5 | -1279.84 | 25627.02 | -8496.81 | -46144.2 | 15132.9 | 48474.71 |
| MODAL | 6 | 3063.397 | 7751.999 | 61132.64 | 161772.9 | -105122 | 1450.254 |
| MODAL | 7 | -13379.8 | -3192.24 | 20767.92 | 56097.27 | -41290.7 | 11395.67 |
| MODAL | 8 | -3481.39 | -25521.8 | 29717.7 | 68927.57 | -25090 | 4618.238 |
| MODAL | 9 | -9520.89 | 14829.95 | 5075.352 | 19342.06 | 19154.19 | 96879.11 |
| MODAL | 10 | -9198.59 | 13637.29 | -4934.27 | -334.405 | 29201.08 | 85610.76 |
| MODAL | 11 | -19340.7 | -7167.36 | -14410 | -46370.4 | 52813.76 | 34227.72 |
| MODAL | 12 | 1644.203 | 6709.4 | -8294.14 | -6094.68 | 7492.623 | 16018.96 |
| LIVE | | -7.1E-08 | -1.4E-12 | 132.851 | 305.5671 | -222.712 | 3.09E-08 |
| FLOOR FINISH | | -3.5E-08 | -7.1E-13 | 66.426 | 152.7835 | -111.356 | 1.55E-08 |
| EQx | | -421.142 | 6.65E-10 | 2E-07 | 9.42E-07 | -2964.76 | 1254.205 |
| EQy | | 2.97E-06 | -421.142 | 8.89E-08 | 2964.757 | 1.37E-05 | -734.706 |

| TABLE D3: Modal Participating Mass Ratios (Building D : without links) | | | | | | |
|---|---|---|---|---|---|---|
| **StepType** | **Step** | **Period** | **UX** | **UY** | **SumUX** | **SumUY** |
| Text | | Sec | Unitless | Unitless | Unitless | Unitless |
| Mode | 1 | 0.351987 | 0.74859 | 3.53E-06 | 0.74859 | 3.53E-06 |
| Mode | 2 | 0.247735 | 5.87E-06 | 0.66081 | 0.74859 | 0.66082 |
| Mode | 3 | 0.163224 | 0.00279 | 2.76E-05 | 0.75138 | 0.66084 |
| Mode | 4 | 0.107333 | 0.13535 | 9.37E-05 | 0.88673 | 0.66094 |
| Mode | 5 | 0.087646 | 0.0004 | 0.16921 | 0.88714 | 0.83014 |
| Mode | 6 | 0.079492 | 0.0013 | 0.01349 | 0.88844 | 0.84364 |
| Mode | 7 | 0.064593 | 0.01614 | 0.00122 | 0.90458 | 0.84486 |
| Mode | 8 | 0.05821 | 0.0005 | 0.03459 | 0.90508 | 0.87945 |
| Mode | 9 | 0.054807 | 0.0082 | 0.01489 | 0.91328 | 0.89433 |
| Mode | 10 | 0.045874 | 0.00713 | 0.00125 | 0.92042 | 0.89559 |
| Mode | 11 | 0.044058 | 0.00199 | 0.00117 | 0.92241 | 0.89676 |
| Mode | 12 | 0.042676 | 5.91E-05 | 0.00445 | 0.92246 | 0.9012 |

| TABLE D4: Modal Participating Mass Ratios (Building D : with links) | | | | | | |
|---|---|---|---|---|---|---|
| **StepType** | **Step** | **Period** | **UX** | **UY** | **SumUX** | **SumUY** |
| Text | | Sec | Unitless | Unitless | Unitless | Unitless |
| Mode | 1 | 0.356823 | 0.75977 | 2.48E-05 | 0.75977 | 2.48E-05 |
| Mode | 2 | 0.249501 | 3.57E-05 | 0.66093 | 0.75981 | 0.66096 |
| Mode | 3 | 0.166998 | 0.00236 | 3.32E-05 | 0.76217 | 0.66099 |
| Mode | 4 | 0.109039 | 0.13936 | 0.00011 | 0.90153 | 0.6611 |
| Mode | 5 | 0.088358 | 0.00045 | 0.17942 | 0.90198 | 0.84052 |
| Mode | 6 | 0.08071 | 0.00178 | 0.01143 | 0.90376 | 0.85195 |
| Mode | 7 | 0.066614 | 0.0158 | 0.0009 | 0.91956 | 0.85285 |
| Mode | 8 | 0.058874 | 0.00065 | 0.03508 | 0.92022 | 0.88792 |
| Mode | 9 | 0.056101 | 0.00402 | 0.00976 | 0.92424 | 0.89769 |
| Mode | 10 | 0.055175 | 0.00351 | 0.00773 | 0.92776 | 0.90541 |
| Mode | 11 | 0.047872 | 0.00881 | 0.00121 | 0.93656 | 0.90662 |
| Mode | 12 | 0.045609 | 5.24E-05 | 0.00087 | 0.93661 | 0.90749 |

| TABLE E1: Base Reactions (Building E : without links) | | | | | | | |
|---|---|---|---|---|---|---|---|
| **Output Case** | **Step** | **Global FX** | **Global FY** | **Global FZ** | **Global MX** | **Global MY** | **Global MZ** |
| Text | | KN | KN | KN | KN-m | KN-m | KN-m |
| DEAD | | -2.3E-12 | 1.74E-12 | 964.991 | 2099.821 | -3326.04 | -2.5E-12 |
| MODAL | 1 | -11490.8 | -43.014 | -31.504 | 136.7598 | -43264.4 | 10337.13 |
| MODAL | 2 | 150.062 | -22043.4 | -784.82 | 84766.17 | 4077.5 | -76393.7 |
| MODAL | 3 | -11076.2 | -742.136 | 556.187 | 3247.495 | -58862.3 | 122227.2 |
| MODAL | 4 | 50327.67 | -450.004 | 244.157 | 1364.008 | 13211.04 | -165203 |
| MODAL | 5 | 47.456 | -33565 | 106320 | 180380.1 | -355616 | -122147 |
| MODAL | 6 | 2936.826 | -819.711 | -6895.9 | -13195 | -14828 | -13677.7 |
| MODAL | 7 | -5146.83 | 30064.42 | 39684.2 | 135511.8 | 30323.46 | 138093.3 |
| MODAL | 8 | -4531.45 | -32238 | -43433.1 | -156625 | 272540.3 | -76916.8 |
| MODAL | 9 | 2244.79 | -16274.1 | -34213.7 | -94822 | 1777.873 | -86359.2 |
| MODAL | 10 | -4535.38 | -14292.7 | -55098.6 | -150037 | 373811.7 | 14695.32 |
| MODAL | 11 | 6830.537 | -5415.92 | -11512.8 | -18895.1 | -97268.2 | -102837 |
| MODAL | 12 | -2065.33 | -45266.7 | -31316.9 | -10319.2 | 139271.6 | -217209 |
| LIVE | | -2.3E-12 | 1.39E-12 | 118.544 | 204.9573 | -397.455 | -4.7E-12 |
| FLOOR FINISH | | -1.2E-12 | 6.94E-13 | 59.272 | 102.4787 | -198.728 | -2.4E-12 |
| EQx | | -312.591 | 1.78E-10 | -4E-12 | -9.1E-10 | -1249.48 | 592.0754 |
| EQy | | 8.56E-11 | -312.591 | 1.0E-11 | 1249.482 | 3.96E-10 | -1068.7 |

| TABLE E2: Base Reactions (Building E : with links) | | | | | | | |
|---|---|---|---|---|---|---|---|
| **Output Case** | **Step** | **Global FX** | **Global FY** | **Global FZ** | **Global MX** | **Global MY** | **Global MZ** |
| Text | | KN | KN | KN | KN-m | KN-m | KN-m |
| DEAD | | -2.1E-07 | -1.8E-11 | 964.986 | 2102.554 | -3327 | -2.9E-06 |
| MODAL | 1 | -10626.5 | -165.318 | -33.761 | 626.938 | -39747.8 | 9258.704 |
| MODAL | 2 | -358.586 | 21533.89 | 686.843 | -82565.3 | -4560.68 | 74591.03 |
| MODAL | 3 | -9262.76 | -616.754 | 509.25 | 2560.482 | -53007.6 | 111172.7 |
| MODAL | 4 | 41359.42 | -25.645 | -1188.49 | -1864.96 | 23272.7 | -135589 |
| MODAL | 5 | -1398.84 | 1375.823 | -4277.29 | -10491.3 | 32075.18 | 9804.991 |
| MODAL | 6 | 1419.483 | -199.355 | -1258.42 | -3377.72 | 11811.77 | -4679.59 |
| MODAL | 7 | -1352.29 | 1056.202 | -8849.34 | -20353 | -11258.7 | 11763.19 |
| MODAL | 8 | 1508.772 | -4669.82 | 13549.0 | 16349.94 | -21840.8 | -22738 |
| MODAL | 9 | 20217.36 | -6189.13 | 22244.3 | 36129.74 | -34932.3 | -83065.6 |
| MODAL | 10 | 10179.06 | 10869.38 | -22787.5 | -26642 | 103653.2 | 7939.245 |
| MODAL | 11 | 1971.099 | 29302.67 | -84846.5 | -125430 | 288342.7 | 95279.72 |
| MODAL | 12 | -3363.83 | 8006.792 | 66256.2 | 201724.1 | -197425 | 35641.36 |
| LIVE | | -1.2E-08 | -9.3E-12 | 118.544 | 204.9573 | -397.455 | -2.5E-07 |
| FLOOR FINISH | | -6E-09 | -4.7E-12 | 59.272 | 102.4787 | -198.728 | -1.3E-07 |
| EQx | | -312.653 | 1.42E-10 | 2.7E-08 | 5.33E-08 | -1249.66 | 621.867 |
| EQy | | 7.89E-07 | -312.653 | -7.7E-08 | 1249.657 | 3.71E-06 | -1110.9 |

| TABLE E3: Modal Participating Mass Ratios (Building E : without links) | | | | | | |
|---|---|---|---|---|---|---|
| **StepType** | **Step** | **Period** | **UX** | **UY** | **SumUX** | **SumUY** |
| Text | | Sec | Unitless | Unitless | Unitless | Unitless |
| Mode | 1 | 0.170558 | 0.67474 | 9.46E-06 | 0.67474 | 9.46E-06 |
| Mode | 2 | 0.126446 | 3.48E-05 | 0.75011 | 0.67478 | 0.75012 |
| Mode | 3 | 0.094467 | 0.059 | 0.00026 | 0.73378 | 0.75038 |
| Mode | 4 | 0.056292 | 0.15358 | 1.23E-05 | 0.88736 | 0.7504 |
| Mode | 5 | 0.050572 | 8.89E-08 | 0.0445 | 0.88736 | 0.7949 |
| Mode | 6 | 0.048382 | 0.00029 | 2.22E-05 | 0.88765 | 0.79492 |
| Mode | 7 | 0.045981 | 0.00072 | 0.0244 | 0.88836 | 0.81932 |
| Mode | 8 | 0.04536 | 0.00052 | 0.02657 | 0.88889 | 0.84589 |
| Mode | 9 | 0.045091 | 0.00013 | 0.00661 | 0.88901 | 0.8525 |
| Mode | 10 | 0.043003 | 0.00042 | 0.00422 | 0.88944 | 0.85672 |
| Mode | 11 | 0.041429 | 0.00083 | 0.00052 | 0.89027 | 0.85724 |
| Mode | 12 | 0.039704 | 0.000064 | 0.03075 | 0.89033 | 0.88799 |

| TABLE E4: Modal Participating Mass Ratios (Building E : with links) | | | | | | |
|---|---|---|---|---|---|---|
| **StepType** | **Step** | **Period** | **UX** | **UY** | **SumUX** | **SumUY** |
| Text | | Sec | Unitless | Unitless | Unitless | Unitless |
| Mode | 1 | 0.177728 | 0.68024 | 0.00016 | 0.68024 | 0.00016 |
| Mode | 2 | 0.128195 | 0.00021 | 0.75612 | 0.68045 | 0.75629 |
| Mode | 3 | 0.097854 | 0.0475 | 0.00021 | 0.72794 | 0.7565 |
| Mode | 4 | 0.06238 | 0.15639 | 6.02E-08 | 0.88433 | 0.7565 |
| Mode | 5 | 0.058905 | 0.00014 | 0.00014 | 0.88447 | 0.75663 |
| Mode | 6 | 0.058062 | 0.00014 | 2.73E-06 | 0.88461 | 0.75664 |
| Mode | 7 | 0.056525 | 0.00011 | 6.88E-05 | 0.88472 | 0.75671 |
| Mode | 8 | 0.05477 | 0.00012 | 0.00118 | 0.88485 | 0.75789 |
| Mode | 9 | 0.054248 | 0.02137 | 0.002 | 0.90622 | 0.75989 |
| Mode | 10 | 0.054112 | 0.00536 | 0.00612 | 0.91158 | 0.76601 |
| Mode | 11 | 0.051051 | 0.00016 | 0.03521 | 0.91174 | 0.80122 |
| Mode | 12 | 0.048657 | 0.00038 | 0.00217 | 0.91213 | 0.80339 |

**APPENDIX: F**

## Determination of Performance point from Capacity Spectrum Method:

### A. BUILDING "A"

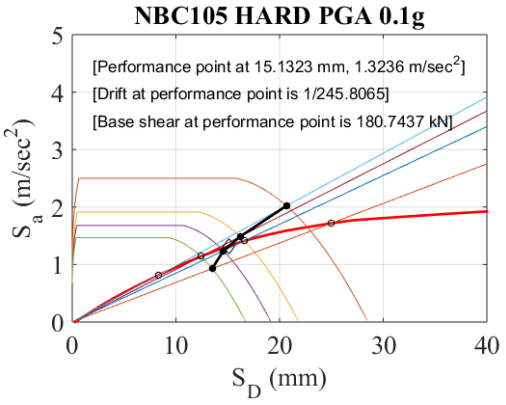


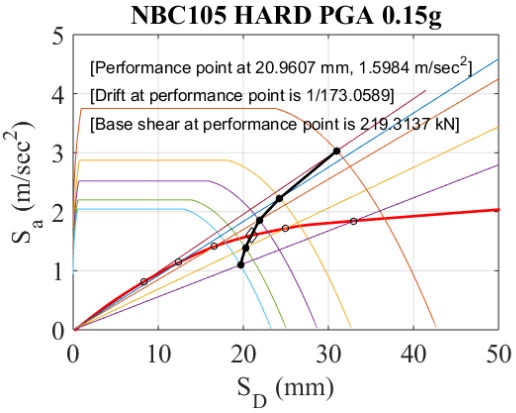


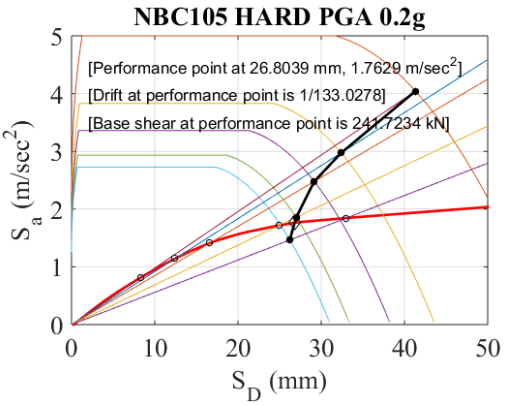


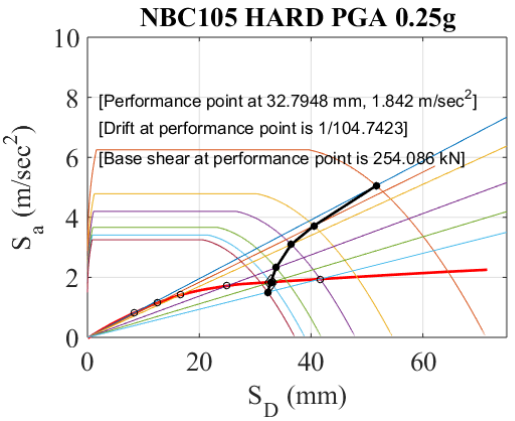


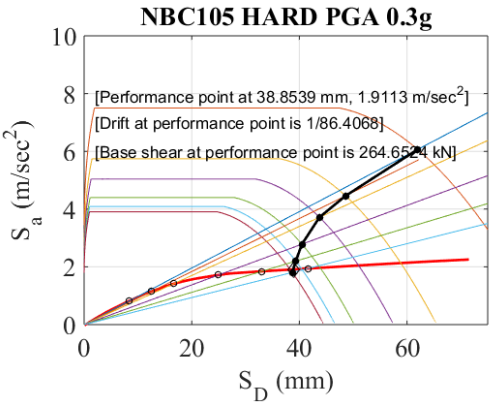


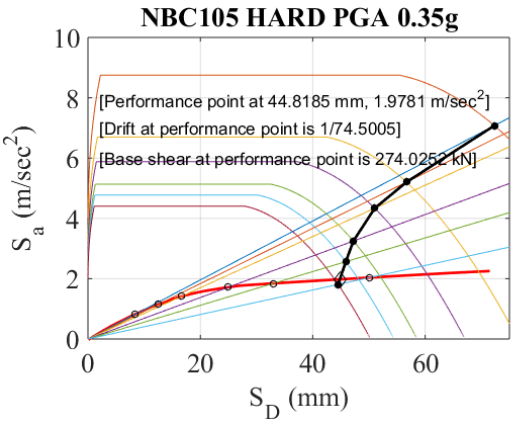

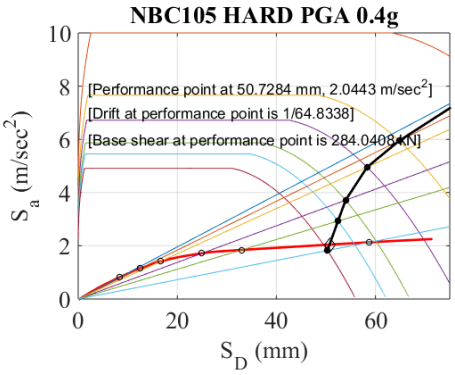
NBC105 HARD PGA 0.4g
[Performance point at 50.7284 mm, 2.0443 m/sec$^2$]
[Drift at performance point is 1/64.8338]
[Base shear at performance point is 284.0408 kN]
S$_a$ (m/sec$^2$)
S$_D$ (mm)

## B. BUILDING "B"

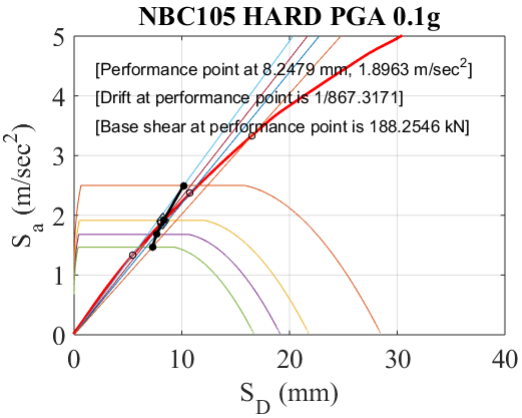
NBC105 HARD PGA 0.1g
[Performance point at 8.2479 mm, 1.8963 m/sec$^2$]
[Drift at performance point is 1/867.3171]
[Base shear at performance point is 188.2546 kN]
S$_a$ (m/sec$^2$)
S$_D$ (mm)

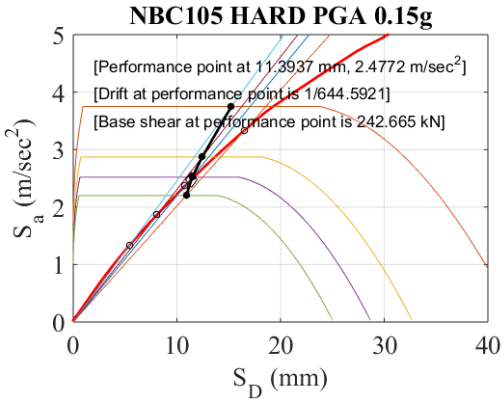
NBC105 HARD PGA 0.15g
[Performance point at 11.3937 mm, 2.4772 m/sec$^2$]
[Drift at performance point is 1/644.5921]
[Base shear at performance point is 242.665 kN]
S$_a$ (m/sec$^2$)
S$_D$ (mm)

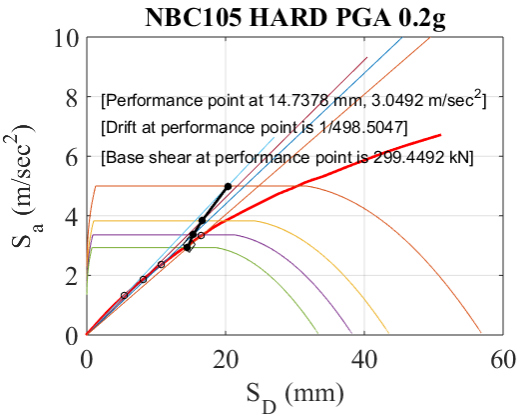
NBC105 HARD PGA 0.2g
[Performance point at 14.7378 mm, 3.0492 m/sec$^2$]
[Drift at performance point is 1/498.5047]
[Base shear at performance point is 299.4492 kN]
S$_a$ (m/sec$^2$)
S$_D$ (mm)

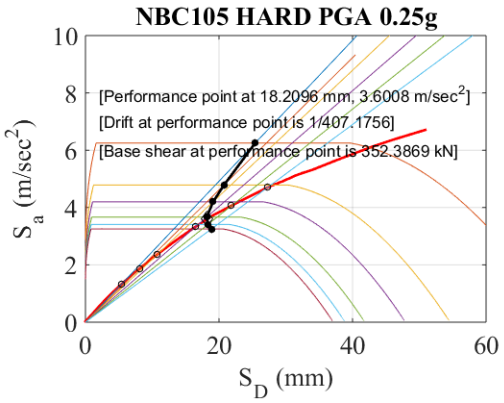
NBC105 HARD PGA 0.25g
[Performance point at 18.2096 mm, 3.6008 m/sec$^2$]
[Drift at performance point is 1/407.1756]
[Base shear at performance point is 352.3869 kN]
S$_a$ (m/sec$^2$)
S$_D$ (mm)

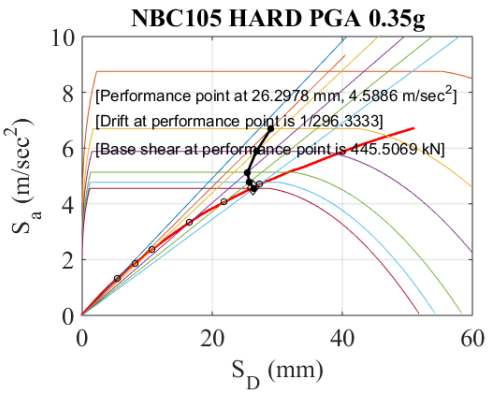
NBC105 HARD PGA 0.35g
[Performance point at 26.2978 mm, 4.5886 m/sec$^2$]
[Drift at performance point is 1/296.3333]
[Base shear at performance point is 445.5069 kN]
S$_a$ (m/sec$^2$)
S$_D$ (mm)

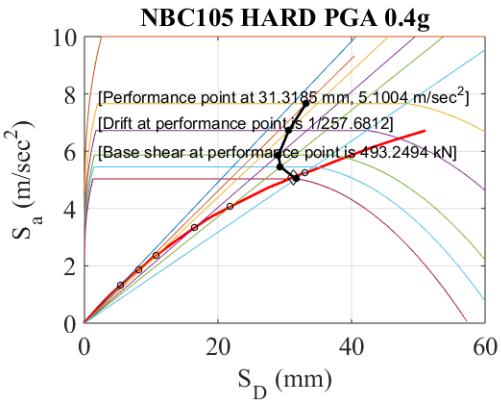
NBC105 HARD PGA 0.4g
[Performance point at 31.3185 mm, 5.1004 m/sec$^2$]
[Drift at performance point is 1/257.6812]
[Base shear at performance point is 493.2494 kN]
S$_a$ (m/sec$^2$)
S$_D$ (mm)

## C. BUILDING "C"

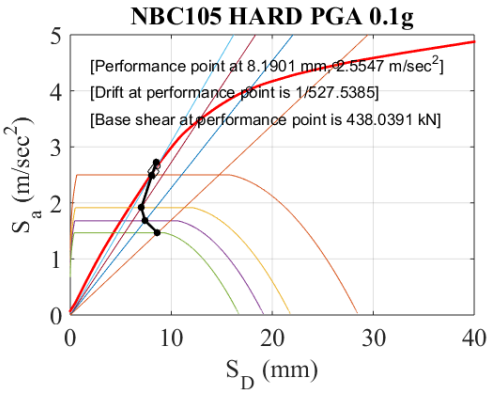
NBC105 HARD PGA 0.1g
[Performance point at 8.1901 mm, 2.5547 m/sec$^2$]
[Drift at performance point is 1/527.5385]
[Base shear at performance point is 438.0391 kN]
$S_a$ (m/sec$^2$)
$S_D$ (mm)

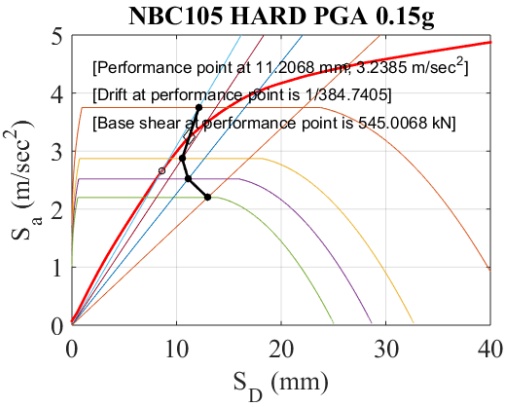
NBC105 HARD PGA 0.15g
[Performance point at 11.2068 mm, 3.2385 m/sec$^2$]
[Drift at performance point is 1/384.7405]
[Base shear at performance point is 545.0068 kN]
$S_a$ (m/sec$^2$)
$S_D$ (mm)

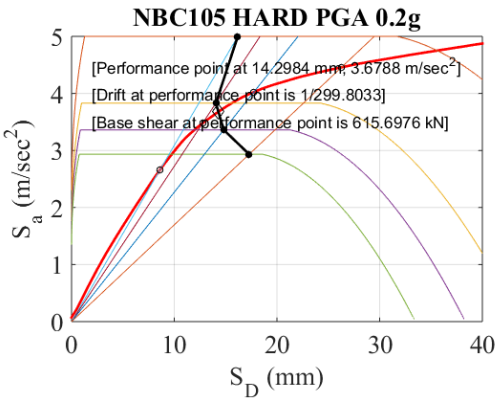
NBC105 HARD PGA 0.2g
[Performance point at 14.2984 mm, 3.6788 m/sec$^2$]
[Drift at performance point is 1/299.8033]
[Base shear at performance point is 615.6976 kN]
$S_a$ (m/sec$^2$)
$S_D$ (mm)

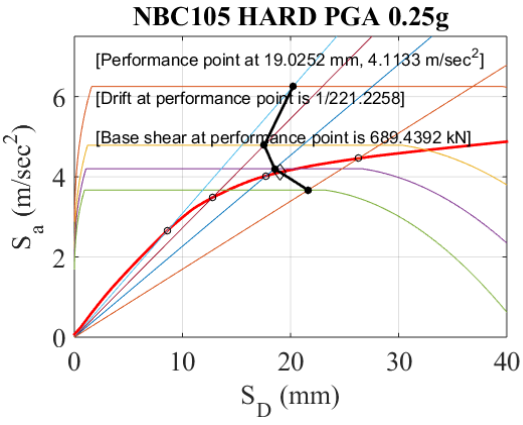
NBC105 HARD PGA 0.25g
[Performance point at 19.0252 mm, 4.1133 m/sec$^2$]
[Drift at performance point is 1/221.2258]
[Base shear at performance point is 689.4392 kN]
$S_a$ (m/sec$^2$)
$S_D$ (mm)

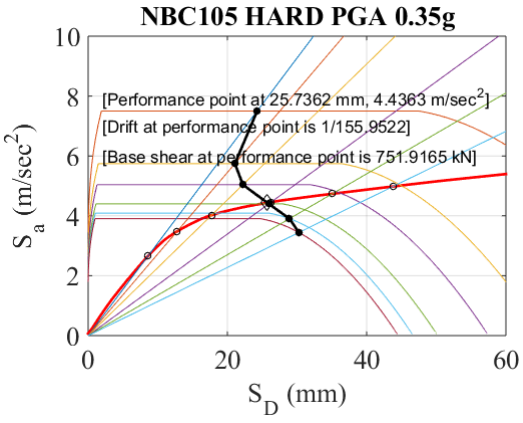
NBC105 HARD PGA 0.35g
[Performance point at 25.7362 mm, 4.4363 m/sec$^2$]
[Drift at performance point is 1/155.9522]
[Base shear at performance point is 751.9165 kN]
$S_a$ (m/sec$^2$)
$S_D$ (mm)

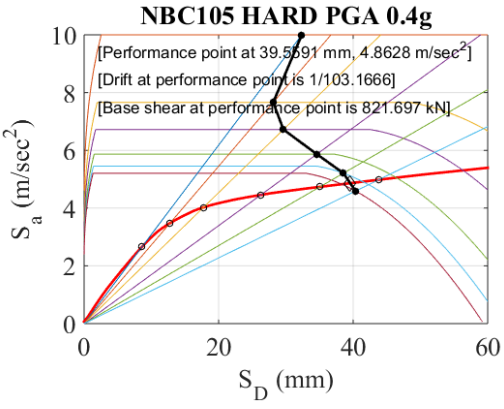
NBC105 HARD PGA 0.4g
[Performance point at 39.5891 mm, 4.8628 m/sec$^2$]
[Drift at performance point is 1/103.1666]
[Base shear at performance point is 821.697 kN]
$S_a$ (m/sec$^2$)
$S_D$ (mm)

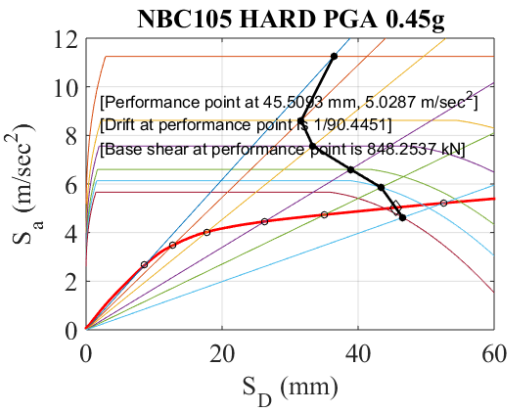
NBC105 HARD PGA 0.45g
[Performance point at 45.5093 mm, 5.0287 m/sec$^2$]
[Drift at performance point is 1/90.4451]
[Base shear at performance point is 848.2537 kN]
$S_a$ (m/sec$^2$)
$S_D$ (mm)

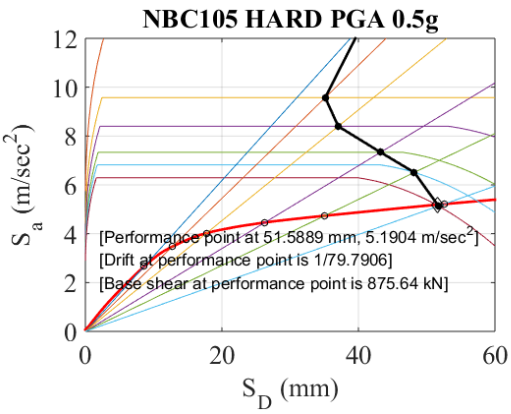
NBC105 HARD PGA 0.5g
[Performance point at 51.5889 mm, 5.1904 m/sec$^2$]
[Drift at performance point is 1/79.7906]
[Base shear at performance point is 875.64 kN]
$S_a$ (m/sec$^2$)
$S_D$ (mm)

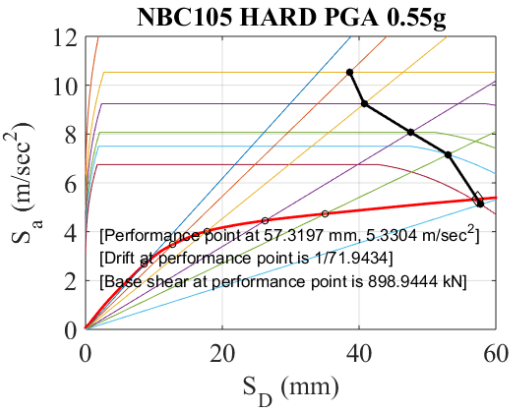
NBC105 HARD PGA 0.55g
[Performance point at 57.3197 mm, 5.3304 m/sec$^2$]
[Drift at performance point is 1/71.9434]
[Base shear at performance point is 898.9444 kN]
$S_a$ (m/sec$^2$)
$S_D$ (mm)

## D. BUILDING "D"

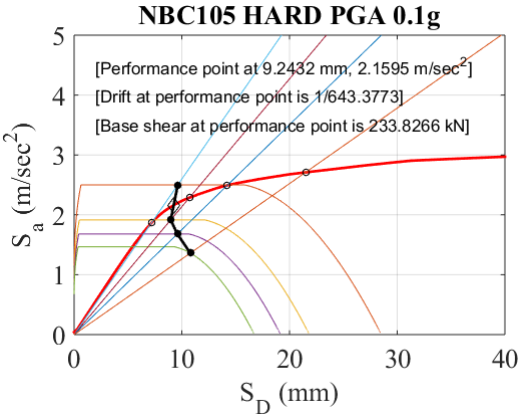
NBC105 HARD PGA 0.1g
[Performance point at 9.2432 mm, 2.1595 m/sec$^2$]
[Drift at performance point is 1/643.3773]
[Base shear at performance point is 233.8266 kN]
$S_a$ (m/sec$^2$)
$S_D$ (mm)

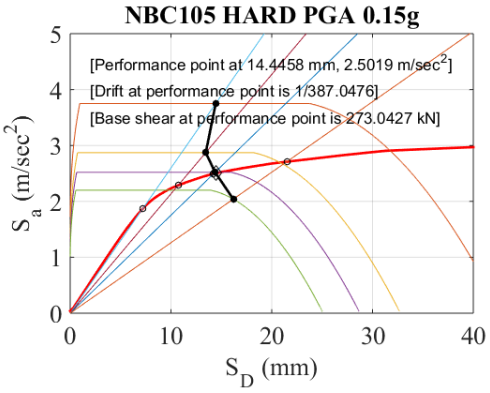
NBC105 HARD PGA 0.15g
[Performance point at 14.4458 mm, 2.5019 m/sec$^2$]
[Drift at performance point is 1/387.0476]
[Base shear at performance point is 273.0427 kN]
$S_a$ (m/sec$^2$)
$S_D$ (mm)

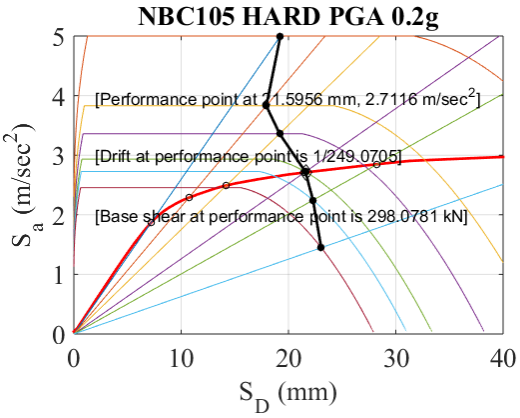
NBC105 HARD PGA 0.2g
[Performance point at 11.5956 mm, 2.7116 m/sec$^2$]
[Drift at performance point is 1/249.0705]
[Base shear at performance point is 298.0781 kN]
$S_a$ (m/sec$^2$)
$S_D$ (mm)

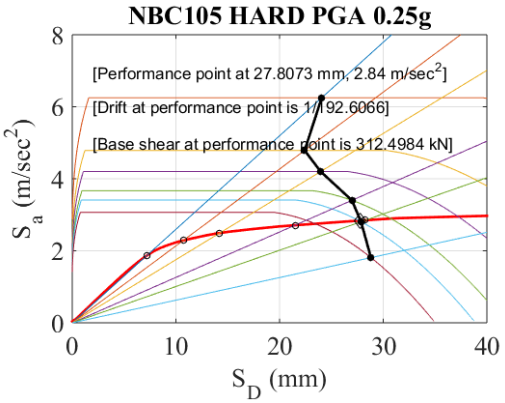
NBC105 HARD PGA 0.25g
[Performance point at 27.8073 mm, 2.84 m/sec$^2$]
[Drift at performance point is 1/192.6066]
[Base shear at performance point is 312.4984 kN]
$S_a$ (m/sec$^2$)
$S_D$ (mm)

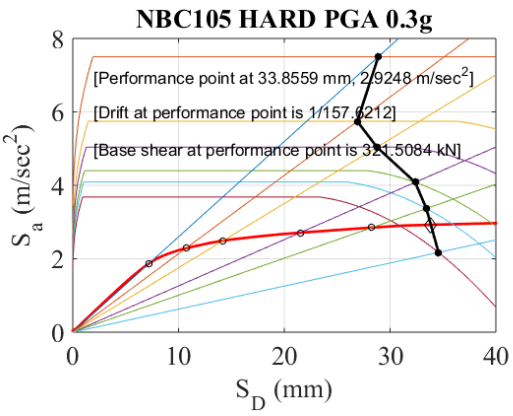
NBC105 HARD PGA 0.3g
[Performance point at 33.8559 mm, 2.9248 m/sec$^2$]
[Drift at performance point is 1/157.6212]
[Base shear at performance point is 321.5084 kN]
$S_a$ (m/sec$^2$)
$S_D$ (mm)

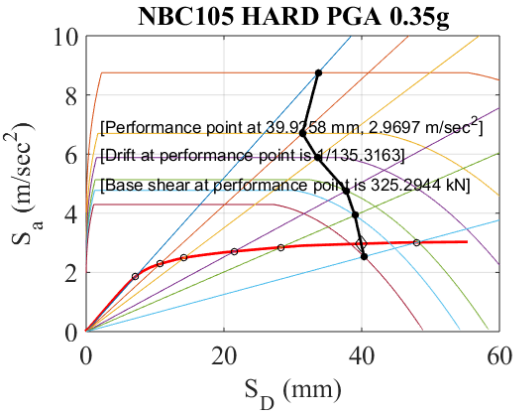
NBC105 HARD PGA 0.35g
[Performance point at 39.9158 mm, 2.9697 m/sec$^2$]
[Drift at performance point is 1/135.3163]
[Base shear at performance point is 325.2944 kN]
$S_a$ (m/sec$^2$)
$S_D$ (mm)

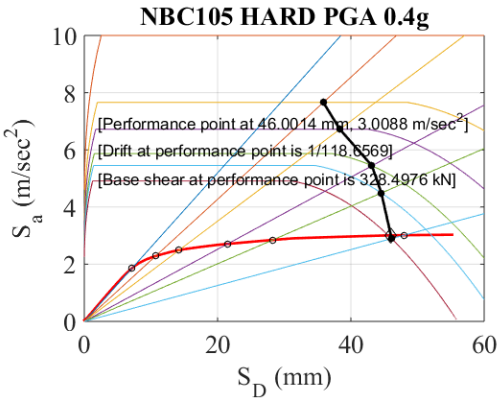
NBC105 HARD PGA 0.4g
[Performance point at 46.0014 mm, 3.0088 m/sec$^2$]
[Drift at performance point is 1/118.6569]
[Base shear at performance point is 328.4976 kN]
$S_a$ (m/sec$^2$)
$S_D$ (mm)

## E. BUILDING "E"

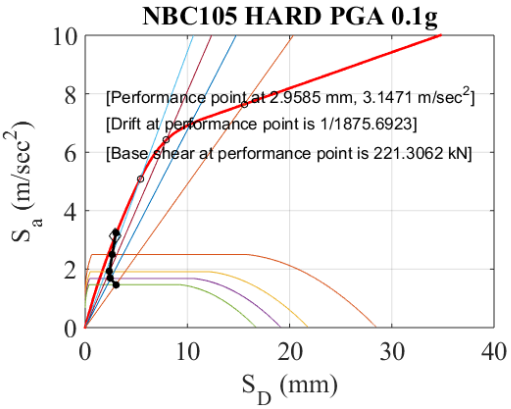
NBC105 HARD PGA 0.1g
[Performance point at 2.9585 mm, 3.1471 m/sec$^2$]
[Drift at performance point is 1/1875.6923]
[Base shear at performance point is 221.3062 kN]
$S_a$ (m/sec$^2$)
$S_D$ (mm)

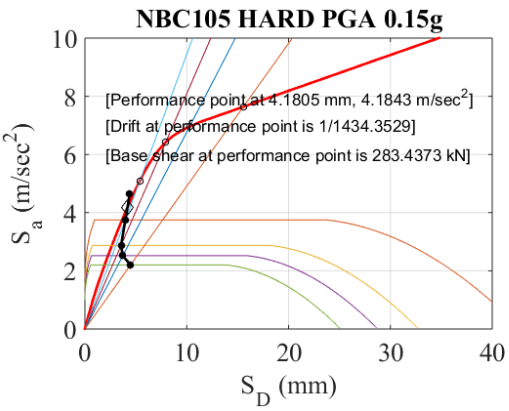
NBC105 HARD PGA 0.15g
[Performance point at 4.1805 mm, 4.1843 m/sec$^2$]
[Drift at performance point is 1/1434.3529]
[Base shear at performance point is 283.4373 kN]
$S_a$ (m/sec$^2$)
$S_D$ (mm)

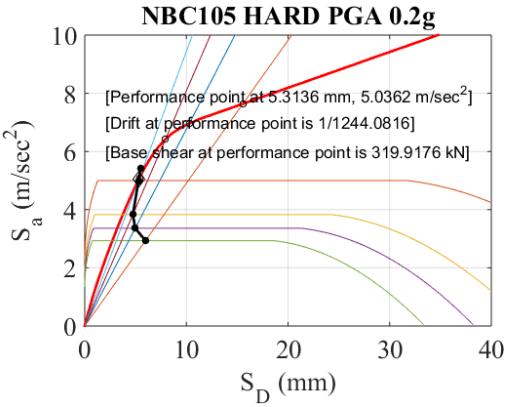
NBC105 HARD PGA 0.2g
[Performance point at 5.3136 mm, 5.0362 m/sec$^2$]
[Drift at performance point is 1/1244.0816]
[Base shear at performance point is 319.9176 kN]
$S_a$ (m/sec$^2$)
$S_D$ (mm)

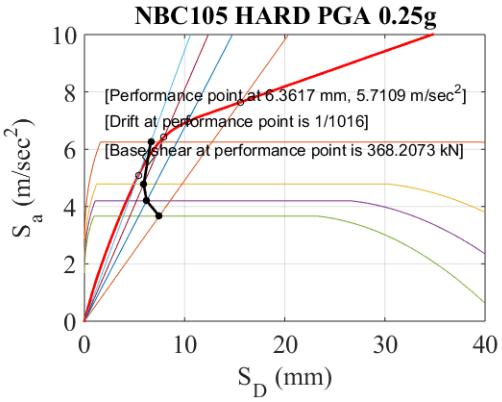
NBC105 HARD PGA 0.25g
[Performance point at 6.3617 mm, 5.7109 m/sec$^2$]
[Drift at performance point is 1/1016]
[Base shear at performance point is 368.2073 kN]
$S_a$ (m/sec$^2$)
$S_D$ (mm)

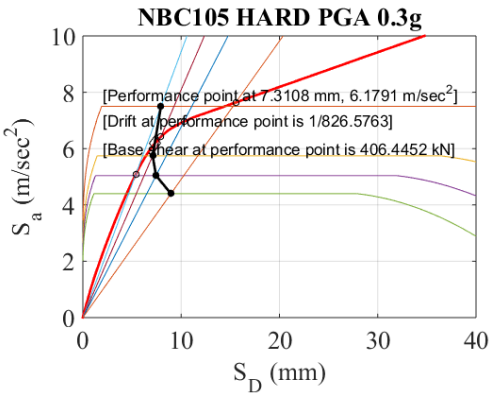
NBC105 HARD PGA 0.3g
[Performance point at 7.3108 mm, 6.1791 m/sec$^2$]
[Drift at performance point is 1/826.5763]
[Base shear at performance point is 406.4452 kN]
$S_a$ (m/sec$^2$)
$S_D$ (mm)

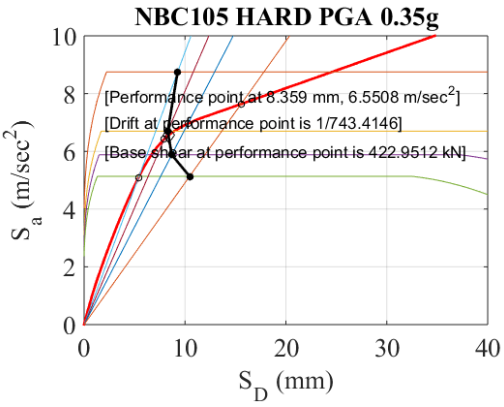
NBC105 HARD PGA 0.35g
[Performance point at 8.359 mm, 6.5508 m/sec$^2$]
[Drift at performance point is 1/743.4146]
[Base shear at performance point is 422.9512 kN]
$S_a$ (m/sec$^2$)
$S_D$ (mm)

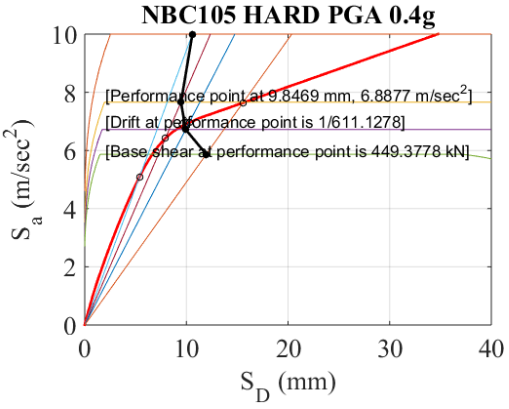
NBC105 HARD PGA 0.4g
[Performance point at 9.8469 mm, 6.8877 m/sec$^2$]
[Drift at performance point is 1/611.1278]
[Base shear at performance point is 449.3778 kN]
$S_a$ (m/scc$^2$)
$S_D$ (mm)
0
2
4
6
8
10
0
10
20
30
40

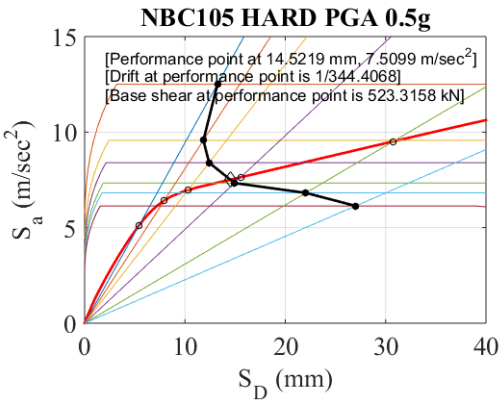
NBC105 HARD PGA 0.5g
[Performance point at 14.5219 mm, 7.5099 m/sec$^2$]
[Drift at performance point is 1/344.4068]
[Base shear at performance point is 523.3158 kN]
$S_a$ (m/scc$^2$)
$S_D$ (mm)
0
5
10
15
0
10
20
30
40